The North Atlantic Ocean in the Greenhouse – Overturning Response and Sensitivities

Dissertation
zur Erlangung des Doktorgrades
der Christian-Albrechts-Universität
zu Kiel

vorgelegt von
Ulf Schweckendiek

Kiel
2003

Referent	Prof. Dr. Jürgen Willebrand
Koreferent	Prof. Dr. Mojib Latif
Tag der mündlichen Prüfung:	9.12.2003
Zum Druck genehmigt:	5.12.2003

Contents

Zusammenfassung

Die Prognosen gekoppelter Klimamodelle dafür, wie sich die thermohaline Zirkulation bei einer zunehmenden Konzentration von Treibhausgasen in der Atmosphäre entwickelt, sind sehr unterschiedlich. Eine mögliche Ursache für diese Diskrepanz ist die Darstellung der Ozeane in gekoppelten Klimamodellen. Im Vergleich zu Messungen oder auch reinen Ozeanmodellen ist die Simulation von Zirkulation und Wassermasseneigenschaften in den meisten Ozeankomponenten in vielerlei Hinsicht noch recht unrealistisch. Treibt man realistischere Zirkulationsmodelle des Ozeans mit diagnostizierten Flüssen aus Treibhausgas-Simulationen gekoppelter Klimamodelle an, lässt sich untersuchen, inwiefern und in welchen Regionen eine realistischere Darstellung des Ozeans zu einer Konvergenz der Prognosen führen kann.

Die Ergebnisse aus dem Ozeanmodell zeigen allerdings, dass der generelle Response der thermohalinen Zirkulation durch atmosphärischen Antrieb im Hinblick auf längerfristige Variabilität und Trends robust und relativ unabhängig von der Ozeankomponente ist.

Die Variabilität der thermohalinen Zirkulation auf verschiedenen Zeitskalen lässt sich relativ einfach auf die recht lineare Überlagerung der Komponenten des atmospherischen Antriebs in verschiedenen Regionen des Nordatlantiks zurückführen. Die interannuale bis dekadische Variabilität hat im wesentlichen im subpolaren Bereich ihren Ursprung. Dabei dominieren Windstressanomalien auf interannualen Skalen, während Wärmeflussanomalien die Variabilität auf dekadischen Skalen bestimmen. Die Ursache für fundamentale Änderungen sowie multidekadischen Schwankungen ist hauptsächlich die Veränderungen in der Dichteschichtung in der Nordischen See, so dass unterschiedliche Prognosen von Klimamodellen im wesentlichen mit der Dichtebilanz in der Nordischen See zu erklären sind.

Die Bedeutung und Sensibilität der Regionen der Tiefenwasserbildung im Nordatlantik sind sehr unterschiedlich. Die zentrale Labradorsee reagiert recht sensibel auf anthropogene Änderungen in den Oberflächenflüssen, so dass hier die Tiefenwasserbildung im Treibhausszenario im Laufe des 21. Jahrhunderts zusammenbricht. In diesem Fall wird die Stärke der meridionale Zelle fast vollständig durch den Transport dichten Wassers über die relativ flachen Overflows bestimmt. Die nördliche Region ist wegen des Reservoirs an dichtem Wasser im Hinblick auf anthropogen bedingte Änderungen in den Oberflächenflüssen im Ozeanmodel robuster; hier entscheidet sich letztlich das generelle Verhalten der thermohalinen Zirkulation.

Abstract

The prognoses of coupled climate models, how the thermohaline circulation evolves under an increasing concentration of greenhouse gases in the atmosphere are highly different. A possible reason for this discrepancy is the presentation of the oceans in coupled climate models. In comparison to observations or pure ocean models the simulation of circulation and water mass properties is in many aspects still quite unrealistic. Forcing a more realistic ocean circulation model with diagnosed fluxes from greenhouse gas simulations permits to investigate, to what extent and in which region a realistic representation of the ocean can lead to converging prognoses.

The results from the ocean model show indeed, that the general response of the thermohaline circulation due to changes in atmospheric forcing in terms of long-term variability and trends is quite robust and relatively independent of the ocean component.

The variability of the thermohaline circulation on different timescales can easily be traced back to a quite linear superposition of atmospheric forcing components in different regions of the North Atlantic. The interannual to decadal variability has its seeds mainly in the subpolar region. On interannual scales, the wind stress anomalies dominate the response, while heat flux anomalies affect the variability on decadal timescales. The reason for fundamental changes as well as for multidecadal fluctuations are primarily changes in the stratification in the Nordic Seas, so that different prognosis from climate models can mainly be explained by the density budget in the Nordic Seas.

The relevance and sensitivity of the regions of deep water formation in the North Atlantic are very different. The central Labrador Sea responds quite sensitive to anthropogenic changes in the surface fluxes, so that the deep water formation in this region breaks down during the 21^{st} century. In that case, the strength of the overturning cell is mainly determined by the dense water transport over relative shallow overflows. Due to the reservoir of dense water, the northern region is more robust in terms of anthropogenic changes in the surface fluxes; in this region the general response of the thermohaline circulation is ultimately determined.

Chapter 1

Introduction

The world's ocean provides an important component in the climate system. Due to its capacity to store and transport large amounts of heat and chemical gases like carbon dioxide, the ocean is both a passive buffer for atmospheric fluctuations and an active conveyor of properties. Fundamental changes in the oceanic state might therefore be responsible for fundamental changes of the earth's climate.

For example, ideas from Philander and Fedorov (2003) suggest that along with the global cooling during the Cenozoic (60 Ma to 3 Ma ago) the thermal structure of the ocean changed gradually. At the beginning the warm deep ocean temperatures at about 12°C in the early Cenozoic could have been the reason for a very deep thermocline in the tropics. Like under today's El Niño conditions winds were unable to bring cold water to the surface in the upwelling zones of low latitudes, with the consequence, that the ocean underneath the thermocline remains mainly uncoupled in these regions. Along with a cooling of the deeper ocean until about 3 Ma ago, the mixed layer depth could have become sufficiently shallow. Significant upwelling could set in to reduce surface temperatures and hence permit atmosphere interactions with the deeper ocean in tropical latitudes.

But also higher latitudes could be affected. A key and much more investigated role in terms of climate change due to changes within the ocean is ascribed to the conveyor belt circulation itself, often associated with the *thermohaline circulation* (THC). This name is to some extent misleading, because the energetics, leading to this overturning conveyor in the ocean are difficult to acquire [1] (Wunsch, 2000). The dynamical characteristic of the THC is its nonlinear behaviour, which is the basis of understanding the possible existence of several equilibrium states and relatively rapid transitions between them. Changes in oceanic circulation, particularly in the Atlantic Ocean could have played an important role in variations

[1] The physical mechanisms driving this circulation are a combination of wind stress, buoyancy forcing as well as diffusive effects. Since the THC cannot be diagnosed, neither in observations nor in models with realistic forcing, in this study, we use changes in the meridional overturning circulation (MOC) (e.g. Schmitz and McCartney, 1993) in the Atlantic Ocean as an indicator for changes of the THC, as it is done in most model studies. It is justifiable, since in models the thermohaline part is essentially similar to the overturning circulation, but lacks the narrow wind-driven cells near the surface (e.g. Rahmstorf, 2003).

of glacial climate. Rapid transitions for instance could have been the reason for 6-10°C temperature increases within about 10 years (Dansgaard/Oeschger events) during the last glacial maximum (GANOPOLSKI AND RAHMSTORF, 2001).

Fortunately today's climate is found to be much more stable. Although never before on our planet the atmospheric concentration of greenhouse gases changed so quickly, anthropogenic future forcing scenarios with coupled ocean-atmosphere models mostly indicate a more or less strong *linear* weakening of the circulation for the next century. Following implications of BROECKER (1987), in most models this is traced back to an advective spindown due to increasing heat and freshwater fluxes in high latitudes of the North Atlantic ocean.
However, the possible impacts of this weakening on northern Europe's climate are still an open question. On the one hand, it is still arguable, to what extent the THC is responsible for the warm winter temperatures on the European continent relative to the temperatures in Newfoundland at a similar latitude (SEAGER ET AL., 2002). On the other hand, it is not yet extracted, whether the role of the THC is mainly a direct or a remote effect:
Since the ocean's heat capacity exceeds that of the atmosphere by more than three orders, the relatively slow ocean currents are able to provide heat transports, which are in some latitudes of the Atlantic ocean in the order of the atmospheric fraction (e.g. HALL AND BRYDEN, 1982). A weakening of the circulation would cause a reduced northward heat transport and could lead to a cooling of the surface.
Beyond its direct ability to transport enormous amounts of heat, the remote effect of this transport in terms of ocean-atmosphere interactions is very important: In subpolar and polar latitudes, lateral transport of warm water affects or even permits interactions between ocean and atmosphere. The mechanisms are to influence the atmosphere above or to constrain the ice coverage with its isolating effect for air-sea fluxes (SCHILLER ET AL., 1997). By opening the ice, the oceanic transport gives scope for a great number of feedback mechanisms concerning sea ice (CURRY AND WEBSTER, 1999). In ocean models, the surface density in these regions and hence the ability of the models to renew deep water in convective areas is found to be very important for controlling the strength of the THC. Therefore possible changes of THC strength and hence the northern heat transport could not only affect the northern hemispheric sea surface temperatures directly but could also affect the atmospheric contribution by changing its meridional temperature gradient. An anthropogenic forced weakening of the circulation could therefore potentially result in a change of the sea ice coverage.
Additionally, PHILANDER's ideas concerning the depth of the thermocline could come into play in terms of the thermohaline circulation as well in higher latitudes. HUANG ET AL. (2000) suggest that reduced sea surface temperatures in the North Atlantic due to a weakening of the overturning circulation could lead to a deepening of the thermocline and hence to an enhanced accumulation of heat into the interior ocean.
With all its self constraining impacts, the THC might have an influence on the meridional atmospheric temperature gradient above and therefore also on the at-

mospheric heat transport. Hence predicting the future climate, the response of the THC must essentially be taken into account.

Although quite uncertain, the only way to get predictions beyond these theoretical dependencies in the future climate is indeed to integrate highly realistic coupled ocean-atmosphere models, forced with the expected increase of anthropogenic greenhouse gas concentrations. In terms of the evolution of the THC in a warmer world, the response of these climate models in anthropogenic forcing scenarios differs fundamentally: Depending on the sensitivity of the THC to changes in the radiative forcing, the slowing down varies between 10% (Mitchell et al., 1995) and 100% (Manabe and Stouffer, 1994) and is quite linear. Anyhow, although suggesting a weakening of the THC, in most of these models the greenhouse gas forcing still leads to an increase in surface temperatures over most of the North Atlantic and the European continent. Only in some regions along the Gulf Stream, where the lateral effect of oceanic heat transport is strongest, a slight cooling can be diagnosed.
However, in some models the THC remains almost constant (Latif et al., 2000; Gent, 2001). In both integrations, the THC is stabilized due to a gain in surface salinity arising from enhanced evaporation, counteracting the destabilizing of the THC. Despite the similar behaviour, the mechanisms are quite different. Gent reported a locally enhanced evaporation in regions of deep water formation in the *CSM* model. Here the THC responds more or less passively to local changes in the atmospheric fluxes, as it is found in a couple of studies (e.g. Delworth and Greatbatch, 2000). In contrast, in the *ECHAM4/OPYC3* coupled model the enhanced evaporation occurs in the tropics and subtropics. The resulting salt signal is ultimately advected into convective regions (Latif et al., 2000). These findings from Latif and recent results from Thorpe et al. (2001) using the *HadCM3* model suggest a more active role of the ocean. As a consequence of changes within the hydrological cycle and hence the ocean's salinity, the ocean dynamics come into play. In both integrations the lateral transport of salt serves to stabilize the THC response to anthropogenic forcing.
If there are indications that it might also be relevant to focus on the dynamics *within* the ocean to predict THC changes, the representation of the ocean in climate models could be a limiting factor, since climate models are seriously mispresenting many oceanic processes. Due to the slower moving of the ocean, the main horizontal momentum balance in large scale geophysical dynamics on the earth between the Coriolis-Force and the pressure gradient has to be examined on much smaller spatial scales in the ocean than in the atmosphere. Hence, in ocean components of most climate models with a coarse horizontal and vertical resolution, the representation of boundary currents and narrow passages along topography is necessarily poor. Döscher and Redler (1997) found in an ocean model, that if a realistic narrow density signal of the Denmark Strait Overflow is implemented, the surface forcing within the subpolar gyre is of less importance for the THC strength. Their argumentation is, that, if coarse resolution models are not able to simulate these (observed) signals, they might be too sensitive to

anthropogenic surface forcing and might therefore overestimate the response of the THC on decadal to centennial timescales.

Furthermore, observational studies provide a relative complete association concerning mechanisms of open ocean deep water formation (MARSHALL AND SCHOTT, 1999). These processes involving the circulation as well as local loss of buoyancy take part on relatively small scales. So, to include this at least as an integral effect, much effort on the parameterization is necessary. Anyhow, realistic properties and the spreading of these water masses in the correct depth are difficult to achieve. Although often flux-corrected at the surface, the majority of models seems to be too diffusive and is not able to provide deep water masses with correct temperature and salinity. JIA (2002) found in a comparison between different coupled models a mean deviation of North Atlantic Deep Water temperature of about 2.5°C relative to observations (ROEMMICH AND WUNSCH, 1985). As a consequence, in these models the depth of the Deep Western Boundary Current is often too shallow. This might have a number of consequences for the distribution and interaction of water masses in the ocean, for instance for the interaction with the Gulf Stream above or for the spreading of Antarctic Bottom Water in the North Atlantic.

Another point is the difficulty of coarse resolution models to differentiate between different regions of deep water formation. In observations, regions of deep convection are found both south of Iceland, mainly the Labrador and the Irminger Sea, as well as in the Greenland-Iceland-Scotland Sea (e.g. FISCHER AND SCHOTT, 1997). This subdivision results in roughly three layers of North Atlantic Deep Water with different properties. Instead, many models show convective events *either* in the subpolar gyre *or* in the Nordic Seas. Beyond the deficit in simulating a realistic mean state of the ocean, for the response of the THC this point can be of great relevance. RAHMSTORF (1999) suggests that not only the strength but also the contribution of the cold branch of the circulation might change due to greenhouse gas forcing, as it is found by WOOD ET AL. (1999) in the *HadCM3* model. In their model, the Labrador Sea convection breaks down under anthropogenic changes of the surface fluxes, while the situation north of Iceland remains almost unchanged. However, in that experiment the THC is only slightly reduced.

The main scope of the thesis is to constrain the number of possible reasons for the deviating response of climate models in greenhouse gas simulations. For this point, not the variability on decadal to interdecadal scales is investigated, instead we mainly concentrate on the trend of the MOC. By forcing a proven ocean model with a quite realistic mean state with anthropogenic fluxes from different scenarios, we focus on the question, whether the deviating overturning response can be traced back to differences within the individual ocean components: Does an ocean model with a more realistic mean state provide fundamental differing results in terms of the THC response?
On account of physical problems of forcing a high resolved ocean with fluxes diagnosed from a coarse circulation pattern, these anthropogenic experiments are performed with a one-degree ocean model. Instead of integrating an eddy-permitting model with greenhouse gas forcing, a number of artifical sensitivity studies with

both resolutions are performed, in order to estimate the dependency of the resolution on the response of the THC. Furthermore, using an uncoupled ocean model, we are able to integrate the model with different combinations of anthropogenic forcing. This is an useful approach to investigate the role of individual air-sea fluxes and also regional dependencies. For instance, with different water mass contributions to the deep western boundary current, we are in the position to investigate the question, if and where there are key regions for the general overturning response of the ocean model to anthropogenic forcing.
Additionally, by simplifying the ocean model in terms of parameterization and topography, we concern to the question, how realistic an ocean model must be to provide a comparable response on surface forcing.

However, the meridional shape of the overturning as well as the thermohaline circulation is an integral parameter and is ultimately determined by local processes within the basin. But since the THC is associated with net meridional oceanic heat transport on longer timescales, comparing its response in global warming scenarios is the most obvious approach. The deficits of representing local features of the circulation in coupled models with a coarse resolved ocean are well known. Hence the purpose of these models is not the investigation of the local but of the integral response. Therefore, finding a fundamentally different response in an ocean model with different complexity and the same atmospheric forcing pattern requires further investigations. In that case we must indeed focus on the individual response of local features of certain parts of the circulation, leading to these deviations.

The outline of this thesis is as follows: Chapter 2 describes the physics of the numerical ocean model, explains the implementation of the anthropogenic forcing and shows some aspects of the oceanic state and circulation at the beginning of the experiments. Additionally, since we mainly use the MOC as diagnostic tool in the following chapters, we summarize its coherency to the THC and the meridional heat transport. In chapter 3, two suites of sensitivity studies with idealized forcing for the coarse as well as for a higher resolution model are presented. Chapter 4 and 5 contain the studies with anthropogenic forcing from two differing greenhouse gas simulations. Since we are not able to investigate the response of the ocean model to a high number of forcing pattern, we chose two scenarios which differ as much as possible in terms of deep water formation regions, response of the overturning circulation and representation of topography. Both chapters focus on the question, whether a different ocean model can be the reason for the deviating response of the THC in climate models. Relatively separated for each of these climate models, specific questions are illuminated. In chapter 4 the stabilizing effect of lateral signals for the North Atlantic is investigated. In chapter 5 we mainly concentrate on the contributions and the interplay of certain components of atmospheric forcing for the variability and the trend of the THC. Finally, in chapter 6 a summary as well as a conclusion about the results of different combinations of the anthropogenic forcing pattern is given.

Chapter 2

The Atlantic Ocean model

2.1 Introduction

The model used in this study is part of *FLAME* (FLAME Group, 1999), a modeling effort focusing on the physical circulation and biogeochemistry of the Atlantic Ocean.
FLAME contains models of resolutions between 4/3° and 1/12° of different regions of the investigation area in order to illuminate different aspects of the ocean's circulation in the Atlantic Ocean.
This family of models is based on the same physical principles and numerical code which is a further development of the *GFDL-MOM 2.1* z-coordinate *primitive equation* (hereafter PE) model (Pacanowski, 1995). This code enables integrations on vector architectures as well as on massive-parallel computers. Recently developed parameterizations can be included to take the effect of unresolved processes into account.
In order to perform several long-term integrations on timescales of 150 years, the majority of the experiments in this study is performed with the coarse resolution OGCM (hereafter *FLAME 4/3*), as it is used in Eden and Willebrand (2001).

2.2 Model characteristics

2.2.1 Topography and vertical boundaries

The horizontal resolution is 4/3° in longitude and $4/3° \cdot cos\phi$ in latitude (ϕ), providing an isotropic grid. This means that independent of latitude, the meridional equals the zonal extent at each grid box. This grid style results in a basin-mean resolution of 1°. The spatial distance between two grid points is 147 km at the equator, decreasing to 50 km at the poleward boundaries.
The vertical dimension is spanned by a vector with 45 levels, the box thickness varies between 10 m near the surface and 250 m in the deep ocean near the bottom.
The model region extends from 70°S to 70°N and from 100°W to 16°E. *FLAME 4/3* has a realistic topography taken from the Etopo5 (1988) dataset. After interpolated to the model's grid, some modifications to the topography have been

made to assure realistic mass transports in certain regions, e.g. the Florida Strait or the Denmark Strait. In the climatological integration, the northern and south-

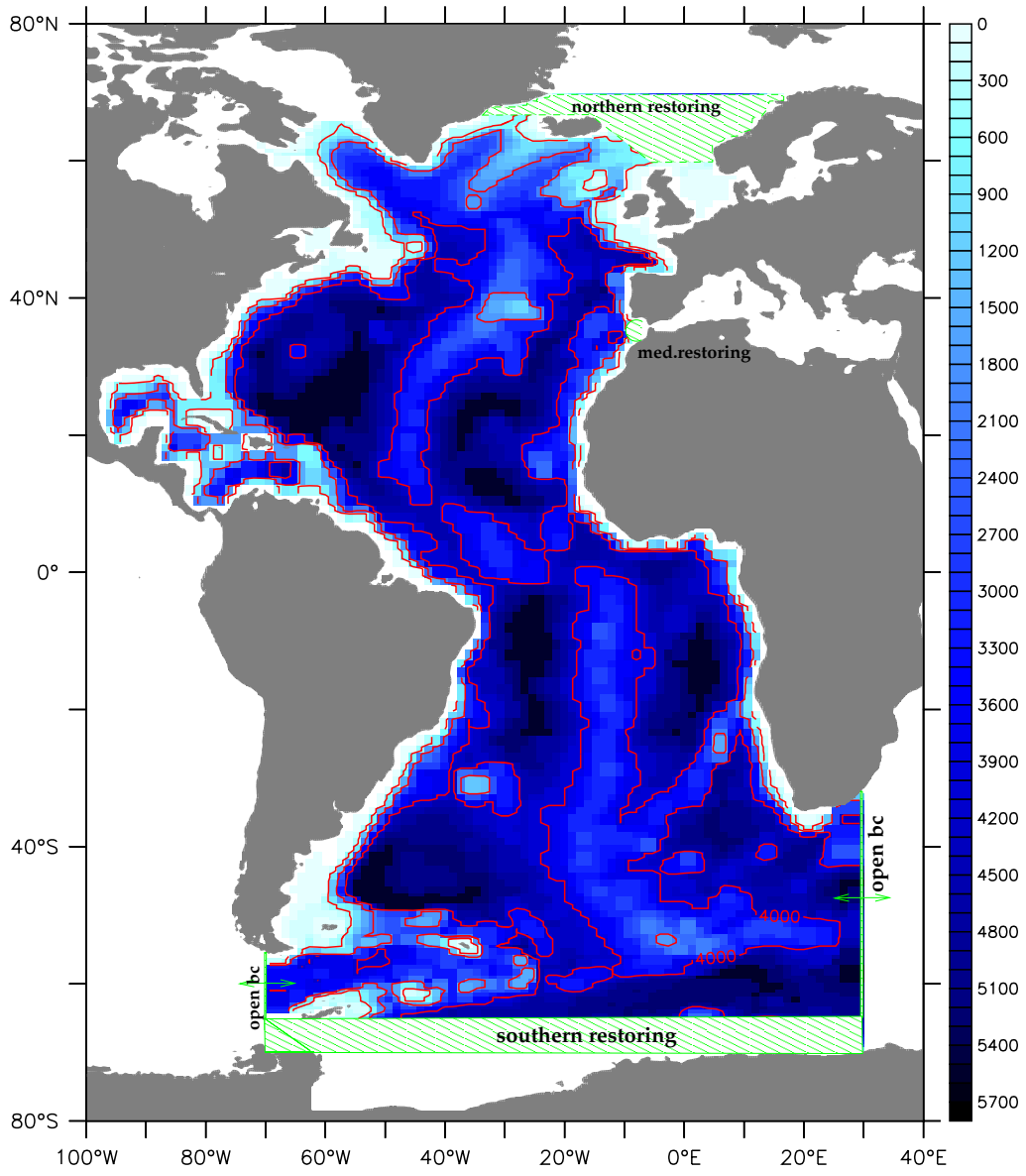

Figure 2.1: *Topography of FLAME 4/3, overlaid are the contour lines of 500, 2000 and 4000 meters, the green shaded regions denote restoring areas.*

ern boundaries are closed with zones of restoring to monthly mean climatological data for salt and temperature. The timescales decrease from 3 days at the outer boundary linearly to 100 days at the inner margin of the restoring region. While the southern sponge area involves the four southernmost grid points, the northern restoring region includes the whole Greenland-Iceland-Scotland-Sea up to 70°N. It reaches down to 67°N at the east coast of Greenland and to 60°N at the west coast of Norway.

As well the Davis Strait within the Labrador Sea at 66°N and the Hudson Strait as well as the North Sea are closed without a restoring zone.
The impact of the Mediterranean is included by a circular restoring zone with a radius of 600 km around the Strait of Gibraltar in the Golf of Cadiz with a constant horizontal relaxation timescale for salinity and temperature. This has a vertical dependence in the shape of a Gauss-Curve centered at 1200 m with 10 days decreasing to 400 days.
The Drake Passage and the model's zonal boundary at 30°E are closed as open boundaries (STEVENS, 1990) with a prescribed barotropic streamfunction and water mass characteristics at inflow points representing the Antarctic Circumpolar Current.
All data for temperature and salinity relaxation are taken from a combination of LEVITUS AND BOYER (1994) and BOYER AND LEVITUS (1997) climatologies except the data for the northern boundary condition, which is supplied by data from the DYNAMO project (DYNAMO GROUP, 1997). This is necessary, since in the strongly smoothed climatological fields, narrow boundary currents like the East Greenland Current as well as overflow water mass properties like the Denmark Strait Overflow are not well represented.

2.2.2 Parameterization

For this coarse resolution model, a harmonic horizontal and vertical viscosity operator A_h and A_v is chosen.

From a water mass and tracer transport point of view, the most natural coordinate system is the one aligned with the local, instantaneous isopycnal surfaces, because mixing across isopycnal surfaces in the ocean is seven orders of magnitude smaller than along isopycnal surfaces. Therefore tracers are approximately mixed along neutral surfaces. COX (1987) implemented isopycnal diffusion in the small angle approximation into *GFDL-MOM 2*. For reasons of numerical stability, there is a need for a small additional horizontal background diffusion.
The isopycnic diffusion coefficient is $2.0 \cdot 10^7 f(z)g(s)$, where $f(z)$ and $g(s)$ are numerical exponential functions for the vertical dependency and the dependency of isopycnic slope s.
The vertical function $f(z)$ has a maximum of 1 at 500 m decreasing to about 0.25 at depths greater than 4000 m. For depths shallower than 200 m the function is forced to zero (figure 2.2, A). A similar vertical shape was used by BÖNING ET AL. (1995) and DÖSCHER AND REDLER (1997).
Tapering the coefficient to the slope function $g(s)$ becomes necessary for numerical reasons in the case of large isopycnic slopes, when the projection on the z-coordinate leads to too high vertical diffusive fluxes. The function $g(s)$ is a *tanh*-profile limiting the along-isopycnic diffusion coefficients for large slopes (figure 2.2, B).

Instead of a constant diffusivity, in the vertical the coefficient is parameterized proportional to the reciprocal of the Brunt-Väisälä frequency N, following GARGETT

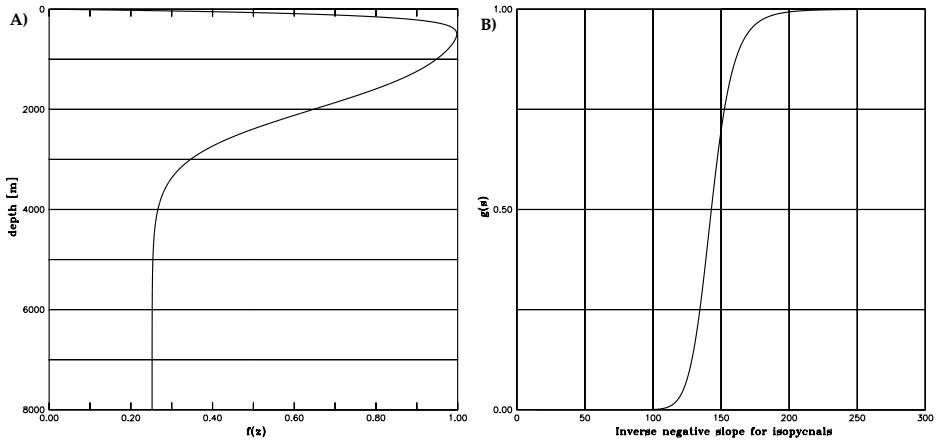

Figure 2.2: *Tapering functions for the isopycnal and the thickness diffusion coefficients: A) The depth dependency $f(z)$ B) The function $g(s)$ for controlling isopycnal fluxes in case of large slopes.*

(1984) and CUMMINS ET AL. (1990):

$$K_v = \frac{K_0}{N}, \quad K_{v,min} <= K_v <= K_{v,max}, \quad N^2 > 0. \tag{2.1}$$

The reason for using a stability depending vertical diffusivity is the attempt to take the effect of turbulent mixing of internal waves into account. This is believed to be more intense in regions of wide spread isopycnals and reduced in regions of strong stratification. K_v is bounded between $K_{v,min}$ and $K_{v,max}$ for numerical reasons and holds for a stable stratification. In the case of vertical instabilities, the scheme of RAHMSTORF (1993) is used, which realizes the vertical exchange by a complete homogenization of vertically adjoining boxes in case of an unstable stratification.

In the presence of baroclinic mesoscale eddies, the conversion of the available potential energy to eddy kinetic energy leads to a nearly adiabatic stirring mechanism that reduces isopycnal slopes (GENT AND MCWILLIAMS, 1990). Since in coarse resolution ocean models these eddies are not resolved, their effect on the tracer transport must be taken into account by a parameterization. Therefore a divergence-free eddy-induced advective velocity (hereafter GM90) is added to the usual tracer velocity (GENT AND MCWILLIAMS, 1995). This thickness diffusion is able to reduce the strong upwelling in midlatitudes in coarse resolution models with the effect of a strengthening of the deep western boundary current (BÖNING ET AL., 1995). For the thickness diffusion coefficients, the same tapering functions $f(z)$ and $g(s)$ as for the isopycnic coefficient were used. At the horizontal boundaries, the continuity demands vanishing thickness diffusivity, here the coefficients are zero.

The friction at the bottom of the basin is parameterized as a function of the

velocity at the deepest grid point:

$$bottomdrag = C_D u \sqrt{u_{tide}^2 + u^2 + v^2} \tag{2.2}$$

Included is the term u_{tide}^2 to take tidal friction into account.

An important deficit of OGCMs with geopotential coordinates is the representation of flows over sills and rough topography. In contrast to the situation in the real ocean, where dense water follows the slope of the obstacles, strong vertical diffusivities simulate a downflow of these waters. The loss of water mass properties on the way down the sill is the consequence. Therefore the meridional circulation has a much shallower structure, because dense water flowing over the sills of Denmark Strait and Island-Scotland Overflow are mixed before they reach a realistic depth of the North Atlantic Deep Water (NADW). To overcome this problem, the Bottom Boundary Layer (BBL) of Beckmann and Döscher (1997) is included to represent a more realistic structure of overflow situations. This parameterization

Viscosity		
A_h	horizontal viscosity	$1.0 \cdot 10^8 cos(\phi) cm^2/s$
A_v	vertical viscosity	$10 cm^2/s$
Diffusivity		
D_{iso}	isopycnal diffusivity	$2.0 \cdot 10^7 f(z)g(s) cm^2/s$
D_{back}	horizontal background diffusivity	$1.0 \cdot 10^6 cm^2/s$
D_{thick}	thickness diffusivity	$2.0 \cdot 10^7 f(z)g(s) cm^2/s$
$K_v = K_0/N$	vertical diffusivity	
K_0		$1 \cdot 10^{-3} cm^2/s$
$K_{v,min}$	min.vertical diffusivity	$0.1 cm^2/s$
$K_{v,max}$	max.vertical diffusivity	$4.0 cm^2/s$
Bottom drag		
C_D	bottom drag coefficient	$1.25 \cdot 10^{-4}$
u_{tide}	tidal friction correction velocity	$5.0 cm/s$
Kraus-Turner mixed layer model		
H_s	scale depth of TKE profil	$50m$
ϵ	TKE mixing effectivty	0.8
Bottom boundary layer		
D_σ	along-isobaths diffusivity	$1 \cdot 10^8 cm^2/s$
$D_{\sigma,min}$	along-isobaths backgrd. diffusivity	$1 \cdot 10^5 cm^2/s$
σ	exchange rate of BBL	1.0

Table 2.1: *Coefficients used in the parameterization of FLAME 4/3*

allows along-isobaths advective and diffusive fluxes along the topographical slope. In cases of a sloping topography and decreasing density with depth, the BBL scheme for diffusion and advection becomes important: In this situation the along-isobaths diffusivity D_σ has a value of $10^8 cm^2/s$, everywhere else it is three orders

smaller. For numerical reasons, this unphysical up-slope diffusion is not zero, but a small diffusivity is retained (DÖSCHER AND BECKMANN, 2000).
The advective velocities of upper box are directed into the down-slope following bottom box. The parameter σ controls the exchange rate of two boxes. In the case of $\sigma = 0$ the exchange is suppressed, for $\sigma = 1$ the advective flow is totally redirected down the slope of the topography. In this study, we used the same parameter as EDEN AND WILLEBRAND (2001) of $\sigma = 1$.

To take the impact of surface fluxes for the structure of the mixed layer depth into account, a simple mixed layer parameterization of KRAUS AND TURNER (1967) is used, which calculates the mixed layer depth by using a vertical integral of the simplified TKE equation. It determines the depth of the mixed layer by comparing the input of turbulent kinetic energy (TKE) from the surface wind field to the potential energy which is necessary to mix layers. Other effects with impacts on the mixed layer depth like buoyancy forcing or the shear of the velocity field are neglected. To simulate the decay of TKE with depth due to frictional effects, an exponential profile with a scale depth of $H_s = 50m$ is assumed. Only a portion ($\epsilon = 0.8$) of the available turbulent energy is used for mixing.
All these parameter values used in *FLAME4/3* are listed in table 2.1.

2.2.3 Surface forcing

The surface forcing in the climatological state of the ocean model contains monthly mean fields which are linearly interpolated onto the model's time.
They originate from a 6-hourly analysis at the ECMWF of the years 1986-88 (BARNIER ET AL., 1995). For the *FLAME* models, this dataset was averaged to receive a climatological year of surface forcing. It was already used in DYNAMO (WILLEBRAND ET AL., 2001), opening the possibility to compare results from older studies. This advantage was weighted more important than the fact, that the dataset falls in a time period with a high North Atlantic Oscillation (NAO), probably having an impact on *FLAME*'s climatological state of the ocean.

In the standard configuration, the surface boundary condition for heat is provided by a combination of a heat flux Q_0 and a flux correction restoring towards climatological SSTs (HANEY, 1971):

$$Q = Q_0 + Q_2 \left(SST_{model} - SST_{clim}\right) \tag{2.3}$$

$$with\ Q_2 = \left.\frac{\partial Q}{\partial SST}\right|_{SST_{clim}}. \tag{2.4}$$

Hereby is Q_2 the temporal and spatial dependent timescale of the relaxation term, which is directly derived from a linearized form of the bulk formula for the surface heat flux (BARNIER ET AL., 1995).
The use of restoring boundary condition alone could lead to the unrealistic situation of suppressed heat exchange, if the model has the "correct" SST in terms of climatology. This combined procedure assures that in this case there is still a heat flux Q_0 between atmosphere and ocean.

However, equation 2.3 can be rewritten as a pure relaxation to the *apparent surface temperature* T^*:

$$Q = Q_2 \left(SST_{model} - T^* \right) \tag{2.5}$$

$$with\ T^* = SST_{clim} - \frac{Q_0}{Q_2}. \tag{2.6}$$

In this formulation the properties for the surface heat flux can easily derived:
An atmosphere with an infinite heat capacity is assumed, what means that changes in the heat flux can only be caused by the reaction of changes in the ocean's temperature on a constant atmosphere. This atmosphere absorbs any additional heat coming out of the ocean (the term $Q_2 SST_{model}$ in equation 2.5). In a physical sense the additional heat is directly spread by divergences of the wind field without heating the air somewhere.
For small scales this assumption may hold, for larger heat anomalies the ability of the atmosphere to change its heat transport as a consequence of SST changes can be an important feedback mechanism of the coupled system (Marotzke, 1996). However, this kind of surface boundary condition for heat is often used in ocean models. Its range of application is mainly to simulate a mean state of the ocean under climatological boundary conditions in order to examine small disturbances and internal variability within the ocean. The ability to force models for problems of climate variability and integrating the ocean model in global warming scenarios on timescales of 150 years is somehow a marginal case. To investigate the coupled system with its variety of ocean-atmosphere feedback mechanisms this procedure cannot be justified. For that kind of application, a coupled model, at least with a simple but responding atmosphere has to be used. Rahmstorf and Willebrand (1995) showed that the role of such an atmosphere could for instance have a damping and in some sense a stabilizing effect on the ocean's circulation.

In the standard configuration, the freshwater flux into the ocean is realized as a restoring to climatological surface salinities after Levitus and Boyer (1994) and Boyer and Levitus (1997) at a constant timescale of 15 days in the surface grid boxes. The reason not to use a boundary condition similar to the heat flux formulation are large uncertainties in the climatological precipitation and evaporation datasets. Due to the small spatial scales of rain and the absence of fields of reliable data covering the whole domain, the salinity restoring is used to receive a preferably realistic climatological state of the ocean. In order to perform integrations on decadal to interdecadal timescales, this boundary condition cannot be justified, since any feedback mechanism concerning the ocean's salinity is suppressed. So using this boundary condition, a salt anomaly advecting through the ocean would be damped by the unphysical mechanism of anomalously high precipitation.
Therefore in this study we use a freshwater flux diagnosed from the restoring boundary condition for salt in a quasi-equilibrium state. Although these fluxes are completely artificial, they provide an oceanic state excluding the unphysical mechanism of precipitation depending on surface salinity. Thus, the model is able to conserve salinity signals advected at the surface.

There is a lot of literature about the use of mixed boundary conditions in models for the investigation of the response of the THC (e.g. MAROTZKE AND WILLEBRAND, 1990). The existence of different stable states of the ocean and the switch from one state to the other due to relatively small freshwater perturbations is often described using highly idealized models. Nevertheless, the use of mixed boundary conditions for driving ocean models is still a compromise. In PE models, the freshwater flux is realized as a equivalent salt flux into an ocean with a rigid lid surface, where the vertical velocity vanishes. This procedure can result in somehow different results concerning the baroclinic gyres. HUANG (1993) found in a circulation model driven with real freshwater fluxes, that relatively small amounts of freshwater flux can be able to drive very strong meridional and zonal cells, which were 100 times stronger than the driving freshwater flux. Moreover the meridional salt flux in the model was better represented with realistic freshwater fluxes at the surface. Since a sensitivity study concerning technical aspects and sensitivities of the implementation of surface forcing is beyond this work, we nevertheless use the mixed boundary condition formulation.
For this study remains important, not to find different climatological stable states but to give the uncoupled ocean as much ability as possible to respond in a physical sense on changes in the atmospheric forcing. Restoring boundary conditions always have the characteristic, that the forcing towards climatological values increases all the more, the system diverges from it. Therefore in this work, this unphysical bounding is as much reduced as possible in order to simulate the behaviour of the ocean as a preferable free component of the climate system.
The spinup and the switch from full surface restoring to freshwater fluxes in combination with temperature restoring is described in section 2.4.

The surface forcing contains also ECMWF data for zonal and meridional wind stress components as well as deduced wind stress velocities necessary for the mixed layer model.
All data sets except restoring timescales are Killworth-filtered (KILLWORTH, 1996). This prevents a systematic error in the forcing with linear interpolated data of monthly averaged rawdata.

2.3 Implementation of anthropogenic forcing

The issue of this study is to force the *FLAME 4/3* ocean model with diagnosed fluxes from anthropogenic global warming scenario integrations of ocean-atmosphere coupled models. To do this, we implemented the fluxes of heat and freshwater as well as wind stress data as forcing anomalies on our model's quasi-equilibrium state. The reason for this procedure is the fact that the coupled systems might have a totally different mean state of the ocean.
Using the full set of forcing would not only force the ocean model in an anthropogenic sense but also into the direction of the (probably less realistic) mean state of the coupled system's ocean. Additionally, due to the different source of the fluxes, implementing the heat and freshwater fluxes of anthropogenic scenarios in

the Atlantic ocean would yield to an enormous drift during the models integration, since the heat and salt budgets are only closed as a global integral. Only if the lateral transport at the vertical boundaries of the regional model would accord with the transport of the global ocean in that region (what cannot be assured due to the formulation of the vertical boundary conditions in *FLAME 4/3*), this could be suppressed.
Implementing the anomalous greenhouse gas signals (index GH) in the ocean model, at the ocean surface the boundary condition for heat (Q_{GH}), freshwater (F_{GH}) and wind (τ_{GH}) become:

$$Q_{GH} = Q + Q_2 \Delta T_{GH}^{skin} + \Delta Q_{GH} \quad (2.7)$$

$$F_{GH} = F + \Delta F_2 \quad (2.8)$$

$$\tau_{GH} = \tau + \Delta \tau_{GH}. \quad (2.9)$$

Hereby is Q the heat flux forcing (equation 2.5). The index Δ denotes anthropogenic flux anomalies relative to the mean state of the climate model between 1860 and 1950. At that time the anthropogenic forcing is still small (figure 2.3), so that the ocean model's integrations start with little anthropogenic forcing in the year 1950.
In contrast to the usual *FLAME* forcing with Q_2 being the temporal and spatial dependent timescale, in the experiments with anthropogenic forcing data we took a constant value of $40 W/m^2/k$. The reason for this procedure is, that the original values of Q_2 are derived from the ECMWF data set. Since the heat flux correction from the climate models need not necessarily fit these values, we chose a constant value for Q_2. This constant value is a widely proven procedure in ocean models (e.g. TREGUIER ET AL., 1999). Using a constant value for Q_2 does not significantly change the quasi-equilibrium state of *FLAME 4/3* relative to the temporal and spatial dependent Q_2.
This procedure assures that, if the climate model maintained its state, all terms

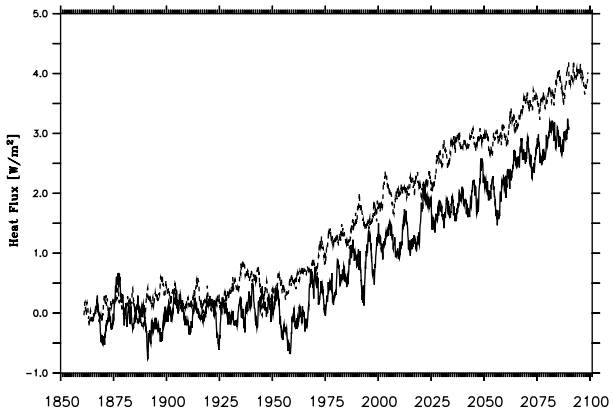

Figure 2.3: *2-year running mean of global mean heat flux anomalies in coupled integrations of ECHAM4/OPYC3 (line) and GFDL-gps03 (dashed).*

on the right side of equation 2.7-2.9 labeled by GH would be zero and the anthropogenic would become the climatological forcing.

The quality of the chosen boundary conditions strongly depend on the difference between the horizontal circulation in the coupled and in the uncoupled case. Because the diagnosed fluxes originate from interactions between certain regimes in the upper ocean of the climate model's ocean and the atmosphere above, the evolvement of the diagnosed fluxes onto an ocean with a different horizontal circulation can cause fundamental problems, even if only anomalies are applied. For instance, if a current has a fundamental different position in the coupled integration, changes in the diagnosed fluxes may have an impact on a completely wrong regime. Only if the horizontal circulation of the uncoupled model perfectly matches the pattern of the coupled model's ocean, the surface forcing can show a "physical" reaction on the model's SST.

Having this constraint in mind, the implementation of freshwater flux anomalies and wind stress anomalies is quite obvious: There is simply no feedback mechanism from the dynamic ocean into the prescribed atmosphere, so there remains a one-way atmospheric forcing.
The resulting boundary condition for heat is less intuitive. Therefore it is worth to illuminate some of its aspects. If we only took the anomalous heat flux ΔQ_{GH} as the only modification of the climatological heat flux Q, in a global warming scenario, in which we have to expect fundamental changes in the model's SST, the anthropogenic signal would be damped by the fixed apparent atmospheric temperature T^*, the more the temperature rises. To avoid this we also include an anthropogenic signal on the apparent atmospheric temperature T^* as well to overcome this damping problem. This is chosen to be the anomaly of the skin temperature ΔT_{GH}^{skin} in the coupled integration. With or without this modification, the shape of the boundary condition for heat as a combination of restoring and heat flux correction has another property:
In contrast to freshwater forcing and wind, the anthropogenic heat flux Q_{GH} in the ocean model can differ from the anthropogenic forcing in the climate model due to the restoring term in equation 2.7.
This deviation must be expected to be strongest in regions of large differences of the horizontal circulation of the ocean in both models, where wrong positioned heating and cooling due to this boundary condition are expected. To clarify this point, the integration of *FLAME 4/3* in the *GFDL gps03* global warming scenario (details in chapter 5) gives a suitable example.
First of all, in an integral point of view, this artificial mechanism seems small in the whole domain of the North Atlantic ocean (figure 2.4,A). Although there is some discrepancy on annual timescales between the anomalous heat flux in the coupled model and the resulting flux felt by *FLAME4/3*, the main trend is well represented.
If we look at the meridional distribution of the anthropogenic signal, some differences in higher latitudes can be seen, which increase in the later part of the 21^{st} century (figure 2.4,B). In lower latitudes the two signal match almost perfect.

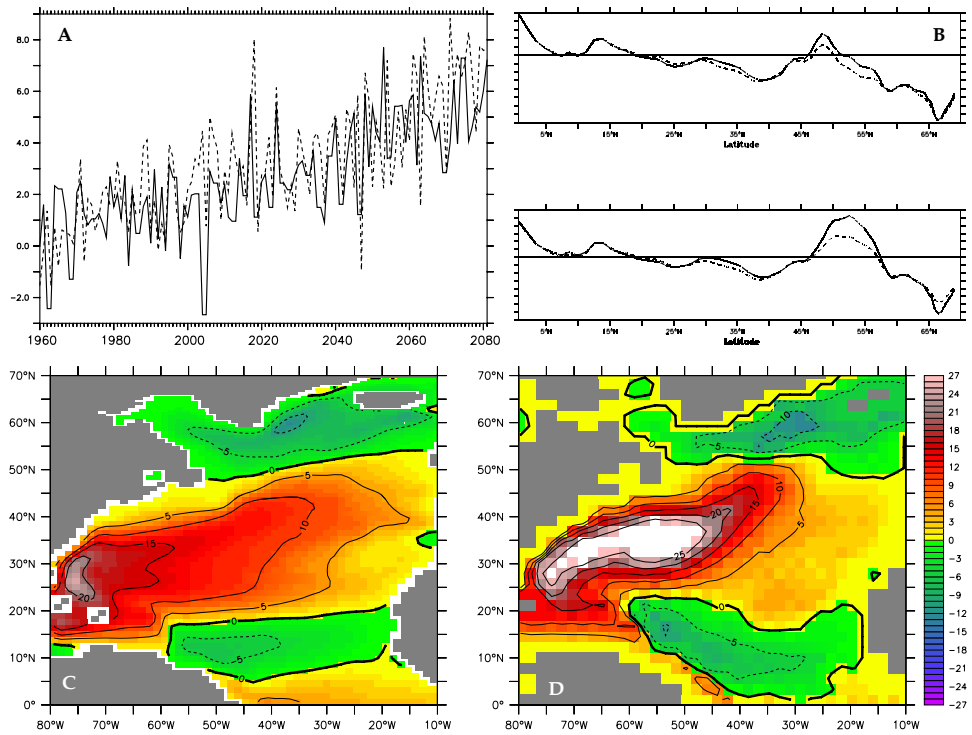

Figure 2.4:
A: *Changes in surface heat fluxes in FLAME 4/3 (dashed) and GFDL gps03 (line) in* W/m^2 *(0° N-70° N/80° W-30° E, averaged);*
B: *Zonally averaged surface heat flux in FLAME 4/3 (dashed) and in the climate model (line) averaged between 1950-1960 (top) and 2080-2090 (bottom);*
*horizontal barotropic streamfunction of FLAME 4/3 (***C***) and of GFDL gps03 (***D***) (averaged between 1950-2090; unit is Sv).*

The deviation in higher latitudes are the consequence of a different shape of the subpolar gyre in both models. This can be studied by looking at the barotropic streamfunction in figure 2.4, C and D. The devolution is the following: During the global warming scenario, the northward heat transport of the climate model decreases, causing a colder Gulf Stream transport. As an atmospheric response, the skin temperature becomes colder. Moreover the atmospheric heat transport and the surface heat flux into the ocean increase. Since the shape of the subpolar gyre and also the position of the Gulf Stream are different in *FLAME4/3*, the uncoupled ocean model responds in a different way. The anomalous high heat flux into the ocean is felt in a region, where the Gulf Stream has already separated from the coast (figure 2.4, C). So an advective signal cannot be found in this region. However, the (cold) restoring signal from the climate model is anyhow included (terms ΔQ_{GH} and $Q_2 \Delta T_{GH}^{skin}$ in equation 2.7).

This combination yields to a less intense heat flux change during the integration in that region, without the ocean model's Gulf Stream being involved (figure

2.4,C). Nevertheless this reaction is appreciated, because the source of this feedback mechanism is the northward heat transport and not a locally caused effect of the atmosphere in the region southeast of the Labrador Sea. In other regions, e.g. downstream the North Atlantic Current, the devolution is vice versa. Here *FLAME4/3*'s oceanic heat transport weakens, the lower SSTs cause the surface heat flux evolution (right side of equation 2.5).
Therefore the heat flux boundary condition can be mainly interpreted to be regime dependent: The atmospheric response is an anthropogenic dominated signal in domains matching the climate model's ocean (terms ΔQ_{GH} and $Q_2 \Delta T_{GH}^{skin}$ with the same algebraic sign) and a physical artificial reaction in deviating regimes (both terms balancing each other in some sense).

However, choosing this kind of boundary condition is still a compromise. This thermal boundary condition contains two parts of restoring to some temperature, a climatological part $Q_2 T^*$ and an anthropogenic part $Q_2 \Delta T_{GH}^{skin}$. In a physical sense, they can be distinguished as follows: The climatological part is the response of an (even changed) oceanic SST to an unchanged atmosphere whereas the anthropogenic part is the response of the ocean to an anthropogenic changing atmosphere. The reason why these contribution is carefully distinguished here are some sensitivity studies in chapter 5, where the anthropogenic surface forcing is switched off in some regions. So, in those experiments there is still GH-induced variability in local heat fluxes due to lateral changes in the SST as a reaction on the fixed atmospheric state. Nevertheless this mechanism is still embraced and also reasonable in a physical sense. Its effect is illuminated in section 5.7, where we calculated heat budgets in order to estimate the relative importance of this restoring feedback relative to the full anthropogenic forcing.

At the vertical boundaries, the restoring terms for the closed boundaries respective the inflow conditions at the open boundaries are as well modified by anthropogenic signals. The restoring term in the tracer equation for salt and temperature at the vertical boundaries is rewritten as:

$$\begin{aligned} &(R_{GH}^S, R_{GH}^T) = \\ &\gamma \left[(S_{model}, T_{model}) - (S_{clim}, T_{clim}) - \Delta(S_{GH}, T_{GH}) \right], \end{aligned} \tag{2.10}$$

where γ is the restoring timescale while the index $clim$ denotes climatological values (section 2.2.1). The last term on the right side is the anomalous anthropogenic signal in the climate model's oceanic tracer distribution. For each month the temperature and salinity anomalies are interpolated on the ocean model's grid in sponge areas. Again, as for the surface forcing, if the climate model remains unchanged, the GH-labeled terms would be zero and *FLAME4/3* was forced by its quasi-equilibrium vertical boundary conditions. Having the constraints in mind, applying the anthropogenic forcing into the ocean model in the described way could help to prove the reliability of results from the coupled model's ocean.

2.4 Spinup

Starting from the LEVITUS AND BOYER (1994) dataset, we integrated the coarse resolution *FLAME4/3* model for 50 years to receive a quasi-equilibrium climatological state relative to the applied forcing under pure restoring boundary conditions. In the last 10 years of this spinup we diagnosed the surface freshwater fluxes resulting from the restoring boundary condition with an interval of two days. After averaging these fluxes into one climatological year, we ran the model with these fluxes for another 50 years in order to control the salinity drift in the model. After 30 years of integration with mixed boundary conditions, the salinity drift is less than $1 \cdot 10^{-5} psu/year$, what is much less than the expected changes due to anthropogenic forcing.
The resulting state of the ocean under mixed boundary conditions is validated and discussed in section 2.6. It is the platform to start the idealized experiments (chapter 3) as well as greenhouse gas forcing experiments (chapter 4 and 5) from.

2.5 Higher resolution models

In addition to a couple of experiments with *FLAME4/3*, we performed some sensitivity studies with a higher resolved version. The implementation of anthropogenic forcing on a coarse grid into a more realistic ocean model has a few limitations (see section 2.3). The most important one is the "regime dependence" of the local forcing. Since the climate model's atmospheric fluxes are the result of interactions with an ocean in a different state, running a model with a different ocean state might result in unrealistic fluxes. In figure 2.5 this problem is demonstrated at the example of the subpolar front. Both in the climate model's ocean as well as in *FLAME4/3*, the position of this front is quite similar, since in both models, the Gulf Stream is not as concentrated as in *FLAME1/3* and the separation of the current is still not correct. Therefore the North West Corner is nearly non-existent in both coarse resolution models. Looking at a section at 52°W (lower right panel), the higher resolution model shows a narrow SST front, while the two other models are much more smoothed. Expected changes in the air-sea interactions within the Gulf Stream could therefore, implemented in the higher resolution model, lead to unrealistic fluxes in adjoining regions like the Labrador Sea.
Additionally, because of computational costs and technical problems for integrating anthropogenic warming scenarios under mixed boundary conditions with eddy permitting models for several hundreds of years, we restricted the adoption of *FLAME1/3* to some sensitivity studies with idealized forcing applications relative to the coarse resolution model in chapter 3.

2.5.1 Model's style and forcing

The experiments used for the validation of the response of the coarse resolution model are all performed with the 1/3° version of the *FLAME* models (hereafter *FLAME1/3*), which bases on the same physical code as *FLAME4/3*. The

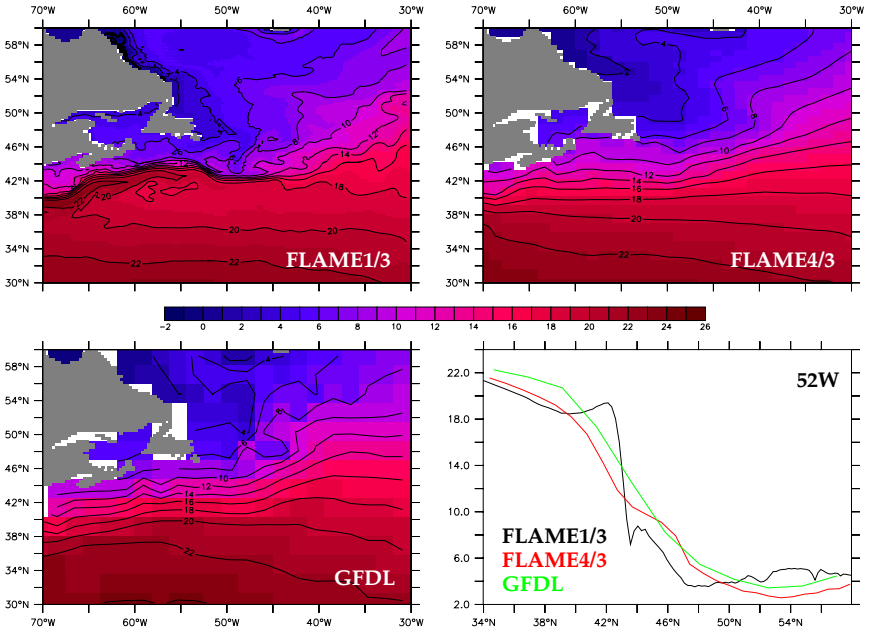

Figure 2.5: *Annual mean SST of FLAME1/3, FLAME4/3 and GFDL in the vicinity of the subpolar front.*

model area is slightly different. While the North Atlantic has a very similar style, the model is closed with an open boundary condition at 20°S. The prescribed barotropic streamfunction is taken from a simple Sverdrup relation, the tracer values at inflow points are again a combination of climatological values taken from Levitus and Boyer (1994) and Boyer and Levitus (1997). As a contrast to the coarse resolution model, the northern restoring zone only reaches from 67°N to 70°N. One reason for this difference is the ability of *FLAME1/3* to have deep convection areas north of Iceland, even though the model is closed within the Nordic Seas.

Like in the coarse resolution model, the bottom boundary layer is employed, the coefficient in these configuration is $A_\sigma = 5.0 \cdot 10^7 cm^2$. Also included is the isopycnal diffusion with an coefficient of $D_{iso} = 4.0 \cdot 10^6 cm^2/s$ and the same tapering functions used in *FLAME4/3* (see table 2.1). The horizontal background diffusion is $D_{back} = 4.0 \cdot 10^5 cm^2/s$. As a difference to *FLAME4/3* configuration, the GM90 parameterization (Gent and McWilliams, 1990) is not used in these experiments. In the case of the higher resolution model, the parameterization of eddy-induced velocity should be unnecessary, since the eddies are resolved at least in lower latitudes. The horizontal viscosity is $A_h = 1.0 \cdot 10^7 cm^2/s$, the vertical viscosity is $A_v = 10.0 cm^2/s$ like in *FLAME4/3*. Finally, the quadratic bottom friction is $1.2 \cdot 10^3$ for the higher resolved version.

The surface forcing consists of the same climatological fields already described in section 2.2.3. In contrast to *FLAME4/3*, the sensitivity studies with the high

resolution model are integrated under restoring conditions for salt and temperature instead of mixed boundary conditions. The reason to use pure restoring at the surface is the problem with unphysical drifts in regional models. Due to high computational costs, long integrations to suppress this drift are not possible. This must be taken into account comparing the experiments in chapter 3.

In the following section, we validate the climatological state of *FLAME4/3* and pass on a description of *FLAME1/3*, since the anthropogenic forcing experiments are performed with the coarse version. However, the mean state and variability of *FLAME1/3* is widely tested in a number of studies based on FLAME Group (1999).

2.6 Validation

In this section, the mean general circulation as well as some aspects of the hydrology of the climatological state of the ocean model are described and validated. For comparison, some properties of the ocean component of both climate models are shown, from which the diagnosed fluxes in chapter 4 and 5 originate and which are used to force *FLAME4/3*. These are the *ECHAM4/OPYC3* climate model as well as the *GFDL* climate model. At the beginning of chapter 4 and 5, technical aspects as well as the specific anthropogenic forcing scenario performed with those models are summarized.

FLAME4/3 has shown reasonable results concerning the interannual to decadal variability in experiments with realistic forcing time series (Eden and Willebrand, 2001). Because the mean circulation under mixed boundary conditions and climatological forcing does hardly deviate form the model under restoring boundary conditions, here we confine on some aspects, which are important for the response experiments with anthropogenic forcing in chapters 4 and 5. These concern mainly the mean state since the variability of the diagnosed air-sea fluxes from coupled GCMs is much more idealized than the realistic forcing used in Eden and Willebrand, where the variability on different scales is capaciously described.

In this thesis the main question is less the variability of the ocean. Instead, the topic is whether a widely proven ocean model shows a fundamental different response on global warming scenarios. In other word, whether a more realistic mean circulation of the ocean results in a general different behaviour of relevant parameters. Hence, the evolution of a model with a quite realistic oceanic state in experiments with anthropogenic forcing diagnosed from in some sense idealized ocean-atmosphere systems is investigated.

In the following the state of the climatological year is discussed, which is the last year of the spinup. By forcing with climatological data for another about 150 years to compare to anthropogenic changes, it does not show significant changes. This must be ascribed to the very low internal variability of the coarse resolution model, unable to resolve eddies and their spreading in the ocean.

2.6.1 The meridional circulation

The meridional overturning cell is a useful parameter in terms of the thermohaline circulation. Since it is the main diagnostic parameter used in this study, in section 2.7.1 we expand on certain aspects of the role of the overturning function relative to the THC. Here we describe the main properties of the meridional overturning circulation in *FLAME4/3*, which is the following integral (e.g. SCHMITZ AND MCCARTNEY, 1993):

$$\Psi(\phi, z) = \int_{\lambda_{min}}^{\lambda_{max}} a \ cos\phi \ d\lambda \int_{z}^{0} v(\lambda, \phi, z') \ dz'. \tag{2.11}$$

In a regional model of the Atlantic Ocean, λ_{min} and λ_{max} are the limits of the zonal extent of the basin and v is the meridional velocity.

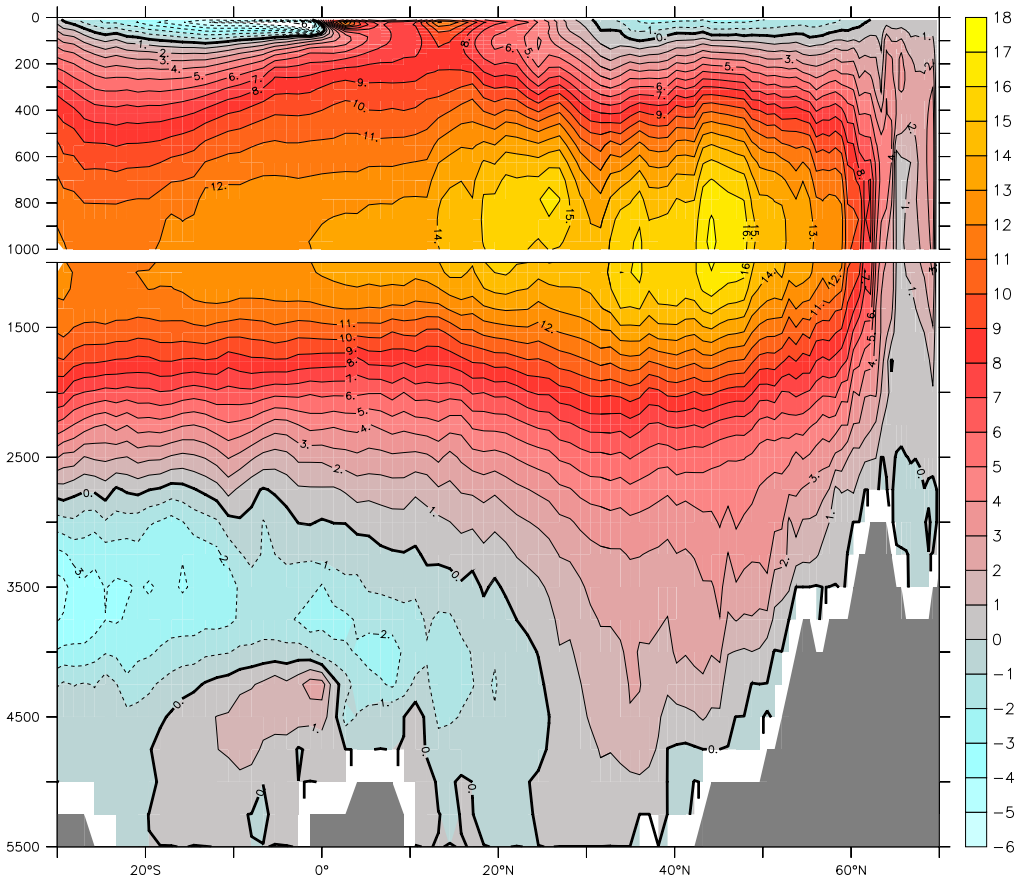

Figure 2.6: *Overturning circulation in the last year of the spinup in FLAME 4/3, the upper 1000 m are stretched, unit is Sv.*

Figure 2.6 shows the annual mean overturning function in the last year of the spinup. The dominant cell is formed by the North Brazil Current, the Antilles Current, the Florida Current, the Gulf Stream and the North Atlantic Current as the upper branch of the cell. The Deep Western Boundary Current with its different

components forms the compensating lower branch. The maximum transport of this cell is about 16.5 Sv at 40°N. This value is close to results in other z-level North Atlantic Models (e.g. WILLEBRAND ET AL., 2001). Observational values are quite similar: ROEMMICH AND WUNSCH (1985) estimated the overturning strength to be 17 Sv, other estimates include 16 Sv by MACDONALD AND WUNSCH (1996) and GANACHAUD AND WUNSCH (2000) and an average of 18.8 Sv from three sets of hydrographic data by LAVIN ET AL. (1998).
Starting in the north, at 66°N the strength is at about 3 Sv. Since at this latitude, the main southward flow goes through the Denmark Strait (figure 2.8), this value can mainly be associated with the Denmark Strait Overflow in different density classes. South of the sill, the transport increases to about 8 Sv until it reaches 60°N. This accretion can be ascribed to entrainment as well as to sinking within the subpolar gyre. At Cape Farwell, the southward transport has grown to 12 Sv. The maximum is reached in a depth of 1000 m in 40°N.
A second local maximum can be found at $25°N$. This arises from strong upwelling within the subtropical gyre and is a well-known problem of coarse resolution models. Although the thickness diffusion is able to reduce this problem (BÖNING ET AL., 1995), it is still present in the model.
Below this dominant cell, a northward flow of Antarctic Bottom Water (AABW) is feeding the lower branch of NADW. It has a maximum strength of about 2 Sv in the North Atlantic.
Above these deep cells, three wind-driven cells with a maximum depth of a few hundred meters can be localized. By diagnosing the overturning on vertical levels by equation 2.11, the source of these cells is that wind-driven waters follow isopycnal layers connected with a vertical motion in the case of isopycnal slopes. Showing the overturning function on isopycnal surfaces therefore leads to a higher overturning cell in the North Atlantic of about 20 Sv (see section 2.7.1). The wind-driven cell vanishes and the transport on isopycnals becomes visible (WILLEBRAND ET AL., 2001).

Although the overturning circulation or at least the overturning index is often used as an indicator for the ocean's role in climate, its magnitude and structure is difficult to compare with observations, since these are very rare. However, the transport through the Denmark Strait of about 3 Sv below the model's upper boundary of the Denmark Strait Overflow of $\sigma_\Theta = 27.75\ kg/m^3$ (figure 2.7) is quite close to observations of DICKSON ET AL. (1990), who found 2.9 Sv below his upper boundary of $\sigma_\Theta = 27.8\ kg/m^3$.

The transport through the Iceland-Scotland sills is at about 1.5 Sv below $\sigma_\Theta = 27.75\ kg/m^3$ in this quasi-equilibrium state of the model (not shown) what within the error bars of DICKSON's 1.5 to 1.9 Sv below $\sigma_\Theta = 27.8\ kg/m^3$ there.
Although these values are quite reasonable for the coarse resolution *FLAME4/3*, they strongly depend on the representation of the topography, which is idealized in some points. Using different cross-sections of the narrow flows, the results can be totally different concerning not even the local behaviour but also the whole overturning function. We performed a sensitivity study on this in section 5.5.8.

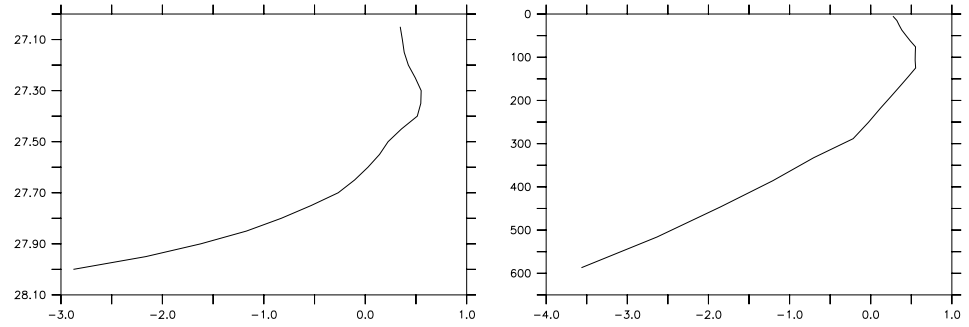

Figure 2.7: *Annual mean cumulative transport through the Denmark Strait at 66° N and 28° W on isopycnals (left) and on the vertical axis (right) in Sv.*

Concerning the main overturning cell in the North Atlantic, an interesting point is the zonal contribution to this structure. Figure 2.8 shows the relative contribution to the upper and lower branch, starting at the eastern boundary. In both branches the western boundary's contribution is mostly important, although the southward flow has a not negligible component in the ocean's interior between 30°N and 48°N. This is also present in higher resolution versions of *FLAME* and is not confuted by observations so far. In these models, although the ocean's interior contributes to the southward flow, the variability is primarily given by the boundary current (*FLAME Group, pers.com.*). Within the subpolar gyre, as well the deep flow shows some northward components whose source is the very barotropic structure of the North Atlantic Current in the model.
The upper branch reflects the gyre circulation with a very concentrated Gulf Stream at the western boundary.
In comparison to the structure of the overturning cell in *FLAME4/3*, the resulting overturning function in the climate models we investigate in chapter 4 and 5 are much more idealized. E.g. in terms of transport between the Nordic Seas' basin and the subpolar basin, the diagnosed transports are quite unrealistic relative to observations. Futhermore, the depth of the southward branch is shallower as the consequence of wrong water mass properties. Additionally, the mean strength is much higher (see the overturning shape of the climate models in figure 5.1). However, whether these are important features of the general response of the overturning function is not answered at this point.

The main role of the ocean in climate is its ability to transport amounts of heat, which are at the same order as the atmospheric transports (Trenberth and Caron, 2001).
Figure 2.9 shows the annual mean meridional heat transport of *FLAME4/3* (black curve). In comparison to results from Macdonald and Wunsch (1996) the values are systematically lower. While their observation was a maximum of 1.4 PW at 10°N, out model's maximum is 0.78 PW at 20°N. At the equator, the northward heat transport is 0.67 PW, while at 40°N, its still 0.53 PW. Across the sills into the Nordic Seas there remains 0.25 PW. All these values are slightly higher in

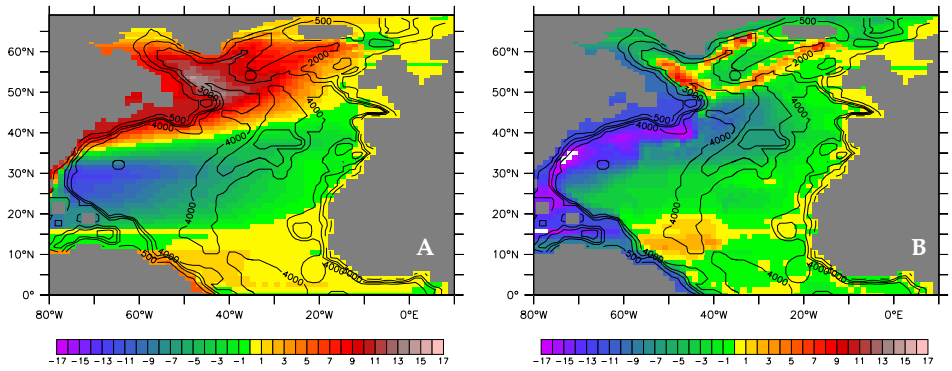

Figure 2.8: *Cumulative contribution to the main overturning cell of the upper branch (A) and the lower branch (B) in the North Atlantic ocean, starting at the eastern boundary; unit is Sv.*

FLAME4/3 with pure restoring boundary conditions, what can be ascribed to the stronger overturning circulation (Eden, 1999). Trenberth and Caron (2001) used the NCEP/NCAR reanalysis data (Kalnay et al., 1996) as well as the ECMWF reanalysis data (Gibson et al., 1997) to estimate the northward heat transport in the Atlantic ocean by calculating heat budgets. While like the observations of Macdonald and Wunsch the NCEP/NCAR data are much higher within the subtropical gyre up to $40°N$, in the subpolar gyre the values are very similar (*brown curve*). Much more similar over the domain of the Atlantic Ocean is the curve derived from ECMWF data (*magenta curve*). Their heat transports peaks at 20°N with about 0.8 PW and decreases at 40°N to 0.6 PW and at $66°N$ to 0.2 PW. In *FLAME4/3* there is a slight local maximum within the subpolar gyre which cannot be found in both reanalysis data sets. This can be ascribed to strong surface warming of the cold southward flows leading to a net gain of heat within the subpolar gyre.

A useful diagnostic is the decomposition of the heat transport into a gyre respective an overturning component. In a mathematical sense, the first one is the integral of the correlation between the deviations of v and T from the zonal mean, while the second is the integral of the product of the zonal means.
These two terms are also shown in figure 2.9. While the overturning (*red curve*) component is reactively close to the whole meridional heat transport, the gyre component (*green curve*) is much lower and not even northward in the whole North Atlantic.

Comparing the climate models resulting oceanic heat transport gives a slightly different result. The two climate models, whose diagnosed fluxes are used in chapter 4 and 5, suffer from too low oceanic heat transport. The *ECHAM4/OPYC3* model has a maximum heat transport of 0.59 PW, the *GFDL* model is at 0.49 PW (e.g. Jia, 2002). Although the overturning function in both models is about 10 Sv to high, unrealistic water mass properties lead to this defect. Since the temperature of the deep southward branch is too warm, the heat transport remains too low.

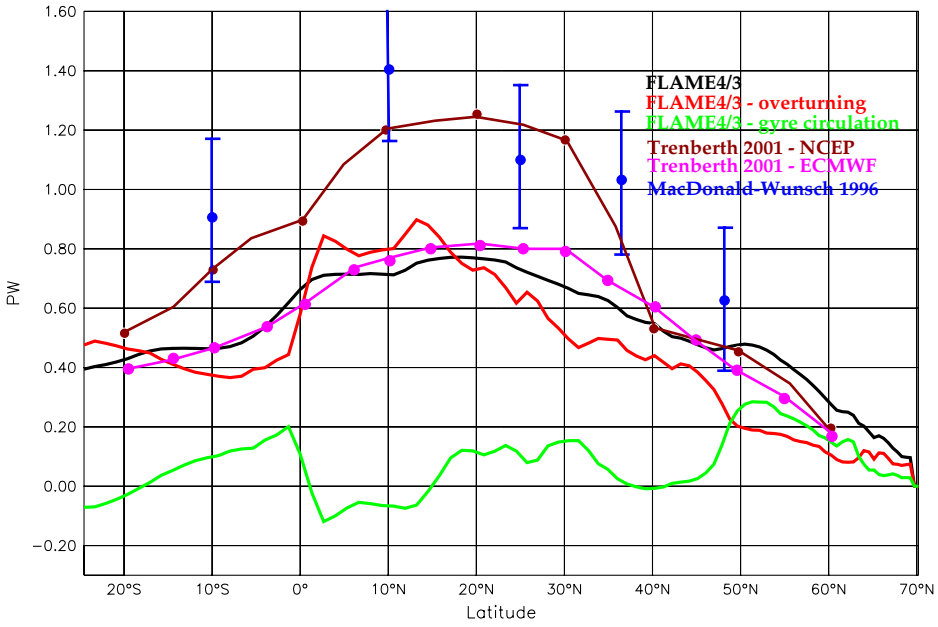

Figure 2.9: *Annual mean meridional heat transport in the Atlantic Ocean as denoted in the figure.*

With a more realistic density of the DWBC the heat transport would be even more unrealistic. So comparing the ocean model in terms of overturning and heat transport to the climate models cannot be done with absolute values. We show an alternate way in section 2.7.2.

2.6.2 Aspects of hydrography and horizontal circulation

In this section we show some features about the (annual) mean state of *FLAME4/3* at the end of the spinup in order to estimate how realistic the representation in comparison to climatological data sets in terms of water mass properties is.

One aspect of the horizontal circulation is the barotropic streamfunction, which is a measure of the depth-integrated horizontal circulation in the model. For the climatological year, this parameter is shown in figure 2.10. The values are smoothed (2-point boxcar window) in order to get rid of subscale noise of *FLAME4/3*, which can be traced back to too low viscosity in the model. The streamfunction has it's highest values of about 150 Sv within the Weddel Sea. Since for the Antarctic Circumpolar Current (ACC) at the open boundaries (section 2.2.1) a barotropic transport of 130 Sv is prescribed, the Weddel Gyre itself has a strength of about 20 Sv. Further north, the subtropical gyre in the South Atlantic has a strength of 30 Sv in the core at 45°W and 38°S. A second local maximum can be found south of the Agulhas Current south of Africa with another 30 Sv of circulation. The Agulhas Current itself contributes with about 20 Sv to the subtropical gyre. In the northern hemisphere the subtropical gyre has a mean strength of 30 Sv

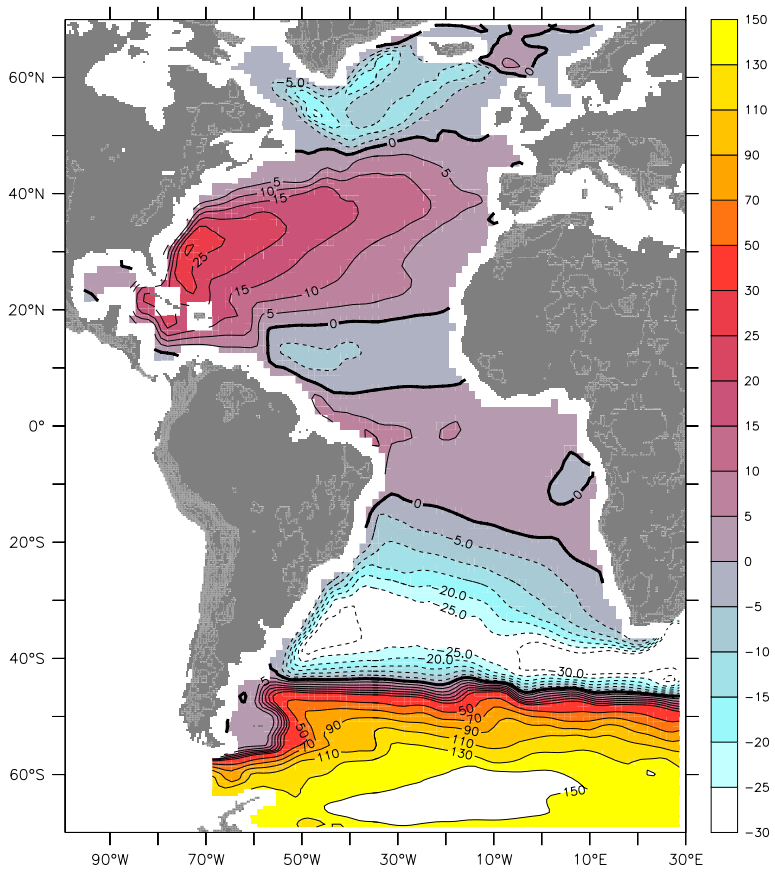

Figure 2.10: *Annual mean barotropic streamfunction of FLAME4/3 in the climatological state, unit is Sv.*

which is almost completely supplied by the currents between the Antilles and the continent. This value is close to observations of SCHOTT ET AL. (1988), who reported about 30 Sv between Florida and the Bahamas Islands.
The cyclonic circulation within the subpolar gyre has a strength of about 20 Sv with its core in the central Labrador Sea.
In section 2.3 the barotropic streamfunction of the *GFDL* model is shown to illuminate difficulties in implementing the diagnosed fluxes. However, that model shows a subtropical gyre with a somehow idealized shape and a maximum strength of about 40 Sv. Also the subpolar gyre is stronger.

To give an overview for the state and the circulation of the upper North Atlantic, figure 2.11 shows the temperature of the ocean model in 100 m depth (*left*) as well as in two widely accepted climatological data sets of BOYER AND LEVITUS (1997) (*middle*) and REYNAUD ET AL. (1998) (*right*).
While the first reference data set is given on an horizontal grid of 1/4° resolution, the second is given on a 1° grid. Therefore, we smoothed the contour lines in order to be able to compare special issues. Additionally, both datasets differ in the

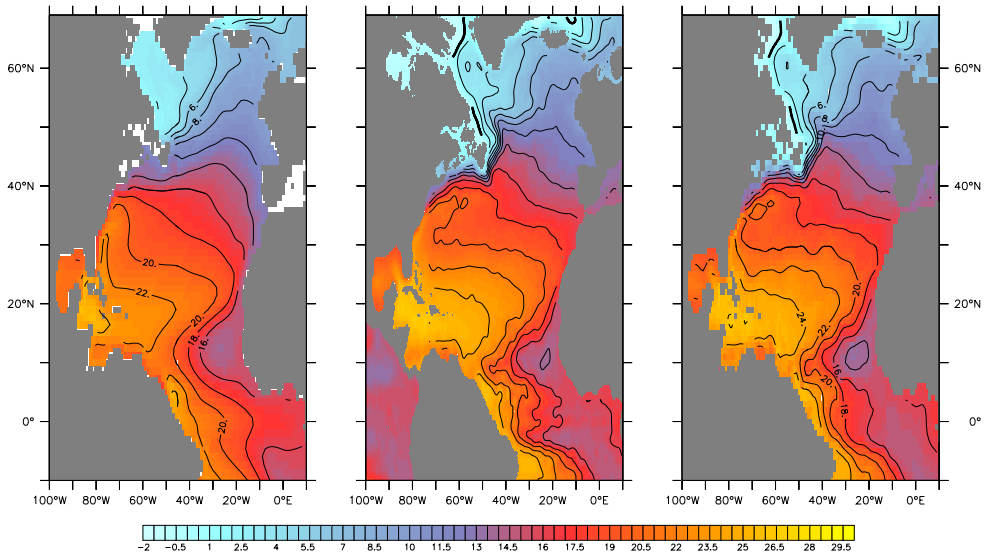

Figure 2.11: *Annual mean ocean temperature in 100 m depth of FLAME4/3 (left), of* Boyer and Levitus *(1997) (middle) and* Reynaud et al. *(1998) (right).*

way they are interpolated. The first one is objectively interpolated on geopotential levels, in the second isopycnals were used.

In first order, there is a high degree of agreement between the coarse resolution model and both climatologies. All three data sets show a very similar temperature both in the subtropical and the subpolar gyre. The temperature within the subtropics is between 25°C at the east coast of North America and 16°C at the African coast. In the subpolar gyre it is between 3°C in the west of the Labrador Sea and 9°C at the west coast of Great Britain. Also quite similar is the temperature distribution north of Iceland with 1-2°C in the East Greenland Current and with 6°C west of the Norwegian coast.

Between the two main wind-driven gyres, even the position of the subpolar front seems to be quite realistic in *FLAME4/3*. Following the North Atlantic Current into the Nordic Seas is also in good agreement with the two reference data sets.

Nevertheless a further inspection anyhow reveals relics of the well known problem of the Gulf Stream separation in ocean models, leading to some kind of unrealistic and simplified circulation along the southernmost part of the Labrador Sea around the Grand Banks east of Newfoundland. This feature is often discussed in model's solutions of the North Atlantic ocean (e.g. Dengg, 1993). Instead separating from the shelf, the front of the isotherms is shifted northward. Using higher resolved ocean models do not necessarily improve the situation. Due to the coarse resolution and high diffusivity, the specific pattern of the Gulf Stream with its distinct eastward jet cannot be represented.

Additionally to the problem of the Gulf Stream separation, the shape of the Labrador Sea Current around the North West Corner is not well represented in *FLAME4/3*. Instead of following the coastline around Newfoundland (Han and

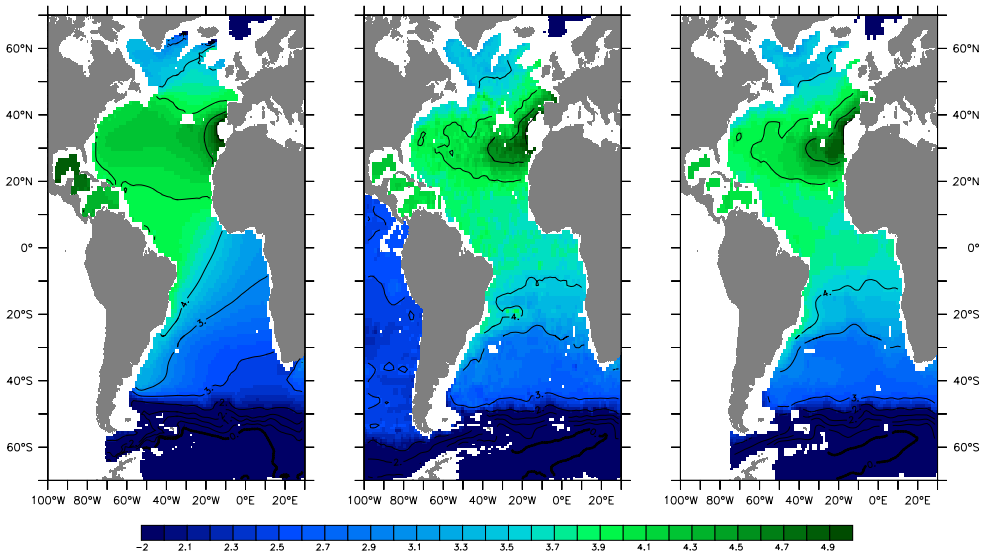

Figure 2.12: *Annual mean temperature in 1800 m depth of FLAME4/3 (left), of* Boyer and Levitus *(middle) and* Reynaud et al. *(right).*

Tang, 1999), in the coarse resolution model this pattern cannot be found in the temperature field in 100 m depth. In contrast to the Gulf Stream separation, this is a problem of coarse resolution models, in which narrow boundary currents are not well represented. In higher resolution models of *FLAME*, especially in the 1/12° version, the circulation is much more realistic here.

Another deficit of the ocean model is the warm water offshore the east coast of North America at 25°N to 35°N. This is connected with the underestimation of the amount of subtropical mode water in *FLAME4/3*, leading to too warm temperatures there (*FLAME Group, pers.com.*). Additionally the Azores Current as the northward nearly zonal branch of the subtropical gyre is missing in the model's solution, what becomes apparent by looking at the zonal spreading isotherms of climatological data sets in that region. The reason is not really known so far, but there are some indication from Jia (2000) that it might be a consequence of a wrong representation and spreading of the Mediterranean inflow into the North Atlantic (figure 2.12) in *FLAME4/3*. Since this Mediterranean outflow is prescribed by a sponge term in the model (section 2.2.1), the water mass properties are correct in the vicinity of the Strait of Gibraltar. Nevertheless the spreading of this warm salty signal into the Atlantic is much more diffusive in *FLAME4/3*. Instead of a concentrated signal along the Portuguese coast northward into the Gulf of Biscaya (Baringer and Price, 1997), in the ocean model the path is in nearly zonal direction. High concentrations of Mediterranean water are still found below the Gulf Stream.

Concentrating on the northern region, the water mass properties in the dense GIN Seas are quite realistic in *FLAME4/3*, since they are restored to observations there (section 2.2.1). In contrast to both climatological data sets, the dense plumes of

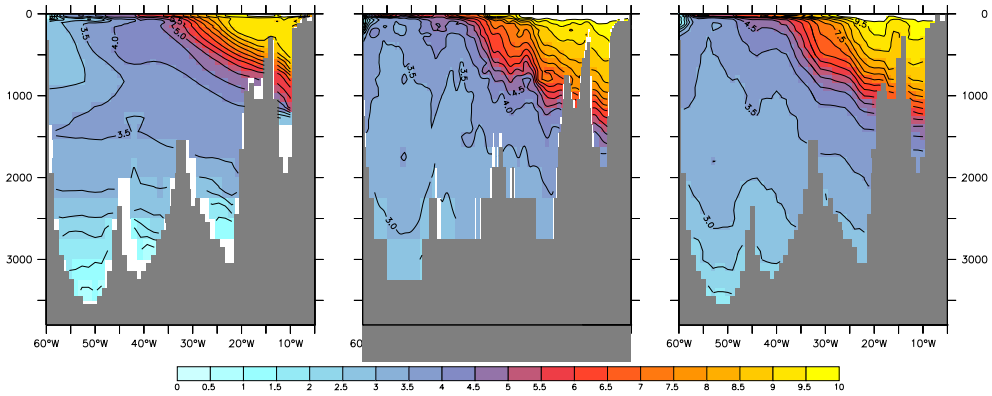

Figure 2.13: *Annual mean temperature at a section at 58° N of FLAME4/3 (left),* Boyer and Levitus *(1997) (middle) and* Monterey and Levitus *(1997) (right).*

the overflows over through the Denmark Strait as well as the Iceland-Scotland Overflow are much more concentrated in the ocean model. By regional smoothing of observational data, signals through narrow passages are often underestimated in climatological data sets. Studying the impact of that point, Döscher et al. (1994) found in a model of the North Atlantic ocean, that a vertical boundary condition in the north including unsmoothed observational data of the dense overflow signals lead to a strengthening and therefore to a much more realistic representation of the overturning function in ocean models than using Levitus and Boyer data solely.

Within the Labrador Sea, the water mass properties at that specific depth are quite similar in both climatological data sets and in *FLAME4/3*. The annual mean temperature is at about 3°C. Again, the lack in the representation of narrow boundary currents is apparently. The water mass properties of Deep Western Boundary Current cannot be found between the coastline and the warmer water within the subpolar gyre.
Finally, further south, the Gulf of Mexico at a depth of 1800 m is much too warm in *FLAME4/3* compared to observations. This must be ascribed to the low water mass exchange in that region in the coarse resolution model.

On a section at 58°N the annual mean temperature distribution is shown in figure 2.13 for all three data sets. It detects some further deficits of the coarse resolution model. While the near surface circulation seems to be quite realistic in terms of the position of the North Atlantic Current, the deep Labrador Sea below 2000 m (in the figures west of 40°W) is too warm. Instead of temperatures of 3-3.5°C in the water column between 500 and 2500 m, the model provides temperatures, which are about 0.5°C higher.
A well known problem of this model, already reported in Eden and Willebrand (2001) is the structure of the isotherms in the deep Labrador Sea basin. They have a very horizontal shape and are the result of a wrong DSOW pathway. Instead of

following the topography as it is found in observations (e.g. Doney and Jenkins, 1994; Strass et al., 1993), the densest water of the NADW fills up the abyssal Labrador Sea, leading to small isothermal slopes and too cold temperatures there.

Although the temperature structure of the deep Labrador Sea basin shows some deficits, at least the density of the Labrador Sea Deep Water (LADW) above is quite realistic. Figure 2.14 shows the density structure in different seasons of the climatological year. In observations the LADW has an upper boundary of $\sigma_\Theta = 27.74 kg/m^3$ (e.g. Rhein et al., 2002), which is quite close to the values in the model. Also the depth of the LADW core seems to be realistic. Since the evolution of the surface density and subsequently of the LADW is an interplay of lateral signals and local surface fluxes, in a couple of ocean models this water mass is, although often restored to climatological values at the surface, too salty. Investigating this point, it is found be an indication for a wrong supply of water entering the central Labrador Sea from the East and West Greenland Current.

Moreover, in higher resolution *FLAME* models, the temperature structure in the deep basin is more realistic and not as cold as in *FLAME4/3*. Therefore, the effect of too high salinity leads to too dense LADW in these models, which in some integrations reaches an unrealistic convection depth down to the bottom.

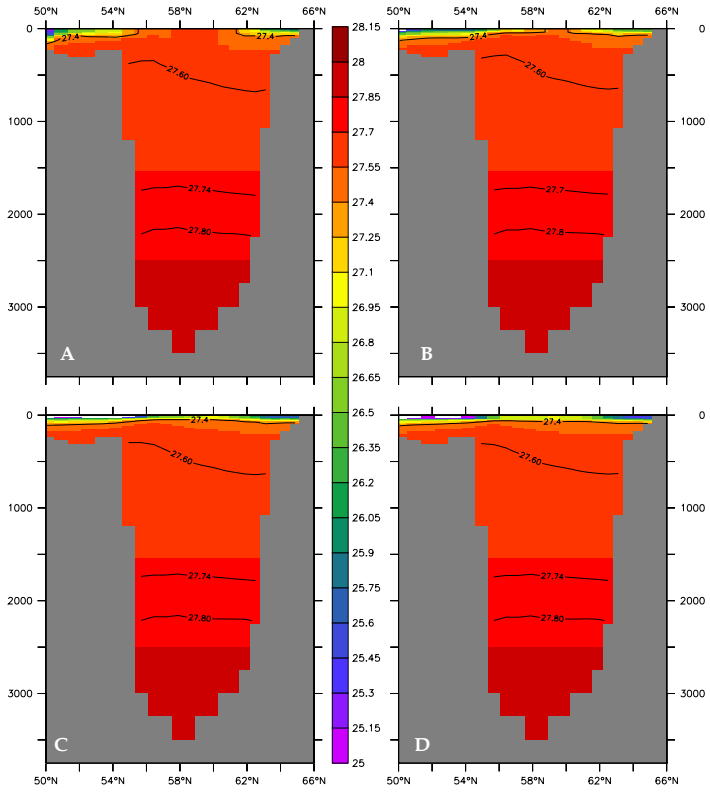

Figure 2.14: σ_Θ *at a section across the Labrador Sea at* 50°*W in March (A), May (B), August (C) and October (D).*

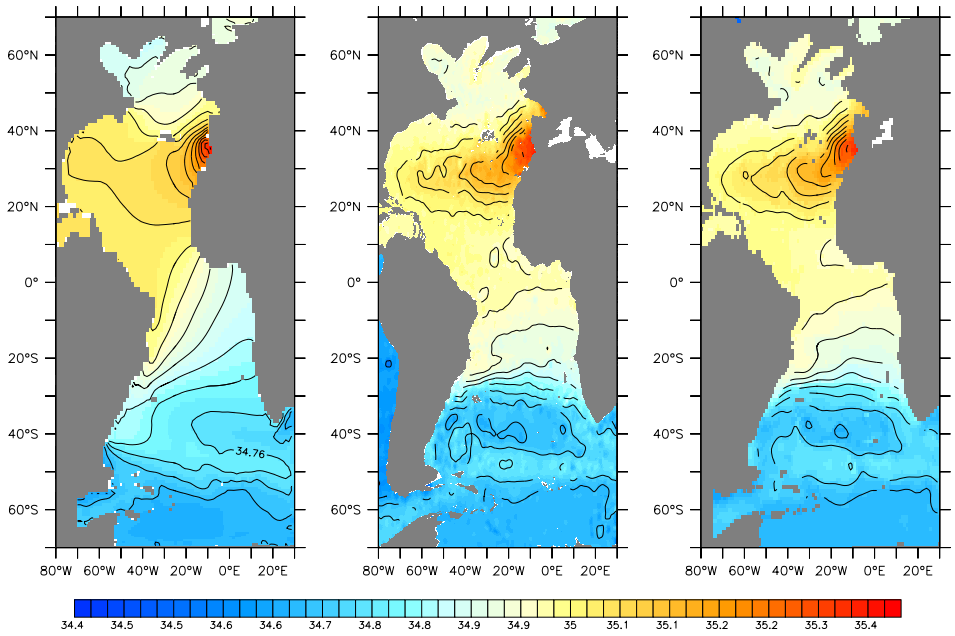

Figure 2.15: *Annual mean salinity in 1800 m depth of FLAME4/3 (left), of* Boyer and Levitus *(middle) and* Reynaud et al. *(right).*

For the sake of completeness, in figure 2.15 we show the annual mean salinity of *FLAME4/3* in comparison to both climatological datasets. The ocean model is quite realistic. Some deficits concern the western tropical gyre with too high values.

Some sensitivity experiments in higher resolution models showed, that, if the properties of these currents are changed on their way around Greenland, the model can overcome the *density problem* within the deep Labrador Sea (*FLAME Group, pers.com.*).

In the case of the coarse resolution *FLAME4/3*, due to the lack of resolved gyres in the model, the transport of water from the boundary currents into the central Labrador Sea seems to be underestimated. Therefore, the properties of the LADW are not as strongly affected by wrong lateral water property signals. This leads to this quite realistic density structure here (*FLAME Group, pers.com.*). The core of cold DSOW at the bottom of the basin restricts the water from too deep sinking. Following the annual cycle of the climatological year, the slope of the isopycnals (*doming*) in the Labrador Sea can be found in March, leading to the renewal of this component of deep water. Due to strong heat loss in the late winter at that time the mixed layer depth reaches about 2200 m, what is quite close to observations in the central Labrador Sea. Curry et al. (1998) respective Lazier (1988) reported of strong interannual variability of the deep water formation in that region. Years of strong convection show mixed layer depths of about 2300 m, talking of low activity means mixed layer depths of about 1000 m. Hence, the situation in the climatological year of *FLAME4/3* is in fair agreement with these

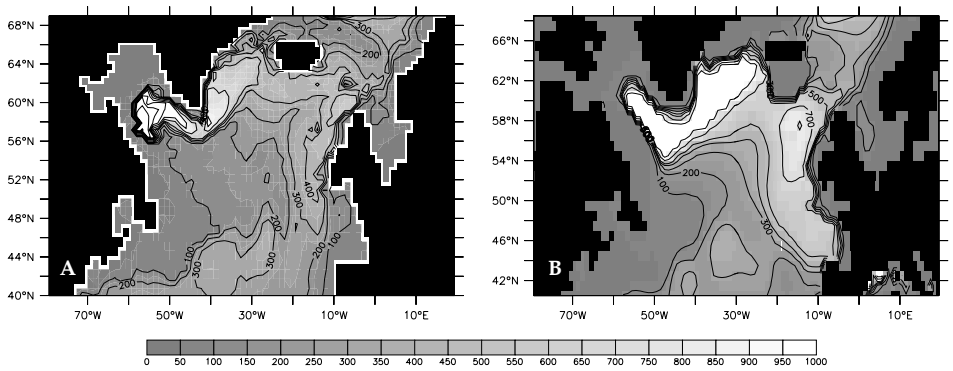

Figure 2.16: *Mixed layer depth in March in FLAME4/3 (A) and from* Monterey and Levitus *(1997) (B). The criterion is* $\Delta\sigma_0 = 0.01 kg/m^3$ *for A and* $\Delta\sigma_0 = 0.125 kg/m^3$ *for B. Note that for B no data below 1000 m are available*

values and can be called a year with quite strong convection activity. Looking at the horizontal map of the convective regime, the solution of the ocean model is quite realistic as well (figure 2.16). At first sight this result is put into perspective by a different definition of the mixed layer depth in model and observations. While the criterion is $\Delta\sigma = 0.01 kg/m^3$ in *FLAME* models, Monterey and Levitus (1997) used a criterion of $\Delta\sigma = 0.125 kg/m^3$, which was found to be more robust in climatological data sets. Using the second criterion in *FLAME* does not alter the results significantly. The deep convection activity mainly takes place within the central Labrador Sea. In the observational map (*right panel*), the calculations are only performed into a depth of 1000 m, so that no comparison about the depth of the convection plume can be made. In May, the seasonal surface warming has set in, so that the communication into the deep basin is suppressed. This situation holds for the rest of the year with slight variations of the seasonal mixed layer (figure 2.14,B,C and D).

Comparing the maps of the mixed layer in March in other regions of the subpolar gyre, some deficits of *FLAME4/3* are obvious. Although the sharp front of values increasing from 200 m to 600 m is present in both solutions, they differ in some aspects. The observations show a much large area of a depth of at least 600 m until 55°N in the western and until 45°N in the eastern basin. In the ocean model, these depths are restricted to a narrow region south of Iceland with a local maximum within the Irminger Sea. In the eastern basin, *FLAME4/3* underestimates the mixed layer depth.

2.6.3 Hydrography of climate models

In the last section, we compared the climatological state of *FLAME4/3* to observational datasets. Here, we show some aspects of the *ECHAM4/OPYC3* as well as the *GFDL* hydrography. Instead of investigating the climatological state of experiments without anthropogenic forcing, we show averaged fields of the first 30 years

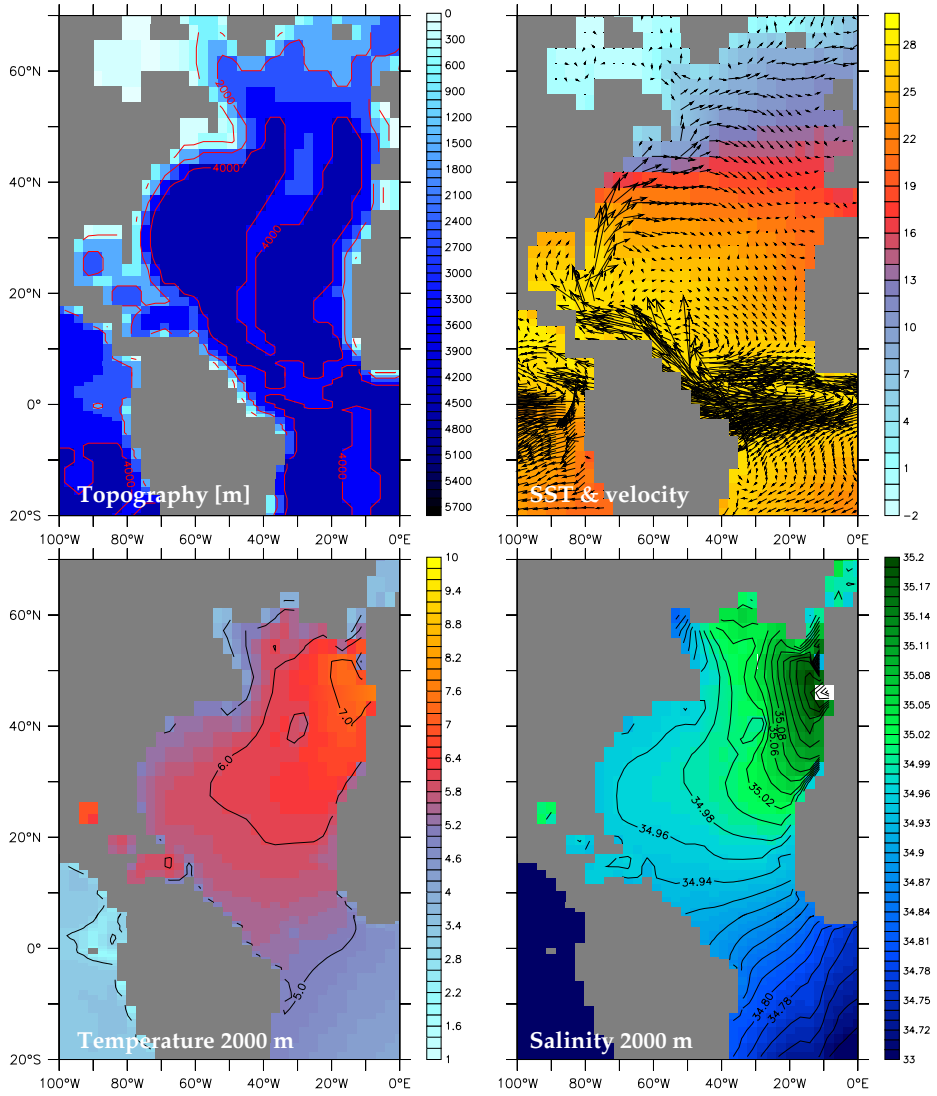

Figure 2.17: *ECHAM4/OPYC3 ocean component:*
Upper left:*Topography (500 m, 2000 m and 4000 m are overlaid in red). The exact topography is not available, so we show the vertical position of the deepest available temperature point. Since these fields are stored for only 10 vertical levels, the shown topography is quite coarse.* ***Upper right:*** *30-years averaged fields at the beginning of the global warming experiments of SST and surface currents.* ***Lower left and right:*** *Temperature and salinity in 2000 m depth.*

in the global warming experiments, when the anomalous forcing is still weak. Since the water mass properties are somehow unrealistic in both models, no details are presented here.

The upper left panel of figure 2.17 and 2.18 show the topography of both climate models' ocean components. Especially the sills around Iceland are highly idealized.

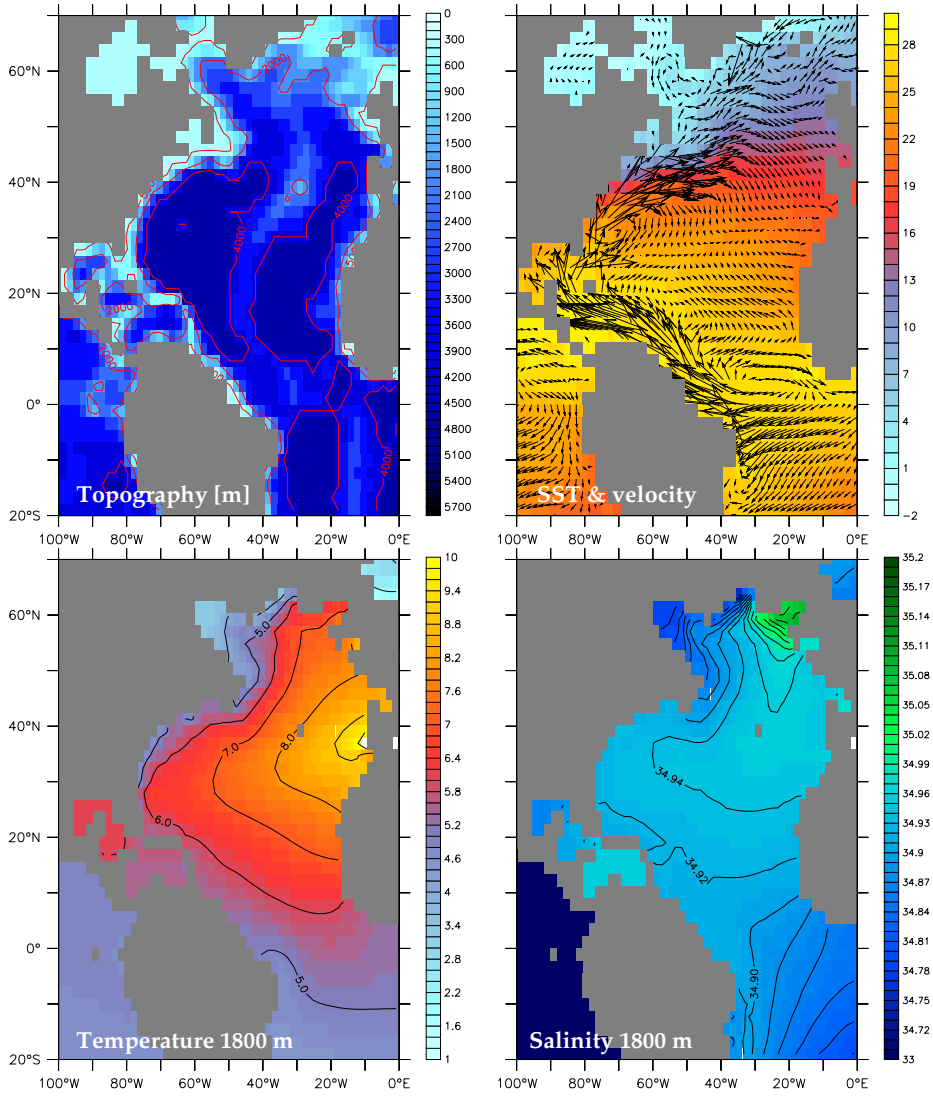

Figure 2.18: *GFDL ocean component:*
Upper left:*Topography (500 m, 2000 m and 4000 m are overlaid in red);* ***Upper right:*** *30-years averaged fields at the beginning of the global warming experiments of SST and surface currents.* ***Lower left and right:*** *Temperature and salinity in 1800 m depth.*

The *ECHAM4/OPYC3* model for instance has a Denmark Strait Overflow depth of 1200 m, the *GFDL* model is 900 m deep at that point. Looking at the surface currents, the *ECHAM4/OPYC3* ocean shows very high values near the equator, which are much stronger than the velocities along the Gulf Stream (figure 2.17, upper right). A special feature of this model is the high horizontal resolution in that region of 0.5°. In comparison, the *GFDL* model shows more realistic velocities in the vicinity of the equator (figure 2.18, upper right). Both models suffer from the Gulf Stream separation, so that especially in the *ECHAM4/OPYC3* model,

the southeast corner of the Labrador Sea is affected by too warm Gulf Stream water of about 9°C. Furthermore, in this model, the cyclonic circulation in that region is very weak and constrained to the northern part. In the *GFDL* model, the Gulf Stream velocities are little higher and the circulation within the Labrador Sea seems to be more realistic, although the temperatures remain too high. The Northwest Corner with a cold Labrador Current cannot be found in both models.

The temperature and salinity in 2000 m (*ECHAM4/OPYC3*) respective in 1800 m (*GFDL*) are shown in the lower panels of figure 2.17 and 2.18. Without going into details, the water mass properties in that depth are highly idealized. So, in the *OPYC* ocean temperatures of 8°C can be found in the outflow region of the Mediterranean, which are about 4°C too high relative to observations (figure 2.12). Even warmer is the *GFDL* ocean in that region. With temperatures up to 10°C, the model is quite unrealistic. Furthermore this warm tongue reaches large areas in the north Atlantic, leading to e.g. high temperatures east of Iceland in that depth. Looking at the salinity of the *GFDL* model, no salt signal from the Mediterranean can be found. Instead the whole North Atlantic has a quite uniform salinity of about 34.9 psu. However, in the *OPYC* ocean, there is indeed a Mediterranean signal. Nevertheless both models suffer from too high salinities within the subpolar gyre. So deep water properties are highly idealized in both ocean components.
Nevertheless, the coarse resolution might be one of the reasons for these unrealistic water mass properties especially in the deeper North Atlantic. However, the purpose of these models is not the representation of local features like the Labrador Sea properties. The use of these models is to estimate the response of integral parameters like the overturning circulation or the heat transport evolution. Therefore, although we can summarize, that the *FLAME4/3* ocean is much more realistic in terms of water mass properties and the resulting circulation, the response of these climate models in terms of greenhouse gas impacts cannot be estimated at this point.

2.7 Diagnostics

The main issue of this thesis is to investigate the general response of the ocean's conveyor in the ocean model to anthropogenic forcing applied at the surface. Different components of atmospheric forcing are the reason for this circulation. Since for diagnosing the response in *FLAME4/3* we mainly use the overturning circulation (equation 2.11), it is useful to differentiate and explain the necessary forcing components like wind and buoyancy forcing for this feature in the ocean.

2.7.1 Thermohaline circulation and overturning

The ocean's conveyor is often associated with the thermohaline circulation. Examine changes of this meridional circulation, the THC is indeed a useful concept but not a useful diagnostic parameter, since it cannot be measured in the ocean and in models with realistic forcing. However, idealized ocean models without surface wind forcing can indeed produce a pure THC by surface buoyancy forcing in

combination with the required turbulent mixing in the interior. This mixing is a necessary part of the circulation, since surface buoyancy forcing, in other words cooling and heating at the same pressure cannot provide kinetic energy for the circulation (SANDSTRÖM, 1908). In ocean models, the mixing is expressed within the hydrodynamic equations and can be varied, no matter whether the surface wind stress is switched on. In the real ocean, the turbulent interior mixing is a *consequence* of surface wind respective tidal forcing (MUNK AND WUNSCH, 1998), so switching the wind off in models means proscribing the wind-driven circulation near the surface but still including its remote effect of mixing. In the first conceptual model of the THC, H.STOMMEL (1961) explictly provided a mixing device for salinity and temperature.
In terms of energy transformation, potential energy for (diapycnal) water mass transformations is supplied by external forcing. Surface buoyancy boundary conditions are needed to provide densification and sinking, but cannot actually drive the circulation.

Anyhow, since the interior mixing is mostly unchanged in one specific model, the variable buoyancy forcing is ultimately responsible for changes in the strength of the conveyor circulation. Because thermohaline forcing is mainly associated with diapycnal transports, investigating the circulation on isopycal surfaces is a useful approach. In this framework, the meridional overturning circulation can be expressed in the following integral:

$$\Psi(\phi, \sigma_{Theta}) = \int_{\lambda_{min}}^{\lambda_{max}} a \ cos\phi \ d\lambda \int_{h(\lambda,\phi,\sigma_\Theta)}^{0} v(\lambda, \phi, z') \ dz'. \qquad (2.12)$$

In a regional model of the Atlantic Ocean, λ_{min} and λ_{max} are the limits of the zonal extent of the basin and v is the meridional velocity in each isopycnal surface. In figure 2.19, this function is shown for the mean state of *FLAME4/3*. Here, "vertical" transports are indeed associated with diapycnal, but not necessarily thermohaline driven transports.
In the case of *FLAME4/3*, this diapycnal mixing can occur due to vertical as well as horizontal diffusion (section 2.2.2) and due to vertical adjustment of an instable stratification, mainly in convective regimes. For the sake of completeness a diapyncal component can also be traced back to truncation in the numerical advection scheme. However, this overturning circulation on isopycnal surfaces results in much higher values in the center of the subpolar gyre between 50°N and 55°N than the overturning function on a geopotential vertical coordinate (figure 2.6), which we already discussed in section 2.6.1. The reason for this difference of about 6 Sv is that ocean currents occur mainly on isopycnal surfaces. Within the subpolar gyre, the contribution of the horizontal circulation to the meridional buoyancy transport is strong, but happens on the same geopotential level and remains therefore invisible in function 2.11. In the isopycnal representation, horizontal transports at different densities become visible. In the specific region of the subpolar gyre, the transport of warm water into the North Atlantic is both compensated by a deep southward flow and a near surface flow along the western boundaries of the basin.

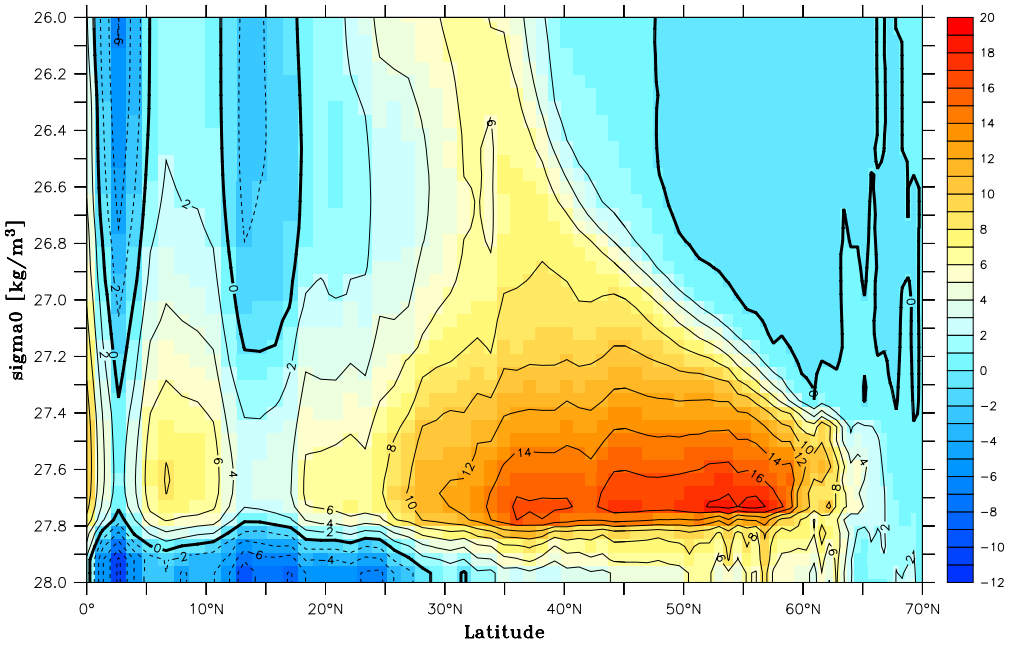

Figure 2.19: *Meridional overturning function of FLAME4/3 calculated on an isopycnal vertical coordinate for the last year of the spinup discussed in section 2.6.*

The found deviation between these two vertical integrals is quite similar to results of Willebrand et al. (2001), who compared overturning circulation in models with a different vertical coordinate. Investigating the overturning circulation in geopotential and isopycnal coordinates can be a useful tool to detect mechanisms in the ocean's overturning circulation. The Deacon Cell in the Antarctic Circumpolar Current is a prominent example, where the different representation leads to totally different results: Studying the circulation in geopotential coordinates shows an overturning circulation which vanishes in the isopycnal framework, since here, vertical is also along-isopycnal motion (e.g. Döös and Webb, 1994).

Returning to the upper example for a pure THC, running the available *FLAME4/3* model in the standard configuration without surface wind forcing, leads necessarily to a breakdown of the wind-driven gyre circulation. Additionally the maximum overturning on geopotential coordinates (figure 2.6) is decreased by about 6 Sv relative to the mean state within 10 years, which is a reduction of about 30%(figure 2.21, left panel). The reason for this response is investigated by Biastoch et al. (2003), who found a strong influence of the gyre circulation around Iceland on the overturning function. When this horizontal circulation is decreasing with a relatively barotropic structure, the transport of dense water within the subpolar gyre is constrained and has an effect on the overturning function, although the thermohaline forcing remains unchanged. Figure 2.20 shows the changes in the barotropic streamfunction after 10 years of integration without surface wind forcing (left panel). Both the subpolar and the subtropical gyre spun down. In the right panel, the vertical structure of the overturning function at different latitudes is

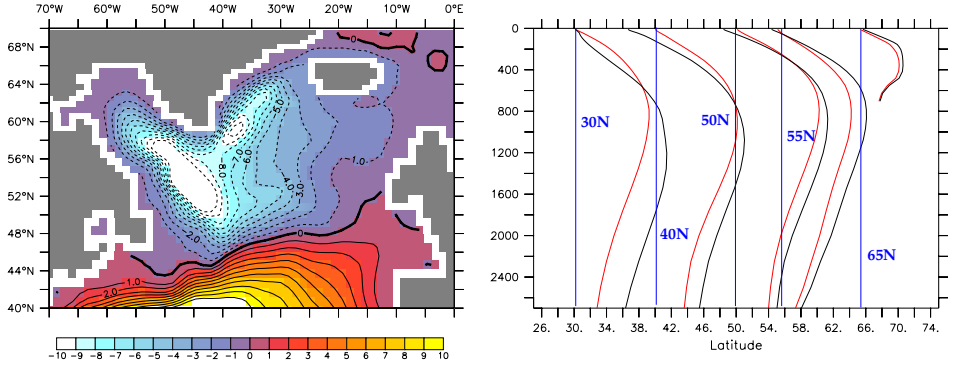

Figure 2.20: *Left: Changes in the barotropic streamfunction 10 years after switching off the wind forcing; right: vertical structure of the overturning function at different latitudes denoted in the figure, red lines denote the situation 10 years after wind forcing stops, the black lines are the climatological values, additionally the horizontal axis denotes relative transports as well, units are Sv.*

shown for the climatological year and for the situation 10 years after switching off the wind. Apparently, the thermohaline cell is affected, although the buoyancy forcing remains unchanged. Starting with weaker nearly barotopic transports in the north at 65°N, the whole cell below the gyre circulation is affected. Near the surface, the negative values of the experiment without wind forcing show the decreased gyre contribution.

In the isopycnal formulation, without forcing the surface gyre circulation, the maximum strength of the MOC also becomes 10 Sv (right panel). This is not self-evident, since the zonal isopycnal slopes could still lead to a difference in both representations. E.g. in the subpolar gyre these slopes can still be found due to buoyancy forcing, even if the wind stress is switched off.

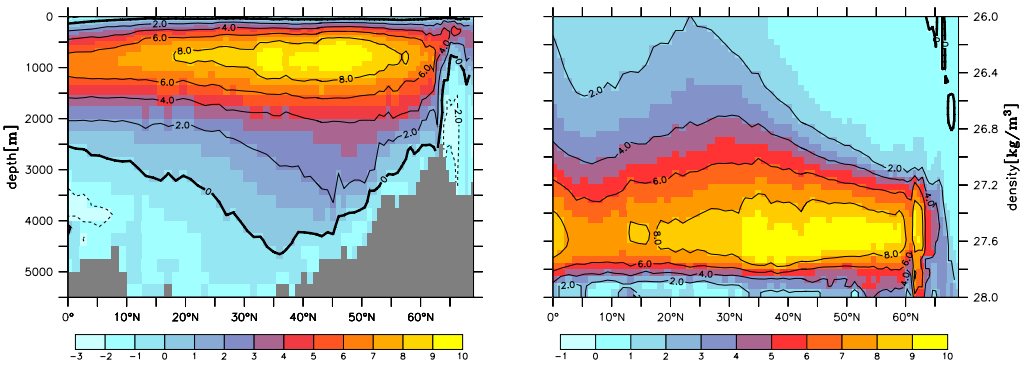

Figure 2.21: *Annual mean meridional overturning function of FLAME4/3 ten years after switching off the surface wind stress; left panel: geopotential vertical coordinate, right panel: isopycnal vertical coordinate; unit is Sv*

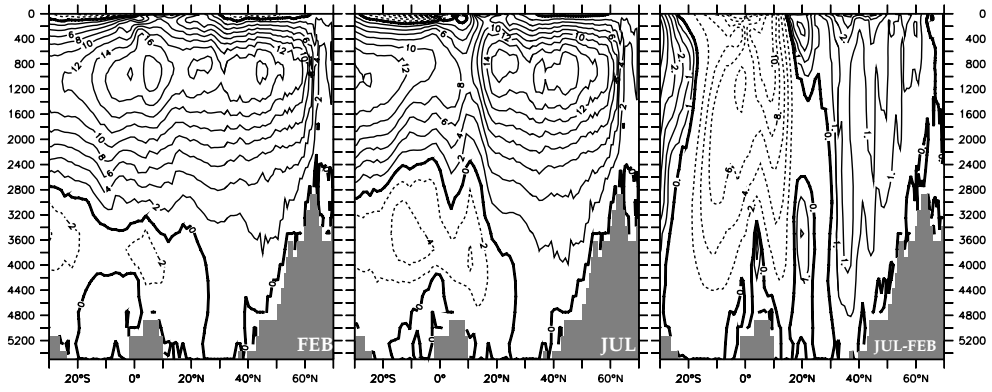

Figure 2.22: *Meridional overturning function in the last year of the spinup in FLAME4/3. Situation in February (left),July (center) and difference of both (right)*

Beyond the non-trivial arguments concerning the energetics of the THC, in terms of investigating the ocean's role in climate, it is not primarily the isolated effect of thermohaline forcing but the oceanic heat transport, which is worth to measure and to study in models. Although the result of a combination of physical mechanism like thermohaline forcing *as well* as wind stress forcing and diffusive processes, the meridional overturning circulation on geopotential vertical levels is a widely accepted approach for a model's response, since it is indeed well correlated with the mean oceanic heat transport in most latitudes (see section 2.7.2).

In terms of global warming, the role of changes in the wind stress relative to changes in the buoyancy forcing are found to be relatively unimportant for the general trend (see chapter 5), since the gyre circulation is not enduringly disturbed, as it is done in the here presented study without wind forcing.

2.7.2 Overturning circulation and heat transport

Using the MOC as an indicator for oceanic heat transport, here we show the coherency on different timescales. Additionally we propose a reasonable way to compare the overturning transport in different models with a different mean state of the circulation. This approach is later used in chapters 4 and 5 in order to compare differences of the ocean model's MOC relative to the climate model's response.

The MOC has a strong seasonal cycle (figure 2.22), especially in the subtropics, which is the result of a variable structure and strength of the circulation within the inclined gyre (Böning et al., 2001). Along with this seasonal cycle goes a nearly barotropic difference between the wintertime and summertime MOC (figure 2.22, right panel).

Due to the strong annual cycle the overturning function cannot be used as an indicator for oceanic heat transport on seasonal timescales (e.g. Jayne and

MAROTZKE, 2001). Figure 2.23 shows the correlation between the meridional heat transport and the maximum overturning function in the North Atlantic for the *FLAME4/3* model in a greenhouse gas simulation (experiment *FULL*, see section 5.3 for details) for different running-mean intervals. Up to 45°N, the correlation is always larger than 0.85, no matter what smoothing interval is chosen. In the subpolar gyre, the coherency is lower, especially on short timescales, anyhow on timescales beyond the seasonal cycle it is still at about 0.85. North of 60°N the correlation with the overturning maximum is low for all running-mean intervals. This can be traced back to two reasons. Due to the segmentation into different basins, the impact of overturning variability at the position of the maximum has little impact on heat transport. Furthermore the proximity of restoring boundaries becomes important. However, in subpolar gyre, the lower correlation can be attributed to the heat transport of the wind-driven gyre circulation, what has a huge impact on the short averaging interval.
Nevertheless, at 40°N the oceanic heat transport still contributes about 25% to the earth's meridional heat transport (TRENBERTH AND CARON, 2001), what justifies

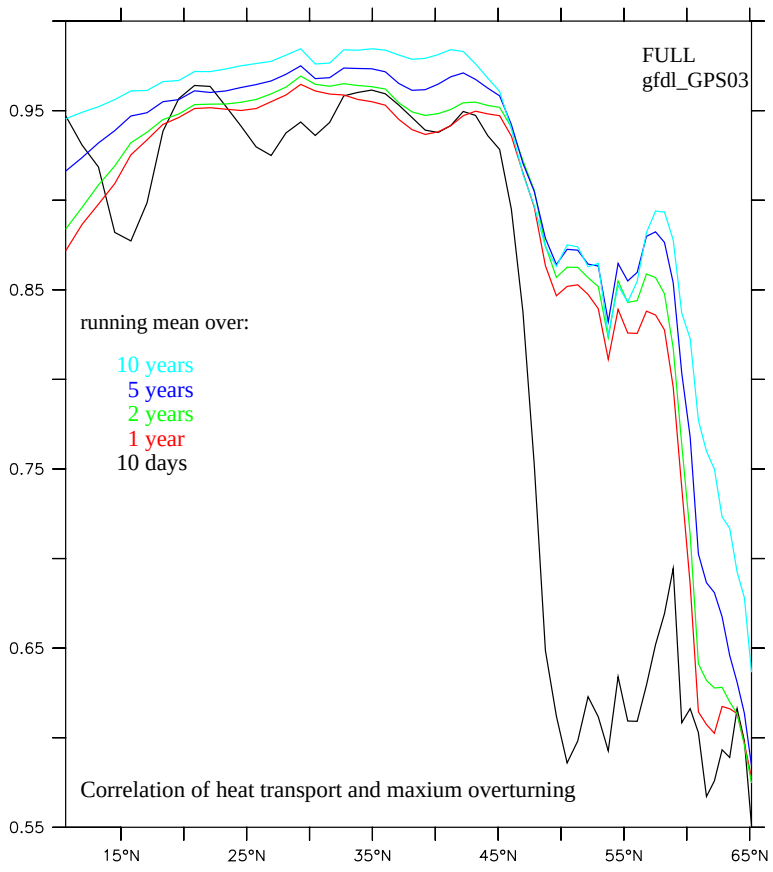

Figure 2.23: *Correlation of meridional heat transport at different latitudes and the maximum overturning function in the North Atlantic for different running-mean intervals in the FULL experiment (see section 5.3 for details)*

the choice of the overturning maximum as an indicator for the oceanic heat transport in most ocean models. Further north the ocean's role is of less importance.

Moreover, it is possible to derive a near linear relationship between oceanic heat transport and overturning strength. This statement holds for several latitudes. For instance BÖNING ET AL. (1996) found that for every 2 Sv gain in overturning rate the heat transport across 25°N increases by approximately 0.1 PW in MOM-style OCMs.
However, in most climate models, the meridional overturning cell is stronger than the observed 16 Sv, while most ocean-only models agree with this value. In the *ECHAM4/OPYC3* coupled model (see chapter 4), the mean transport is 25 Sv, the *NCAR* model even shows 32 Sv. For comparison ROEMMICH AND WUNSCH (1985) suggest a strength of 17 Sv at 25°N. Other observations of MACDONALD AND WUNSCH (1996) and LAVIN ET AL. (1998) suggest a strength between 16 Sv and 18.8 Sv. However, the resulting northward heat transport is a function of the temperature difference between the upper (northward) and the lower (southward) branch of the overturning circulation. Accordingly JIA (2002) found in a comparison between different coupled models a mean deviation of North Atlantic Deep Water temperature of about 2.5°C relative to observations (e.g. HALL AND BRYDEN, 1982). So, although suffering from too high overturning, since the lower branch is often too warm, this leads to a smaller heat transport than the overturning strength would suggest (see WOCE). Apparently the resulting maximum meridional heat transport in climate models is often in the vicinity of 1 PW and therefore more realistic than the overturning strength.

Although often shown (e.g. figure 4.1), to compare the response of climate models in greenhouse gas simulations, the absolute variability or decrease is not a useful parameter in terms of changes in the oceanic heat transport. To compare the climate models' response to the response of the *FLAME* ocean model, another approach is chosen. We use the response of the climate model relative to the quasi-equilibrium state of the climate model. The so weighted response can directly be compared to changes in the ocean model's overturning. Mathematically, the scaled overturning index of the climate models is

$$O_{scale}(t) = \frac{O_{climate}(t)}{O_{climate,equ}} \cdot O_{FLAME,equ}. \tag{2.13}$$

Hereby is $O_{climate}$ the time-dependent overturning strength of the climate model, $O_{climate,equ}$ is the averaged strength before significant anthropogenic forcing sets in and $O_{FLAME,equ}$ is the ocean models state at the end of the spinup. In the case of a linear relationship between heat transport and overturning for each model, the resulting scaled overturning time series O_{scale} is also scaled with respect to the heat transport, even though the mean states of climate and ocean model are different. This approach is chosen for the comparison between *FLAME4/3* with the *ECHAM4/OPYC3* model (figure 4.6) respective the *GFDL* model (figure 5.3) in chapters 4 and 5.

However, using the *FLAME4/3* model with a constant parameter set, we take the overturning function as an indicator for the meridional heat transport. Only in section 5.5.8 we performed a few experiments with modifications in the parameterization as well as the topography, so the dependency of overturning and heat transport is altered, what is illuminated there.

Chapter 3

Idealized forcing experiments

3.1 Motivation

Before running the model with anthropogenic surface forcing, in this chapter we show some sensitivity studies concerning the isolated response of the ocean model on artificial modifications to boundary forcing. By adding a disturbance with a singular shape to the climatological forcing, its specific impact on the circulation can be studied without the necessity to distinguish between different combined mechanisms for changes in the ocean.

All these experiments were performed both with *FLAME4/3* and with the higher resolved *FLAME1/3*, in order to compare a different response of changes in the boundary conditions.

Due to high computational costs and problems to implement the climate model's fluxes into the high resolution model, the anthropogenic forcing experiments with several sensitivity studies are only performed with the coarse resolution model. To classify those results in comparison to the higher resolved version, here we show the response of a number of highly idealized experiments for both resolutions.

Furthermore, since we drive the high resolution model with the standard surface restoring boundary conditions, the impact of mixed boundary conditions in *FLAME4/3* for the overturning function can be estimated.

This chapter is organized as follows: In section 3.2 the different regions of deep water formation, which are the Labrador Sea and the Greenland-Iceland-Scotland Sea are artificially suppressed, to estimate the different impacts on the strength of the overturning circulation. Thereafter, in section 3.3 the timescales of a density signal starting in the overflow of the Denmark Strait are traced along the Deep Western Boundary Current (hereafter DWBC). This timescale becomes important in the anthropogenic forcing experiments, when changes in the dense reservoir due to greenhouse gas forcing take place.

3.2 Isolation of convection regions

3.2.1 Introduction

It is often shown in numerical models, that on decadal to interdecadal timescales the strength of the MOC strongly depends on the deep water formation rate in areas of convection activities (e.g. EDEN AND WILLEBRAND, 2001).
In this section, the relative contributions of different regions of deep water formation to the strength of the overturning circulation and hence the THC is examined for *FLAME4/3* and for the higher resolved *FLAME1/3*.

3.2.2 Performed experiments

Starting from the climatological state under climatological forcing (section 2.2.3) the coarse resolution model is integrated for 30 years until the year 1980 and thereafter in four different combinations of modified boundary conditions for at least 80 years. For comparison, *FLAME1/3* is integrated under climatological forcing, as it is specified in section 2.5.1. Afterwards the same modified boundary conditions are implemented. These experiments integrated for at least 15 years.
The sensitivity experiments performed with both resolutions are listed in table 3.2.2 and shortly described and discussed in terms in the following section.

Name	***Anthrop.Forcing***		***Integr. period***
	Labrador Sea convection	**Northern sponge zone**	
CTRL	on	on	101 y (1980-2080)
NOLAB	off	on	81 y (1980-2060)
NOREST	on	off	101 y (1980-2080)
NOCONVECT	off	off	84 y (1980-2063)
CTRL-H	on	on	20 y (1923-1942)
NOLAB-H	off	on	15 y (1923-1937)
NOREST-H	on	off	15 y (1923-1937)

Table 3.1: Sensitivity studies performed with FLAME 4/3 and FLAME1/3 (appendix -H) under different combinations of climatological forcing.

Experiment *NOLAB*

In the first sensitivity experiment (hereafter *NOLAB*), we shut off the formation of Labrador Sea Deep Water in order to understand its contribution to the MOC under quasi-equilibrium conditions.
This artifical switch for the Labrador Sea is realized as follows: We defined an empirical function for the lower limit of the apparent atmospheric temperature T^* between $5°C$ at center of the Labrador Sea at $58°N$ and $50°W$ exponentially

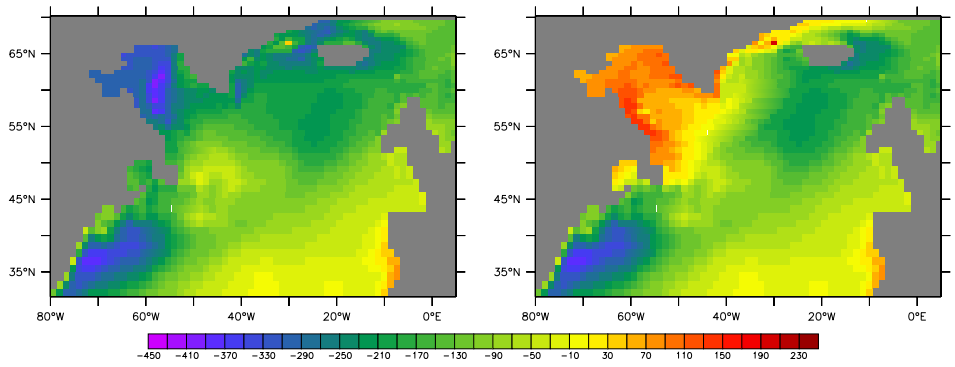

Figure 3.1: *Surface heat flux of CTRL (left) and NOLAB (right) in March due to a different apparent atmospheric restoring temperature in FLAME4/3 in* W/m^2. *The cooling of the Labrador Sea is mainly cut off.*

decreasing to $-2°C$ on a spatial scale of 1000 km. This function is given by

$$T_{lim} = 7.0 \cdot exp(-0.005 * r^2) - 2.0. \tag{3.1}$$

with

$$r = \left[0.4 \cdot (lon - 310.0)^2 + (lat - 58.0)^2\right]^{\frac{1}{2}}, \tag{3.2}$$

where *lon* and *lat* are the longitude respective the latitude axis of the model. The apparent atmospheric temperature T^* in equation 2.3 is afterwards modified:

$$T^{*\prime} = max(T^*, T_{lim}) \tag{3.3}$$

The impact of this modification can be studied by comparing the surface heat flux in March in the *CTRL* integration with the situation after 10 years of integrating experiment *NOLAB* (figure 3.1). While the usual situation at this time of the year is a very cold temperature over the Labrador Sea (right panel) associated with strong heat loss of the ocean, our constraint leads to a high heat flux anomaly over this region (left panel). In March, the oceanic heat loss is reduced by about $300W/m^2$, leading instead to a slight warming of the surface waters even at that time of the year. But not only the central Labrador Sea but also the boundary currents around the core are affected: In the *CTRL* integration, the apparent atmospheric temperature is quite cold east of Greenland, keeping the surface currents from the Nordic Seas cold. The surface heat fluxes of *CTRL* are quite small in this region and the temperature of the East Greenland Current is mainly given by lateral transports from the Nordic Seas. Therefore, although our modification function for the apparent atmospheric temperature provides an exponential decrease from the central Labrador Sea, here the air-sea interaction is, compared to the *CTRL* situation significantly enhanced. The consequence is a remarkable warming along the East Greenland Current. This is seen in figure 3.2, which shows the temperature evolution after 30 years of integration relative to *CTRL* at two

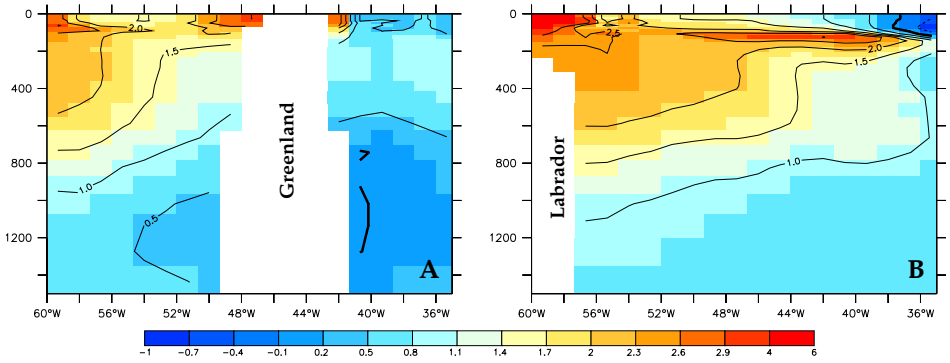

Figure 3.2: *A) Anomalous annual mean temperature at a vertical section at 60° N (A) and at 57° N (B) in experiment NOLAB after 30 years of integration, experiment CTRL is subtracted, unit is ° C. The Labrador Sea as well as the boundary currents are anomalously warmed*

vertical section. The East and West Greenland Current are warmed by about 2.5°C (left panel). For comparison, the central Labrador Sea is warmed by about 4°C (right panel). Not only the surface waters but also subsurface waters are affected in regions with a deep mixed layer. This effect must be taken into account by estimating the role of the Labrador Sea for the overturning function. Since we also warm the boundary current system, its not only in the central Labrador Sea, where we prohibit deep water formation.
This is expected to be more important in *FLAME4/3* than in the higher resolution model, since the southern boundary of the sponge zone is at 66°N. In *FLAME1/3* the effect is weaker, because the East Greenland Current is only prescribed until 69°N, so that the nudging to prescribed values is weaker at the vicinity of the Denmark Strait sill. Instead, the exponential of modified heat fluxes can be felt.
However, as a consequence, the deep water formation within the Labrador Sea, which takes place every single year in winter in the quasi-equilibrium run *CTRL* (see section 2.6), is cut off immediately. Due to the shape of the singular signal, the impact of switching off the renewal of Labrador Sea Water on the MOC can be studied explicitly in this experiment.

Experiment *NOREST*

In the second sensitivity experiment, the renewal of dense water masses north of Iceland, more precisely in the GIN Seas (figure 2.1) is suppressed. Since in *FLAME4/3* this region is realized as a restoring area towards climatological values (see section 2.2), we realized this as follows: The sponge term in equation 2.10 is set to zero. In the quasi-equilibrium integration, to simulate the impact of the Arctic ocean surface waters following the North Atlantic Current lose there characteristics in this region due to cooling and freshening. At the surface, the properties of the East Greenland Current are prescribed. Setting the restoring to zero removes the ability of the model to communicate any water into and out of the Arctic region

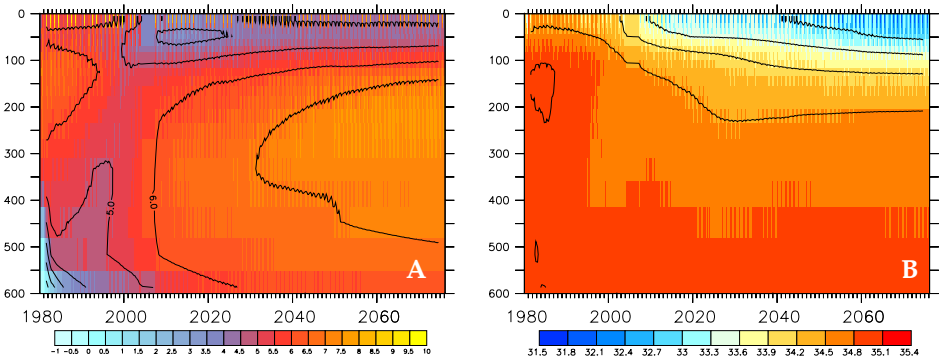

Figure 3.3: *Temperature (A) and salinity (B) evolution of experiment NOREST at 66° N and 28° W. The surface becomes warmer and fresher, the DWBC becomes mainly warmer.*

north of 70°N. In this experiment surface waters, entering this region are reflected into the subpolar gyre, so that the water mass characteristics are only changed by the surface forcing up to 70°N. Figure 3.3 shows the evolution of temperature and salinity in that region. At the surface, this region becomes colder and fresher, since the balance between lateral transports and surface forcing is disturbed. Below the surface, the water mass properties become warmer and more saline, which is indeed the consequence of the missing sponge term. Since due to the model's style, water masses cannot abandon the model's area into the arctic region, it is somehow like a short-circuit of the response in the northern North Atlantic. In a realistic experiment, the timescale of the waters changing their properties are expected to be longer because of the buffering role of the Arctic Ocean.
This experiment is highly idealized in the case of *FLAME4/3*, since this model has no own deep water formation north of Iceland. A little more realistic is *FLAME1/3*, where there is indeed some dense deep water formation in this region due to local surface forcing (*Flame Group, gers.com.*), no matter whether the northern restoring is switched on. Therefore the water mass properties, which are communicated in the subpolar region are expected to be less affected in the higher resolution experiment.

Experiment *NOCONVECT*

To complete these sensitivity studies concerning the different contributions of deep water formation to the MOC, we combined experiments *NOLAB* and *NOREST*. The result is an experiment, in which the renewal of deep waters due to convection mechanisms is totally suppressed.
Since the deep water formation within the Labrador Sea essentially depends to some extent on the properties of lateral transports from the boundary current, we expect a non-linearity between the upper two experiments *NOLAB* and *NOREST*. Experiment *NOCONVECT* is integrated to answer the question, to what extent the two previous sensitivity studies respond linear on almost linear changes in

surface forcing. Unfortunately, an experiment with *FLAME1/3* under this forcing configuration is not available.

3.2.3 The overturning response

All these experiments show a high dependency of the deep water formation activity on the strength of the MOC, what is already found in earlier studies concerning the subpolar gyre (e.g. Eden and Willebrand, 2001) and the overflow properties (e.g. Döscher and Redler, 1997) .
Shutting down the Labrador Sea convection (experiment *NOLAB*) in the coarse resolution model, the overturning weakens at about 3 Sv at a latitude of 40°N compared to the climatological run (figure 3.4, red curve). This state is approximately attained 15 years after the temperatures within the Labrador Sea are limited. Integrating this experiment for another 65 years leads to no further modification of the strength of the MOC.
This result underlines suggestions of Döscher and Redler (1997), who found in a *CME* model, that if an adequate dense overflow is prescribed, variability in the convective regime within the Labrador Sea can not significantly weaken the meridional overturning cell.
In experiment *NOLAB*, the overflows maintain their density due to the style of the sponge area. Independent of the strength, lateral signals entering the region

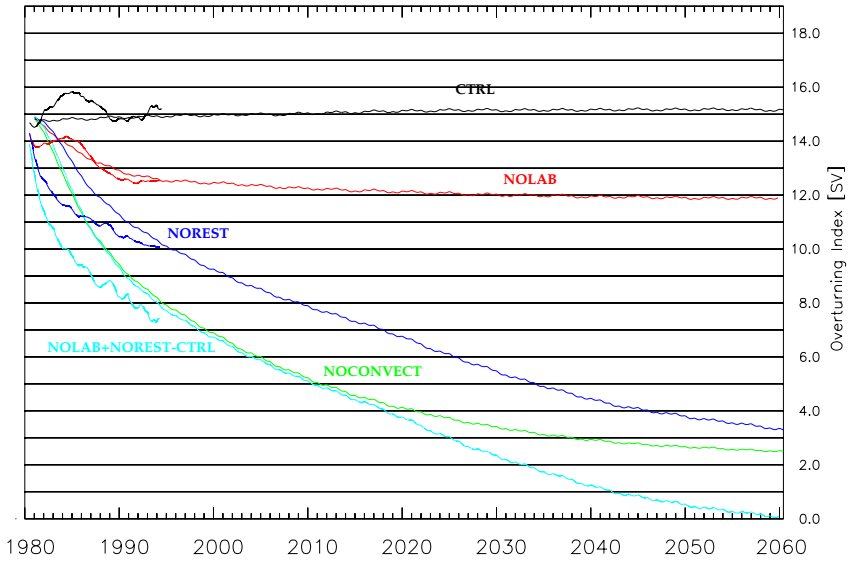

Figure 3.4: *Time series of maximum overturning at 40° N of the sensitivity studies labeled in the plot in FLAME4/3 (line) and in FLAME1/3 (dashed), the higher resolution curves are scaled (see section 2.7.2 for details). Additionally the dashed magenta lines are linear superpositions of the individual response (NOLAB+NOREST-CTRL) of both resolutions. Both models show a similar response.*

north of Iceland, e.g. due to variability of the North Atlantic Current, the water mass properties communicated back into the subpolar basin remain constant. In a physical sense, this nudging condition to climatological constant salinity and temperature must be ascribed to variability in surface freshwater and heat fluxes supplied into the ocean in northern latitudes.
In comparison to this result, the equivalent study *NOLAB-H* with the higher resolution model generates a similar result: The overturning strength is reduced at about 3.5 Sv, decreasing from 17.5 Sv to 14.0 Sv after 15 years of integration. Mind that in figure 3.4 the overturning decrease is weighted with the meridional heat transport, as it is proposed in section 2.7.2, in order to compare the response of models with a different mean circulation. Here the impact after 15 years of switching off the Labrador Sea convecting is about 0.5 Sv stronger. However, in this study we cannot investigate the details of this issue. A possible reason could be the density structure within the Labrador Sea. In the higher resolving case, the density within this region is at about $0.10 kg/m^3$ too high compared to observations (Dorow, 2001). This defect is not found in *FLAME4/3* (figure 2.14, see section 2.6 for details). This difference might explain a part of the slightly different response: The renewal of LADW in *FLAME1/3* is too dense and might lead to an overestimation of the impact of convective events.
Anyhow, the decrease after 15 years of integration remains quite similar. Since the response of the higher resolved version is not available beyond 15 years of integration, it is difficult to estimate its equilibrium state. Döscher et al. (1994) suggest a more rapid response of higher resolution model after changing vertical boundary conditions in the north. Due to the rich spectrum of oscillations possible in an eddy-resolving model, it would generally require a multi-year averaging in connection with a longer integration to define a new statistical equilibrium state.

The response of the overturning function in experiment *NOREST* differs fundamentally to *NOLAB*. Within the integration period of 100 years with the coarse resolution model, no new equilibrium state is reached. In year 2060, the overturning has weakened at about 13.5 Sv, what is about 85%. This can directly be attributed to the loss of density within the northern restoring area (figure 3.3). However, this is indeed no realistic experiment, since the temperature evolution in the Denmark Strait Overflow Water changes by at least 5°C until the year 2080, leading to a reduction of the outflow density of about 0.7 kg/m^3. However, the different role of the two convective areas in these experiments can be distinguished. While switching off the Labrador Sea convection is responsible for a stable 3 Sv reduction of the overturning function, a breakdown of the circulation can be traced back to changes in the density structure north of Iceland. Although not realistic, due to fundamental changes of the temperature and salinity profiles in the Nordic Seas, the weakening does not stabilize in the coarse resolution experiment.
Looking at the results of *NOREST-H*, the experiment cannot be compared directly to the coarse resolution model's results. The reason is the different shape of the restoring area in both models. The southernmost grid point of the sponge in the higher resolution model is approximately at 67°N, enabling deep water formation

due to surface buoyancy loss north of Iceland. Therefore the density of the Denmark Strait Overflow is only reduced at about 0.3 kg/m^3 (not shown). Hence, after 15 years of integration, the overturning is reduced at about 40%(figure 3.4). Due to the limited integration time of experiment *NOREST-H*, the further evolution cannot be estimated. But because of the deep water formation north of Iceland, we do not anticipate an advective spindown like in *NOREST*. However, in spite of the different sponge configuration, the response is very similar in both resolutions.

The green curve in figure 3.4 shows the overturning response of experiment *NOCONVECT*. As in *NOREST*, the artifical forcing leads to a spindown of the circulation until the year 2060. This sensitivity study makes it possible to estimate the interaction between the two upper experiments and hence the linearity of the response in different regions of deep water formation. Combining the relative decrease of *NOLAB* and *NOREST* shows an almost identical response (magenta curve). This hold until the year 2020. Afterwards the state of the ocean is fundamentally changed, so that an interaction between the polar and the subpolar region sets in, leading to a non-linear response. However, in the first 30 years of integrating *FLAME4/3*, the linear contribution of both regional disturbances is very similar.

Since data from a *NOCONVECT*-style experiment with the higher resolution version are not available, no comparison can be made. Figure 3.4 (green dashed curve) shows a linear composition of *NOLAB* and *NOREST* relative to *CTRL-H*. In a realization of this experiment we would expect a less independent response between Nordic Sea and Labrador Sea. The difficulties concerning the salinity in the central Labrador Sea in the higher resolved version are an indication for the lateral impact even if the ocean's state is still close to the situation at the beginning. The interaction in *FLAME4/3*, which becomes important for the overturning function not before the year 2010, when the disturbing lateral signal is quite large (figure 3.3), is expected much earlier due to enhanced eddy transports into the central Labrador Sea in *FLAME1/3*.

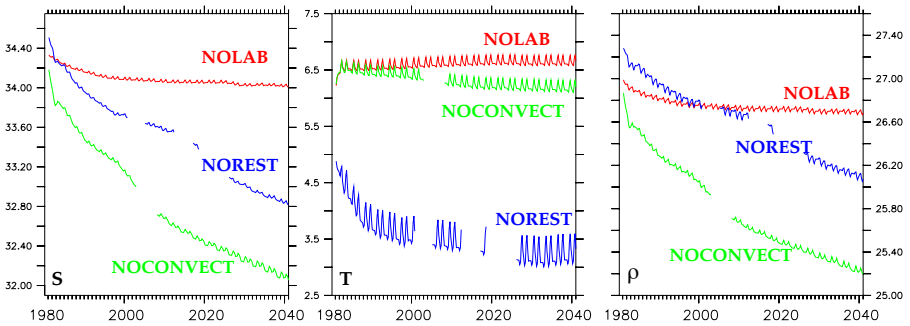

Figure 3.5: *2-year averaged time series of annual mean salinity (left, unit is psu), temperature (middle, unit is °C) and resulting density (right, unit is kg/m^3) in the central Labrador Sea (averaged between 56° N-58° N and 49° W-51° W). The gaps in the time series are corrupt values.*

Using the Labrador Sea tracer distribution as an indicator for such interactions, even in experiment *NOREST* the surface salinity and hence the deep water formation is reduced due to lateral transports of fresh water (figure 3.5, left panel). Since we use mixed boundary conditions in the coarse resolution case, the surface waters following the horizontal gyre are influenced by positive surface freshwater fluxes in that region. In contrast the surface heat flux remains almost constant. Therefore, almost any reduction of surface density in experiment *NOREST* within the Labrador Sea can be ascribed to surface freshening. In experiment *NOCONVECT*, the long-term salinity response is quite similar. Furthermore in experiment *NOLAB*, only a slight reduction of salinity is found, which can be traced back to the instantaneously suppressed sinking of water. When the transport of LADW out of this region is constrained, the local freshening leads to further reduction of salinity.

However, the temperature response is quite different. Since here we use a restoring boundary condition, within the central Labrador Sea the temperatures show almost no trend in experiment *NOREST*, although the state of the ocean changes fundamentally during the integration. Apparently, the surface temperatures are dominated by local heat fluxes and to less extent by lateral transport of properties. Both in experiment *NOLAB* and *NOCONVECT* a quick increase due to the modification of the surface boundary condition is seen. An interesting point after this instantaneous warming is the deviating response in these two experiments in the second part of the integration time. Here, due to fundamental changes of the boundary current system, the Labrador Sea is indeed influenced in experiment *NOCONVECT*.

Finally, the right panel of figure 3.5 shows the resulting density evolution for the three sensitivity studies. The long-term response in the Labrador Sea is indeed given by lateral transports, since the density of *NOREST* and *NOCONVECT* evolve similarly. At shorter time scales the local impact dominates, as it is seen in comparison to *NOLAB* at the beginning of the experiment.

However, the density response within the Labrador Sea and the whole subpolar gyre highly depends on the surface boundary conditions used in this study. Since the higher resolution model is integrated under restoring conditions either for temperature and salinity, the remote effect of lateral transports is damped by surface forcing. The first-order difference between both resolutions is therefore an underestimation of the lateral effects of freshwater anomalies in the full restoring case. However, this could possibly damp the higher lateral transport of water into the Labrador Sea in comparison to *FLAME4/3*.

Anyhow, the overturning response in both resolutions is similar and somehow robust, no matter what type of surface boundary condition is used. However, the artificial impacts in this section are much stronger than any variability expected in experiments with realistic forcing. Therefore a comparable response in *FLAME4/3* and *FLAME1/3* is expected even in greenhouse gas forced experiments.

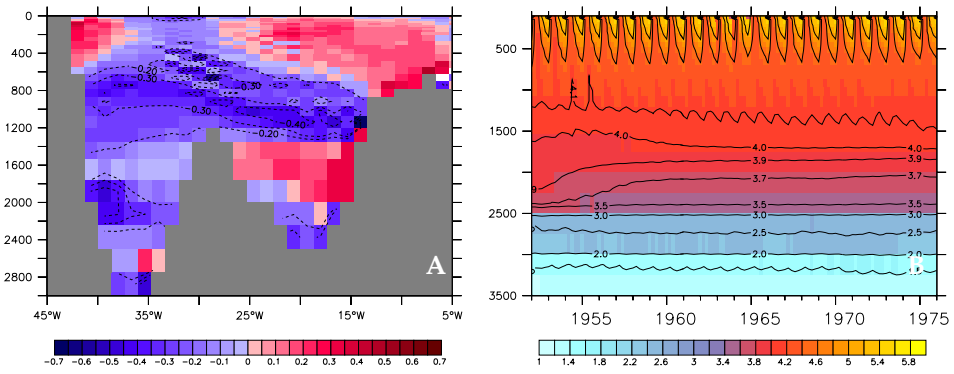

Figure 3.6: *FLAME4/3 temperature response in the signal-spreading experiment with the modified northern boundary condition.* ***A:*** *Vertical section through the Irminger Sea at 60° N 10 years after starting the experiment relative to the beginning.* ***B****:Hovmoeller diagram of the temperature in the central Labrador Sea at 58° N and 50° W between 1952 and 1975; unit is ° C. The Labrador Sea is filled with anomalous cold water from the north.*

3.3 Signal spreading in the North Atlantic

3.3.1 Introduction

In the former section we found the changes in the overflows from the Nordic Seas to be the crucial factor for fundamental changes in the overturning circulation. In comparison to changes in the deep water formation within the subpolar gyre, which accounts in that idealized experiment for about 3 Sv of overturning strength, reducing density in the overflow region is a way to slow down and ultimately interrupt the meridional cell.

In this section, we concentrate on the timescale of the signals spreading into lower latitudes following the Deep Western Boundary Current (DWBC). The question is, how long does it take for a density signal in the specific northern region to have an impact on the overturning circulation at a latitude, where the oceanic heat transport is an important fraction of the total heat transport?

Again we are interested in the point, whether there are differences between higher and lower resolution models, in order to classify the response of *FLAME4/3* in comparison to *FLAME1/3* in the anthropogenic experiments in chapters 4 and 5.

Because in a system with variability in the deep water formation north and south of the sills, the deployment of transport anomalies into the subpolar respective the subtropical gyre is difficult to examine, here we only implemented artificial density anomalies in the overflow waters. Again, like in section 3.2, the signal has a a singular structure in order to be able to trace it as far as possible. Except this modification in the Nordic Seas the ocean model is integrated under climatological forcing for both resolutions.

3.3.2 A dense signal from the Nordic Sea

To investigate the spreading of a density signal from the Nordic Seas, we performed a sensitivity study in which we reduced the restoring temperature in the northern restoring zone by 1°C from one time step to the other. Starting from the reference state of the ocean, we integrated this study for 45 years for the coarse resolution case and for 20 years for *FLAME1/3*. By having a singular switch in the forcing conditions, we are able to follow the signal on its way along the DWBC into the subpolar and subsequently into the subtropical region. For simplicity, we implement this modification uniformly in the whole water column. Although we are mainly interested in the outflow of NADW, this approach might by justifiable, since the main southward signal from that region in the overflow signal. Southward currents near the surface like the East Greenland Current are also affected. In section 3.2 we showed the quite isolated response of convective regions for both model configurations. Hence, the expected response of the overturning function is less due to lateral transports affecting the convective regions within the subpolar gyre but mainly directly due to changes in the density of the overflows. Starting in year 1923 in the higher resolution model and in year 1952 in *FLAME4/3*, we integrated both experiments for at least 15 years. The starting time of these models becomes important for the interpretation of the age-tracer spreading used in the following section.

3.3.3 The response of the temperature field

Figure 3.6 shows the temperature impact due to the modification of the northern sponge zone in the coarse resolution case. In panel (A) the temperature evolution after 10 years in the central Irminger Sea at 60°N is seen. The temperature of the core of the NADW signal, which is at this latitude in a depth between 800 and 1400 m decreased by about 0.4°C. Some warmer patches are also found in this figure. Since we did not increase any temperature relevant parameter, this is traced back to changes in the overturning circulation: By strengthening the northward transport of warm water enhances. In panel (B) a Hovmoeller diagram of the temperature evolution in the central Labrador Sea is shown. Here, changes in the stratification are only found below 1500 m depth. Above, the convective regime in the Labrador Sea is still an nearly undisturbed. Thus, this picture is a further justification for implementing a depth independent signal in the northern sponge term.
30 years after switching on the modified restoring, the temperatures in 2000 m depth are 0.2° cooler. Below 2500 m the temperatures remain unchanged during this integration.

3.3.4 The response of the meridional circulation

Concentrating on the overturning response at 40°N, in *FLAME4/3* a new equilibrium circulation is reached after 9 years of integration. The overturning is 1.5 Sv stronger relative to the climatological state (figure 3.7, right panel). This diag-

nostic is much more difficult for the higher resolution case. Since in *FLAME1/3* the internal variability is much larger due to the eddy activity, it must have been necessary to take the average of an ensemble integration. Here, we can only estimate the response relative to the undisturbed control experiment and find a new equilibrium state after 8-10 years of integration. This is also about 1.5 Sv stronger than the reference state (left panel), but 3 Sv stronger than at the beginning of the experiment. While up to 40°N, in *FLAME4/3* the increase is quite uniformly,

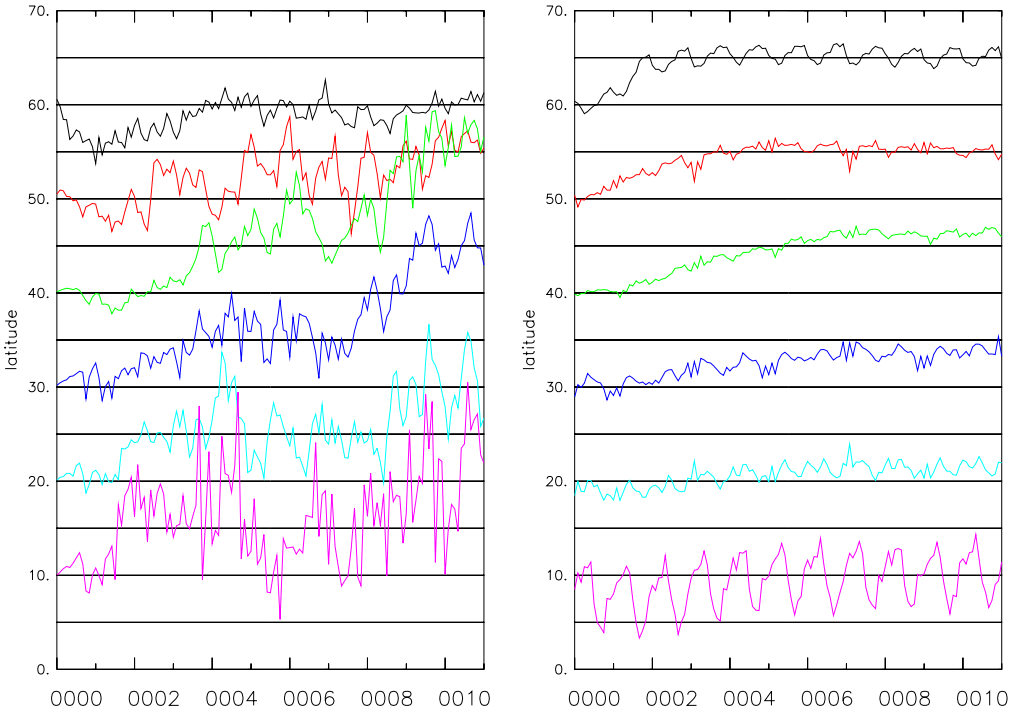

Figure 3.7: *Time series of the vertical maximum overturning response of FLAME1/3 (left) and of FLAME4/3 (right) relative to the control integration for different latitudes, the horizontal lines denote the deviation with a contour interval of 1 Sv. The higher resolved model shows a strong internal variability superposing the response. Anyhow, the spreading timescale is quite similar.*

in the higher resolved model, the gain in overturning is strongest at that latitude and smaller further north. Although the higher internal variability of the circulation in *FLAME1/3* makes it difficult to follow the anomalous overturning signal, up to this latitude a good agreement between both resolutions can be found: It takes about four years of time to communicate the whole overturning increase to 40°N. This timescale is quite slow and is more an advective than a wave propagation timescale. Surprisingly, in *FLAME1/3* and in *FLAME4/3* this scale is nearly identical.

Within the subtropical gyre, the situation is much more difficult. In *FLAME4/3* the signal seems to accelerate. The overturning increase seems to reach 30°N respective 20°N almost at the same time. Further south, the signal has lost a sig-

nificant strength. In *FLAME1/3*, this acceleration can also be found. In contrast, at 10°N, the higher resolved ocean feels the modification of the northern boundary condition. Anyhow, here the communication seems to be much faster. Already after 1.5 years, an increase seems to take place, which is however superposed by high internal variability in the tropical region.
Another difference is the response at 60°N. Here in the coarse resolution model, the spreading of the anomalous overturning strength can already be seen. In contrast, in *FLAME1/3*, a slight decrease of the maximum strength is diagnosed for the first 3 years. Afterwards it reaches its initial state but shows no further strengthening.

Not only the strength but also the vertical structure of the overturning cell in the North Atlantic changes in these experiments. Due to changes in the density distribution the core of the circulation reaches a higher depth. Figure 3.8 shows a vertical view of the spreading of the anomalous overturning strength into the subpolar and subtropical basin. For a better visualization, we calculated the annual mean increase of the experiments relative to the maximum increase for each latitude during the integration period relative to the control integration. For instance, the value "1" in these diagrams is an indicator, that the maximum increase at that latitude is reached at that time.
Both models show the relatively slow deepening of the MOC. In the coarse resolution case (right panel), the spreading seems to be blocked at that latitude somehow, the spreading into the subtropical basin is less intense, what we already found in the vertical maximum. In the higher resolution case (left panel) the deepening of the overturning cell reaches further south. This happens apparently at a somehow advective timescale.
Another interesting point is the overturning response across the sills of the Nordic Seas' basin. Although at that latitude the zonal integral of the meridional velocity is separated into different basins, since the strongest contribution is indeed given by the overflow waters (figure 2.8), it seems to be justified. In *FLAME1/3* a strong signal at the beginning is followed by a situation, in which the circulation is almost identical to the initial situation. Instead of a higher transport the increase of density is responsible for changes further south. In *FLAME4/3*, the situation is again quite similar for the long-term response. As a consequence of the modified boundary condition, not the circulation, but only the density is modified. However, an initial response like in *FLAME1/3* cannot be found in the coarse resolution model.

Anyhow, much investigation is addicted to the mechanisms of signal spreading in the ocean. Johnson and Marshall (2002) integrated a reduced gravity ocean model to determine the timescale of the ocean's response to a change in the thermohaline forcing. Starting with an ocean at rest, they switched on a thermohaline overturning of 10 Sv. Like Kawase (1987), they found a fast coastal Kelvin wave response, which reaches the equator on a monthly timescale. Upon reaching 0°N, the signal crosses the equator as an equatorial Kelvin wave. The coastal Kelvin wave at the eastern coast of the basin travels both northward and southward. The interior adjustment is provided the radiation of the westward propagation of Rossby wave. After this quick response, the long-term adjustment in Johnson's

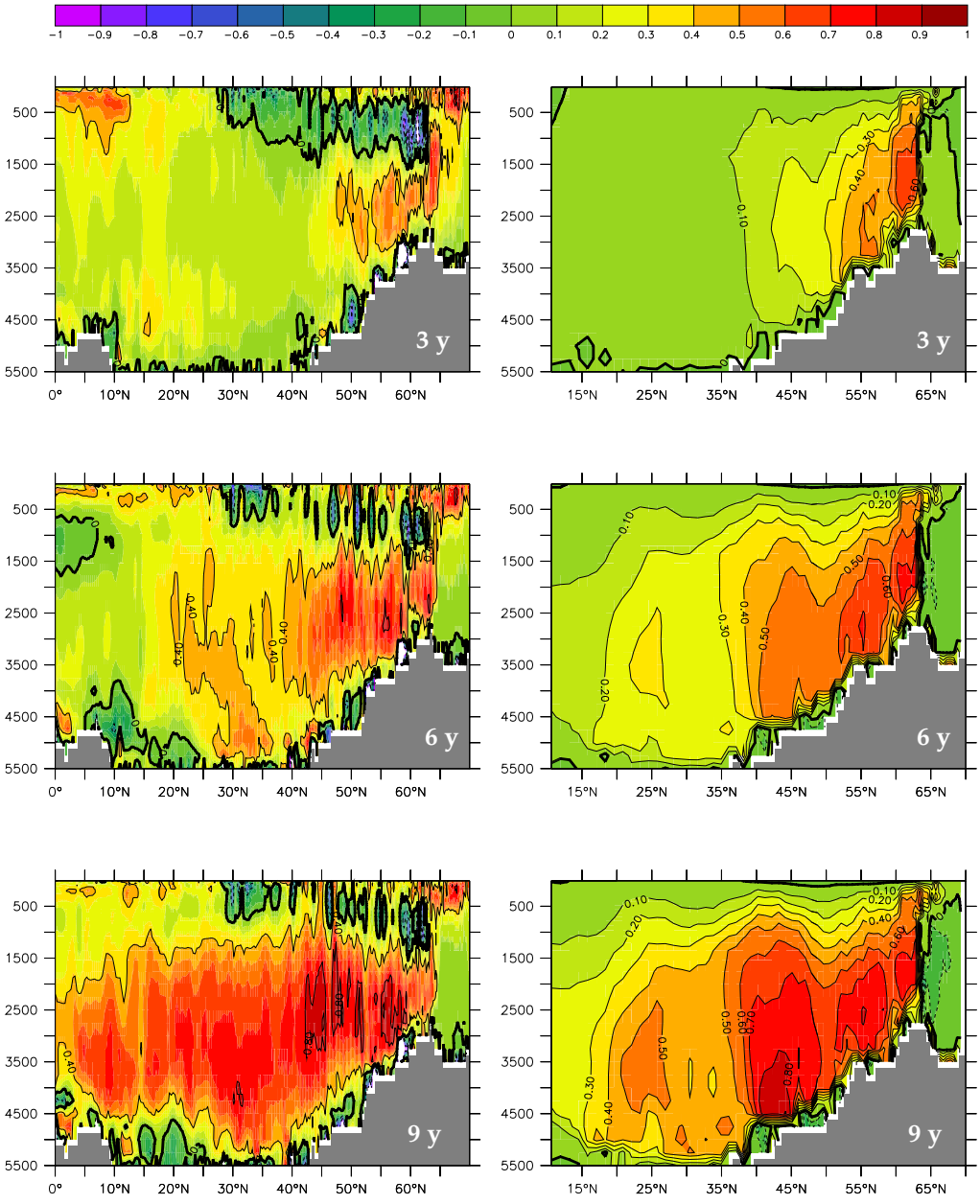

Figure 3.8: *FLAME1/3 (left) and FLAME4/3 (right):The evolution of the overturning function relative to the maximum annual mean value during the integration period. The years denoted in the figure give the elapsed time since the implementation of the minus-one-degree northern restoring condition.*

model takes about 12 years. However, in their model is highly idealized, since no complex stratification and basin geometry as well as realistic forcing structure is used. Anyhow, results from DÖSCHER ET AL. (1994) with a OGCM in two different resolutions showed a similar result: The adjustment to a new quasi equilibrium is attained in less than two decades. The mechanism leading to this adjustment was

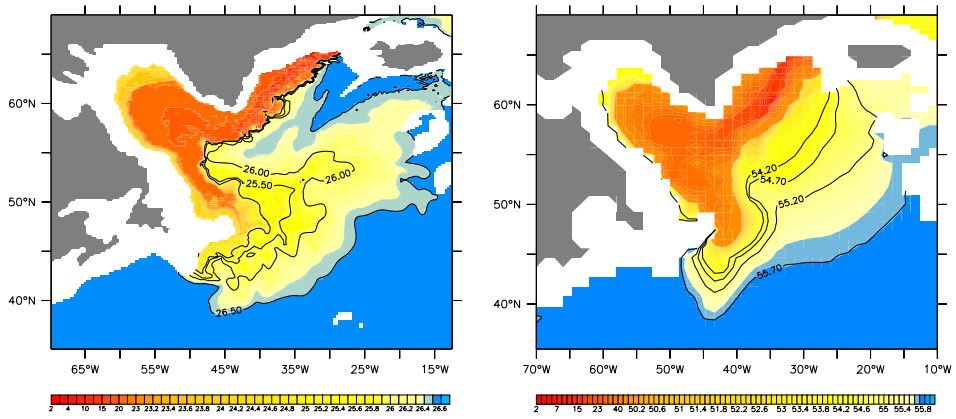

Figure 3.9: *Age tracer* [2] *distribution in the NADW signal after four years of integration for FLAME1/3 (right) and FLAME4/3 (left). Note, that the individual time labels denoted in the figure depend on the starting time of the tracer experiments.*

found to be wave dynamics.
However, the timescale we found in the two experiments above goes with the advective timescale of a tracer spreading in the Deep Western Boundary Current north of 40°N. Figure 3.9 shows the spreading of an age tracer 5 years after starting the integration. Surprisingly, the southward spreading is very similar in *FLAME4/3* and in *FLAME1/3*. Although in the higher resolution case, the deep current velocities are much higher, recirculation pattern seem to prohibit a quicker dispersion. To detect the responsible mechanism Eden and Greatbatch (2003) used a semi-prognostic approach. By integrating an OGCM with a modified density equation, they are able to control wave speed. This modification is a linear combination of the free model density and certain specified density. In their integration, controlling the wave speed leads to no different timescale of a signal evolution in the North Atlantic north of 40°N. Their argumentation is that therefore the spreading can be traced back to advective processes.
However, further south, the mechanism seems to be much more difficult.

As a short summary of this section, we find three different timescales in the available experiments. The first one is the wave signal, reaching the equator in several months in a 1/3° model and in two years in a 1° configuration, as it is already found in Döscher et al. (1994). This one is not discussed here. The slowest is the advective timescale of the Deep Western Boundary Current. A tracer induced in the Denmark Strait Overflow needs about 35 years to reach the equator in our coarse resolution model (figure 3.10). Somewhere in between these two is the spreading timescale of a density signal of about 10 years. This can be called "dynamical", since this is the timescale for a density signal to be communicated

[2] The source region of the age tracer is between 66°N – 67.5°N and 38°W – 20°N below 300 m in water colder than 1.5°C in boxes with southward velocity. It is restored to a value of zero with a timescale of 1 time step in this source region.

from the Nordic Seas into tropical regions as it is seen in the adjustment process of the overturning cell in figure 3.8.
The important result of this section is indeed the similar response scale of both resolutions on fundamental changes in the Nordic Seas water mass properties. Up to 40°N, it takes four years for an overturning anomaly both in *FLAME4/3* and *FLAME1/3*. Further south, the response of the coarse resolution model is much weaker, but a similar timescale can still be found.

3.4 Consequences

These idealized hierarchy of experiments with both the coarse and the higher resolution version of *FLAME* models show the important point, that the overturning circulation in both resolutions responds quite similar to fundamental (and artificial) changes in the boundary forcing. Although the integration period with *FLAME1/3* was limited, changes in the overturning function in terms of strength and timescale, at least within 15 years of integration, are comparable.
Therefore forcing the coarse resolution model instead of *FLAME1/3* with anthropogenic fluxes in chapter 4 and 5 seems to be justified. The sensitivity studies of this chapter are expected to have much greater impact on the meridional circulation than any of the (more realistic) global warming simulations (e.g. a warming of the DSOW by about 4°C in 100 years). Therefore, the general response of the THC in *FLAME4/3* under greenhouse gas forcing is expected to be similar to the behaviour of the higher resolved version, since the models remain closer to the climatological state.

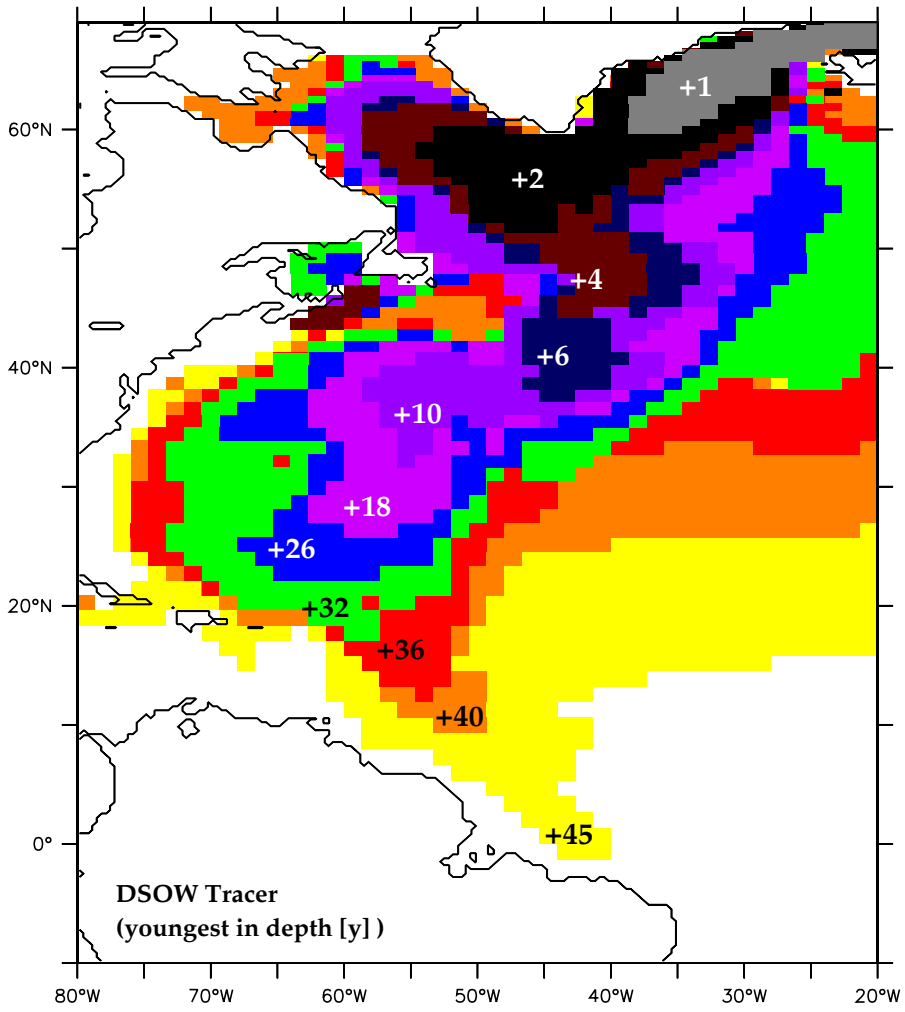

Figure 3.10: *FLAME4/3: The Denmark Strait Overflow tracer spreading in the North Atlantic Ocean; shown is the horizontal position of the youngest water in the water column at the time denoted in the figure.*

Chapter 4

Experiments with ECHAM4/OPYC3 fluxes

4.1 Introduction

Instead of artifical modifications to the forcing, in this chapter the ocean model is forced with anthropogenic fluxes, diagnosed in a coupled global warming simulation. The first scenario which is investigated is integrated with the

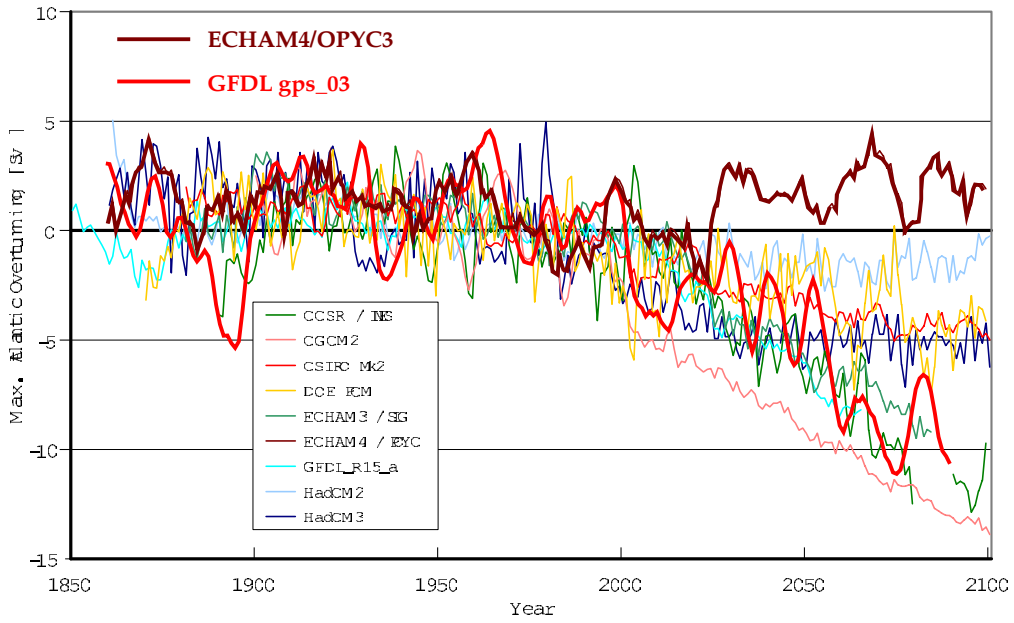

Figure 4.1: *Time series of the maximum overturning function in the North Atlantic ocean in several GCMs, unit is Sv (source:* IPCC 2001*), the index of ECHAM4/OPYC3 is brown, the index of the GFDL model in the gps03 experiment we investigate in chapter 5 is overlaid in red. The prognoses of the different climate simulations are quite different.*

ECHAM4/OPYC3 climate model (hereafter *MPI* model). In contrast to most climate models, this coupled model shows no significant weakening of the meridional overturning circulation in the Atlantic Ocean in a global warming simulation, as it is seen in figure 4.1 (brown curve).

In contrast, in most climate models, the reason for slowing down of the overturning circulation is the anomalous warming and freshening in high latitudes, leading to a reduction of open ocean convection and hence of the thermohaline circulation (e.g. Broecker, 1987). In the *MPI* model, large scale atmospheric interactions between the Atlantic and the Pacific Ocean lead to great pattern of enhanced evaporation in the tropical and subtropical Atlantic. Therefore the surface salinity is fundamentally enhanced. This anomalous signal is spread in the North Atlantic basin, leading to strongly enhanced salinities as well in regions of deep water formation (Latif et al., 2000). This effect compensates the local warming and freshening from the atmosphere, serving for a nearly undisturbed rate of renewal of dense water.

The objectives of this chapter are to focus on the differing response of the THC by forcing *FLAME4/3* with diagnosed fluxes of the *MPI* simulation. Integrating a higher resolution model, we are able to detect whether the deviating response of the *OPYC* ocean component still holds for a more realistic ocean model. In this connection, we concentrate on the detection of the crucial mechanism for this differing response by switching off certain components of atmospheric forcing in the uncoupled ocean model. Moreover, since the Labrador Sea is known as a region of strong convective variability and is therefore possibly an important region for variability in the overturning circulation, we attend to the specific response of this area within the subpolar gyre. This is possible, because in contrast to the *OPYC* ocean, the more realistic representation of the mean circulation and the distinction between different regions of deep water formation allow an estimation of the regional impact for the Labrador Sea.
In section 4.2, a brief description of the *ECHAM4/OPYC3* coupled model and of the anthropogenic fluxes diagnosed in this specific greenhouse integration are given. The experiments we performed with certain combinations of anthropogenic forcing are described in section 4.3; section 4.4 contains some aspects of the anthropogenic surface forcing. The response of *FLAME4/3* in terms of tracer distribution and overturning impact of the different components of surface forcing for the THC is shown in sections 4.5 and 4.6. Furthermore, section 4.7 includes the specific response in the Labrador Sea. Section 4.8 summarizes the results. Finally, in section 4.9 the results and some caveats of our method are discussed.

4.2 The ECHAM4/OPYC3 climate model

4.2.1 Technical aspects

The ocean component *OPYC3* is an updated version of the isopycnal model developed by Oberhuber (1993). The horizontal resolution is $2.8° \times 2.8°$. A special feature compared to other CGCMs is the high meridional resolution of $0.5°$ used

in the tropical oceans, which permits a rather realistic simulation of the ENSO phenomenon in seasonal forecasts.
In order to simulate the ocean interior as nearly conservative fluid with water mass propagation nearly along isopycnals, the concept of an isopycnal vertical coordinate is chosen. Additionally, a surface mixed-layer model is coupled to the ocean, to overcome the problem that this concept of conservative fluids fails in near surface regions of significant turbulence activity. This assures a more realistic response of the mixed layer depth to atmospheric forcing.

To represent the feedback mechanisms in high latitudes as realistic as possible, a sea ice model with rheology is included. This assures the winter-time decoupling of the ocean from the atmosphere in high latitudes and treats the salinity forcing due to melting and freshening of sea ice, which can have an enormous impact on the mechanism of deep water formation, quite realistic. The configuration of the *MPI model* in its greenhouse warming scenario is capaciously described in A.Bacher et al. (1998).

The atmospheric component *ECHAM4* has been developed based on the ECMWF atmospheric model. It has 19 vertical atmospheric layers and uses the T42 horizontal resolution, which approximates to about $2.8° \times 2.8°$. It is part of the *ECHAM* model line (Roeckner et al., 1992), the development regarding the model physics and a description of the simulated climate of the obtained with the uncoupled *ECHAM4* model is given in Roeckner et al. (1996). The initial conditions at the ocean surface originate from the COLA/CAC AMIP SST and the sea ice data set. The topography is supplied by the US Navy high resolution data set.

4.2.2 Anthropogenic forcing

The forcing fields used in the chapter originate from a global warming integration of the *MPI* model integrated between 1860 and 2100. This coupled experiment uses historical greenhouse gas forcing from 1860 to 1990 (Roeckner et al., 1999) followed by a 1% annual increase in radiative forcing after the IPCC IS92a scenario (IPCC 1992) from 1990 to 2100. This scenario is slower than our current 3 % increase of greenhouse gas forcing, reflecting a slowing of economic growth and incorporation of some conservation measures. In this integration, the direct as well as the indirect effect of anthropogenic sulfate emissions are not included.

4.3 Experiments with MPI output

We performed several experiments with an integration period of 150 years. Starting in years 1950, we used different combinations of anthropogenic forcing diagnosed in the *MPI* model global warming integration, which are listed in table 4.1 and shortly described in the following. To have a control run, we performed an integration without any anthropogenic forcing, in order to have a reference run for all sensitivity experiments. Some of the features derived in this experiment we used

in section 2.6. Since the *FLAME4/3* is not eddy resolving, this integration shows very low internal variability on interannual to interdecadal timescales, which is in contrast to the higher resolution models.

CO2

In this experiment, the complete set of anthropogenic forcing diagnosed from the global warming experiment with *ECHAM4/OPYC3* is used. This experiment is the direct approach to estimate the anomalous response of an ocean with a much more realistic state when it is forced by the same atmospheric fluxes.

NOFRESH

The remarkable point of this specific greenhouse integration is the persistence of the overturning strength in spite of local warming and freshening. The reason for this behaviour in the climate model are strong evaporation rates in tropical and subtropical regions. The anomalous high salinity signals follow the mean circulation. Entering regions of deep water formation, they density budget is balanced in some sense in order to allow further deep water formation and consecutively maintaining overturning strength (LATIF ET AL., 2000).
To prove this specific role of the ocean for a more realistic basin, we calculated experiment *NOFRESH*, in which we switched off all anomalous forcing concerning the salinity in the model. This is the surface freshwater flux, where we used the climatological fields as well as the salinity anomalies within the vertical boundaries. A deviating result of this integration relative to experiment *CO2* can answer the question, whether the salinity being the crucial factor is robust as well in ocean models of a more realistic style.

NOFRESHSURF

The second sensitivity experiment is performed in order to study the role of different regions of deep water formation. Hence we used the climatological surface freshwater fluxes, but used the anomalous salinity time series in the northern vertical boundary zone. Doing this the transmitted signal is a slight decrease of salinity

Name	***Surface***			***Vert. BC***	
	Heat	**Freshw.**	**Wind**	**Tmp.**	**Salt**
CTRL	off	off	off	off	off
CO2	on	on	on	on	on
NOFRESH	on	off	on	on	off
NOFRESHSURF	on	off	on	on	on

Table 4.1: Experiments performed with *FLAME 4/3* and *MPI* model forcing anomalies between 1950 and 2100.

due to local forcing followed by a strong salinity increase due to the anomalous advective signal. Since we use a restoring boundary condition, this salt anomaly in the sponge region is as strong as in experiment *CO2*, were the salt time series is the result of both advective and local effects.

4.4 MPI fluxes in *FLAME4/3*

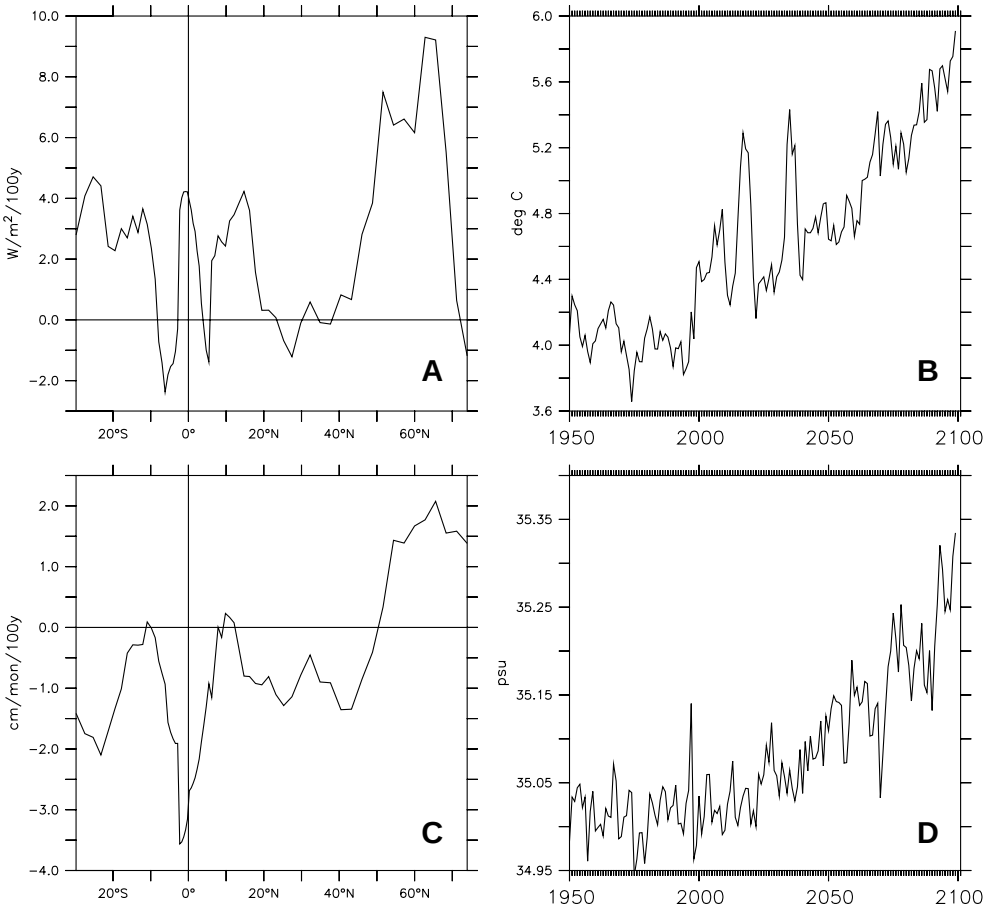

Figure 4.2: *Warming scenario data in the* MPI model *between 2000 and 2100:* **A***: Zonally averaged heat flux trend in* $W/m^2/100y$*;* **B***: Temperature at* $70°N/20°W$ *in 600m depth in* $°C$*;* **C***: Zonally averaged freshwater flux trend in* $cm/mon/100y$*;* **C***: Salinity at 70° N/20° W in 600m depth in psu. Large interhemispheric interactions lead to strong evaporation rates in the lower latitudes of the Atlantic Ocean.*

The main difference between the *MPI* model and other CGCMs in global warming circulations is the strongly enhanced hydrological cycle in the tropical and subtropical regions leading to a reduced freshwater flux into ocean by about $-0.3Sv$, whereas in middle and high latitudes the freshwater flux is similar to other global warming integrations and enhances at about $0.1Sv$ during 1950 and 2100 (Latif et al., 2000). Figure 4.2 shows the anthropogenic forcing felt by *FLAME4/3*. The

increase in heat flux over the North Atlantic ocean (A) is strongest between 45°N and 65°N. Both in lower and higher latitudes, the heat flux gain is less. While in regions north of 65°N the missing of additional heating can be attributed to a reduced sea ice extent, in the tropics respective subtropics this can be traced back to the strongly enhanced evaporation in this areas (C), counteracting the anthropogenic heating.
Looking at the response of the hydrological cycle during the global warming scenario (C) in the domain of the North Atlantic, the area can be split into a region north of 50°N with increased freshwater fluxes and a region in the tropics and subtropics with strongly enhanced evaporation and reduced fluxes into the ocean. LATIF ascribes this special feature to large air-sea interactions in the tropics of the Atlantic and Pacific Ocean.
Concerning the vertical boundary conditions, since we use the salt and temperature fields of the *MPI* model for the restoring in those regions of *FLAME 4/3*, the evolution of salinity and temperature of the coupled integration at the boundaries of the regional model acts as a forcing term (see section 2.3 for details). At the northern boundary of the ocean model at 70°N/20°W in 600m, the temperature of the *OPYC* ocean is raising from 4°C to almost 6°C between 2000 and 2100 (Figure 4.2,B). In comparison to insitu profiles, the temperature is about 2°C too warm, before the anthropogenic forcing sets in (e.g. DICKSON AND BROWN, 1994) The time series of the salinity at that point shows a similar shape (D). After a slight decrease until year 2010, a strong increase of about 0.3 psu until the year 2100 starts to evolve. The origin can be traced back to a signal in the lower latitudes, advecting into regions of deep water formation, because in the northern North Atlantic, there is no additional decrease of surface freshwater at the ocean surface (C), which could lead to increasing salinities (LATIF ET AL., 2000).

4.5 Salinity and temperature response

Forced by these anomalous fluxes, the response of the *FLAME 4/3* ocean in terms of the salinity evolution is very comparable to the coupled integration: A strong salt anomaly develops within the subtropical gyre after the year 2000 and accumulates at about 30°N (figure 4.3). Already at that stage, the salinity in the subpolar gyre of the *MPI* model is at about 0.6 higher than in *FLAME4/3*. This feature is not the result of any response during the global warming integration but can also be found in the *ECHAM4/OPYC3* control integration (not shown here) as a problem of the mean state.

The anthropogenic salt signal follows the mean circulation into the north and reaches the GIN Seas at about 2007 (figure 4.5, upper panel) at a somehow diffusive mean velocity scale of about $1 cm/s$. It results in a salinity increase in the whole North Atlantic (figure 4.4). Since due to the enormous extent of this gain in ocean salinity, it cannot be characterized as an anomalous signal spreading on an advective timescale. At that point the slight local freshening due to anthropogenic surface forcing turns into an increase in salinity, which can also be found in the

core of the Denmark Strait Overflow a few years later (Figure 4.5, A). Comparing the salinity gain at different latitudes of the North Atlantic ocean, it is strongest along the Gulf Stream between 25°N and 35°N, has a local minimum along the North Atlantic drift and finally is again strong in the region around Iceland (B), where the salinity is enhanced at some points at about 0.4 psu at the end of the integration period.

The communication of water from the Nordic Seas into the subpolar gyre is mainly achieved through the narrow passages of the Denmark Strait and the Iceland-Scotland Overflow. Therefore the core of the Denmark Strait Overflow is chosen as an indicator for changes in the tracer contribution in the northern basin. Looking at the compensating effect of increasing temperature and salinity the huge salt signal counteracts the density loss due to the locally increasing temperature (Figure 4.5, B), so that the Denmark Strait Overflows maintains its density during the integration time (C).

Beside the stabilizing signal from the south, even on timescales of a few years, a compensating effect of salinity and temperature can be found, leading to a quite smooth time series of the overflow density without much variability compared to the individual curves. This can be attributed to the local temperature evaporation feedback in high latitudes: Higher surface temperatures lead to enhanced evaporation and higher surface salinity. This response is often found in climate models (e.g. GFDL, section 5.5.4).

As a consequence of the increased salinity transported into the region north of Iceland, not even the overflows but also the East Greenland Current of *FLAME 4/3* becomes saltier, following the boundary currents into the Labrador Sea (figure 4.4). Nevertheless, the central Labrador Sea is mainly unaffected before 2040 (figure 4.5, A) and the formation of Labrador Sea Deep Water (LADW) is cut off after 2035 with mixed layer depths of less then 300 m in March (Figure 4.9, line) due to local heating and freshening (Figure 4.5, B). We will focus on the particular

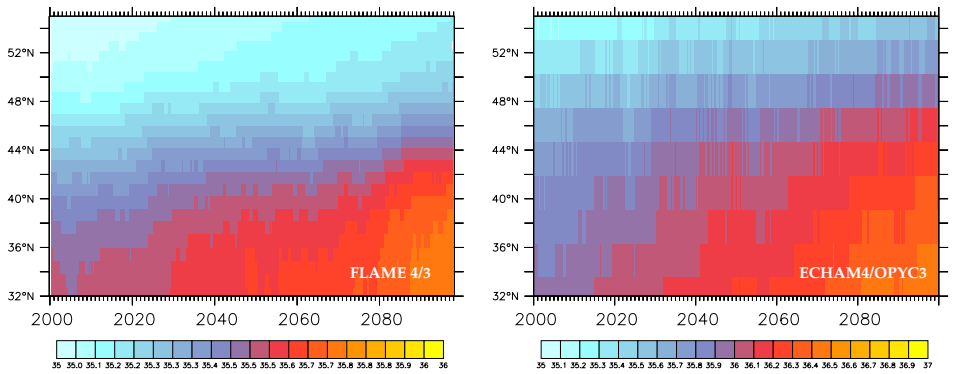

Figure 4.3: *Temporal evolution of salinity between 2000 and 2100 at 35° W in 500 m depth of experiment CO2 (left) and the MPI model (right) psu. The labeling of the color bars is different. Unit is psu. The evolution in the climate model and FLAME4/3 is quite similar.*

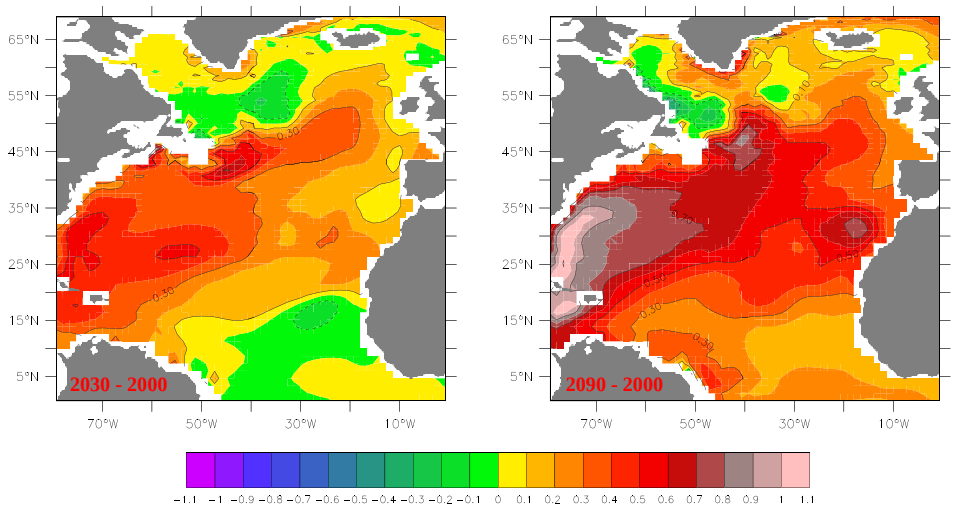

Figure 4.4: *Salinity difference between year 2000 and 2030 (left panel) respective 2090 (right panel) in experiment CO2 of FLAME 4/3 in 100 m depth. The whole North Atlantic is affected by the anomalous salt signal.*

response within the Labrador Sea in the different sensitivity studies in the section 4.7.

4.6 The overturning response

4.6.1 The stabile behaviour

To compare the response of the thermohaline circulation in the ocean model when forced with anthropogenic fluxes, in figure 4.6 the anomalies of the Atlantic overturning at 40°N in 1000 m depth as an indicator for changes within the ocean is shown.

Like in the *MPI* model, using the full set of anomalous forcing in *FLAME4/3* (experiment *CO2*), also shows no significant trend of the thermohaline index (figure 4.6, A). In comparison to the *CTRL* experiment, there is indeed a slight reduction of about 1.5 Sv between the years 2015 and 2030, what can be attributed to the shut down of the deep water formation in the region of the central Labrador Sea. This response is very similar to the changes in the *HadCM3* coupled model, in which the Labrador Sea convection is shut off during the integration period, going along with a slight reduction of the index (Wood et al., 1999).
In the second half of the 21^{st} century, experiment *CO2* falls into a new quasi-equilibrium state of 14.5 Sv. Although the anthropogenic forcing is still increasing, this situation remains stable until the end of the century. In contrast to the *MPI* model, the strong variability on timescales of about 40 years with an amplitude of 2 Sv (figure 4.6, B) cannot be reproduced in *FLAME4/3*. The reason for this cannot be extracted comparing these two integrations.
In former studies (Eden and Willebrand, 2001; Döscher and Redler, 1997)

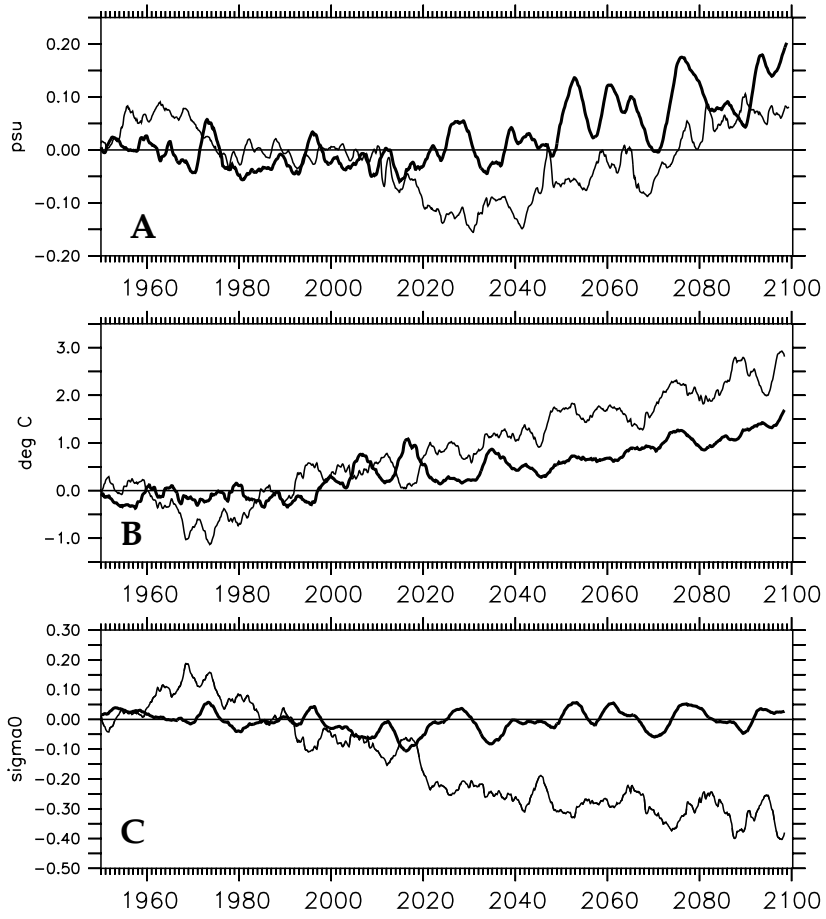

Figure 4.5: *2-year averaged anomalous time series of experiment CO2: Salinity* **(A)**, *Temperature* **(B)**, σ_Θ**(C)**, *in the Labrador Sea at 58° N/50° W at the surface (thin line) and in the core of the Denmark Strait Overflow at 66° N/32° W in 500 m depth (thick line). In the Denmark Strait, salinity changes compensate temperature changes, whereas in the Labrador Sea, the temperature effect dominates.*

as well as in the idealized experiments in chapter 3 we found the strong dependency of the overturning strength from the density provided within the Labrador Sea respective the overflows.

Looking again at figure 4.5, C shows the relative constant density of the Denmark Strait Overflow due to the compensating effect of salinity and temperature in the outflow region. In contrast, the surface density in the Labrador Sea is reduced at about $0.4\,kg/m^3$ mainly due to local warming, leading to a shut down of deep water formation. The density signal of the overflow does not show this strong variability on a 40-years timescale we would expect looking at the overturning index of the *MPI* model. Therefore we can only speculate about this feature. Since none of the anomalous boundary conditions forcing experiment *CO2* shows this variability, we ascribe it to an internal mode of the coupled model.

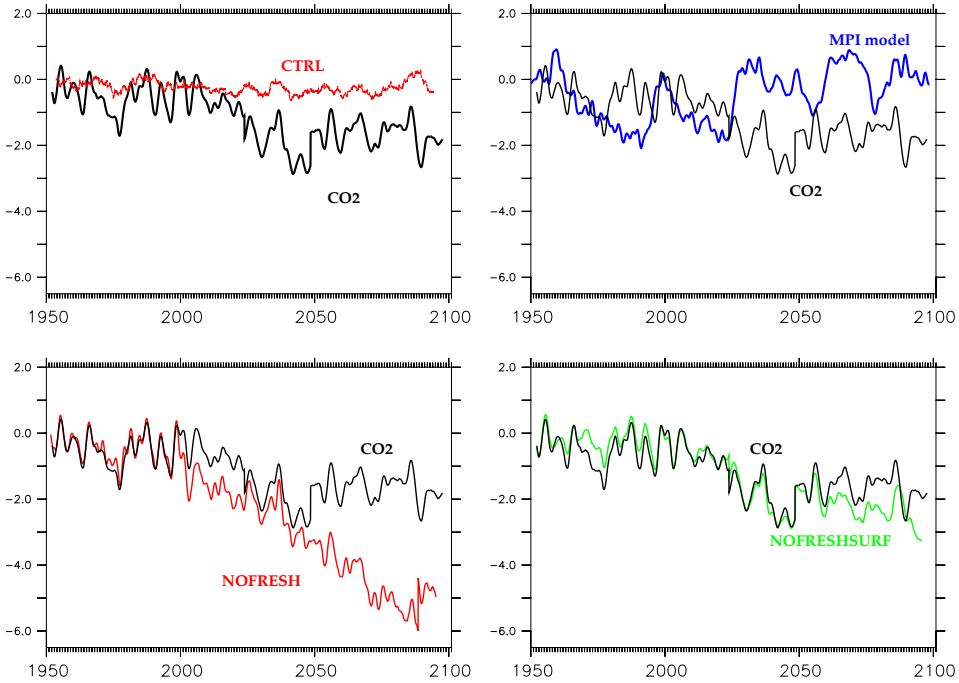

Figure 4.6: *Time series of the anomalous overturning at 40° N in 1000 m in integrations performed with diagnosed fluxes from the MPI model global warming simulations. The experiments are denoted in the figure, unit in Sv. The general response of FLAME4/3 is similar to the climate model, salinity changes indeed stabilize the circulation.*

4.6.2 Saline stabilization

In *NOFRESH*, all anomalies concerning changes in ocean's salinity, where switched off. Here LATIF's result of the stabilizing effect of the salt signal in experiment *CO2* is tested for the higher resolution *FLAME4/3* model. This sensitivity study allows to analyze the role of the changes in the hydrological cycle in *CO2* during the global warming experiment.

The total heat budget of the model's ocean is raising like in *CO2*, whereas the total salt budget stays conserved. Any response of the salinity in the northern sponge zone of *FLAME4/3* on *local* forcing cannot be included in this model. Because the wind driven circulation is mainly unchanged (not shown here), the horizontal distribution of heat is very similar to the upper experiment.

Any change in the meridional overturning circulation in this experiment can be attributed to a modification of sea surface density as a consequence of increased atmospheric heat fluxes.

Contrary to experiment *CO2*, the THC slows down after the year 2005 quasi linearly (Figure 4.6, C) . Due to the temperature effect only, after the year 2080 the overturning is reduced at 6 Sv, what is about 30% of its strength at the beginning. However, a separation of both the lateral and the local effects on the salinity cannot

be done exactly. Due to the style of experiment *NOFRESH*, a slight reduction of salinity in the Nordic Seas as the result of local freshening, which can be seen before the year 2010, is not included. Therefore an experiment in which this local effect can be separated, could result in a reduction of the overturning index, which might even be stronger than it is in experiment *NOFRESH*. To approximated this possible response, we performed a sensitivity study, in which we reduced the sponge salinity until the year 2100 with the trend extracted between 1980 and 2010 (not shown here). The result is reduction at about 7 Sv until the end of the integration period. Eliminating the stabilization due to the enormous salt signal, this dominating temperature impact in the *MPI* model on the strength of the overturning circulation is quite similar to results of Mikolajewicz and Voss (2000) (see section 5.5.2).
We can also extract the well-known temperature-driven response within the Labrador Sea: Switching off the anomalous freshwater fluxes into this region of deep water formation does not prevent the Labrador See deep water formation to maintain during the 21^{st} century.

4.6.3 Different regions of Deep Water formation

In experiment *NOFRESHSURF*, the anomalous surface freshwater forcing term was switched off, while the lateral boundary in the north still include the changes in salt of the *MPI* model (Figure 4.5, C) as an impact on the hydrological cycle. After a slight reduction of salinity until about year 2007, this boundary condition takes effect as an internal salt source for the model's domain at the northern boundary, matching the density loss due to increasing temperatures in the northern restoring area. Following *NOFRESH*, the salt anomaly moving northward into the regions of deep water formation was detected to be the crucial mechanism to stabilize the THC. Moreover *NOFRESHSURF* might answer the question, at which state of the northward spreading this effect starts to become effective.
Looking at the thermohaline index of this experiment, the response is an almost complete conservation of the strength of the THC (Figure 4.6, D). Just including the density signal in the northern sponge area gives the *FLAME4/3* model the ability to stabilize the circulation.
Again, like in the two previous experiments the Labrador Sea cannot be stabilized, the local warming signal dominates the response. This experiment shows the dominate role of the density flux of the overflow waters for the strength of the meridional overturning cell and puts the role of entrainment south of the sills for the thickness of the NADW tongue for our model into perspective.

4.7 The Labrador Sea under MPI forcing

Within the subpolar gyre, the Labrador Sea is a region with strong variability in deep convection events (e.g. Rhein et al., 2002; Lilly et al., 1999).

Its impact on the strength of the overturning circulation is investigated in many OGCMs. Forcing *FLAME4/3* with NCEP data between 1958 and 1997, Eden

AND WILLEBRAND (2001) found a maximum amplitude of about 1.5 Sv between periods of strong deep water formation and years, when the deep convection is suppressed. Furthermore, we showed in section 3.2 a maximum reduction of 3 Sv in an experiment, in which the convection is suppressed artificially over the extended Labrador Sea.

Investigating the response of the Labrador Sea in global warming scenarios is a difficult point to study in most coupled models. Due to their coarse horizontal ocean resolution (often at about 2.5°), there are only a few models, in which the regions of deep water formation match the observations. In most climate models, there is a region "somewhere in the north", where deep convection takes place. So in *ECHAM4/OPYC3* the deep water formation is localized mainly in the Nordic Seas, the subpolar region is mainly unaffected.

However, in recent coupled model's integrations, more realistic regions of deep water formation can be found. With this improvement, questions concerning the impact of anthropogenic forcing in different regions of NADW formation can be investigated.

WOOD ET AL. (1999) found in the *HadCM3* model a reduction of the overturning function at about 20% (figure 4.1, dark blue curve). The reason is a collapse of the deep water formation within the Labrador Sea between 1999 and 2029 together with slightly decreasing density of water communicated into the subpolar during the 21^{st} century. As a consequence of the changes in the Labrador Sea, here the cyclonic circulation around the stops. So RAHMSTORF (1999) mentioned, that not only the strength of the overturning circulation, but also the contribution to the deep branch of the NADW might change.

In the climatological integration, the *FLAME4/3* model shows deep water formation in the subpolar gyre both in the Irminger Sea and the Labrador Sea. In this section we examine the response of the Labrador Sea as the region of the deepest convection activity on the greenhouse warming scenario. Because the wind stress shows no significant change in the 21^{st} century of the *ECHAM4* atmosphere in the coupled integration over the North Atlantic, even in this regional study we concentrate on the changes of sea surface density due to local fluxes and lateral signals for the subpolar region of the Labrador Sea.

The ocean of the *MPI* model has no explicit formation of LADW during the whole integration period. Moreover, the deep water formation can be mainly be localized in the region north of Iceland. Looking at the structure of overturning function of the *MPI* model (figure 5.1), we find the underestimated relevance of the subpolar gyre. Instead, the GIN Seas are the crucial region where deep water formation takes place, going along a unrealistic high southward transport into the subpolar region. The reason for the absence of deep convection in the central Labrador Sea can be attributed to the horizontal circulation near the surface (vectors of figure 4.7, left panel), which is more like a branch of the Gulf Stream than a cyclonic gyre formed by the Greenland and Labrador Current, transporting too warm water in this area to permit convection. Looking at the development of the near surface density, the *MPI* model shows the impact of an unrealistic pattern on the system, even if there are no convection processes to be stabilized in the climate model's

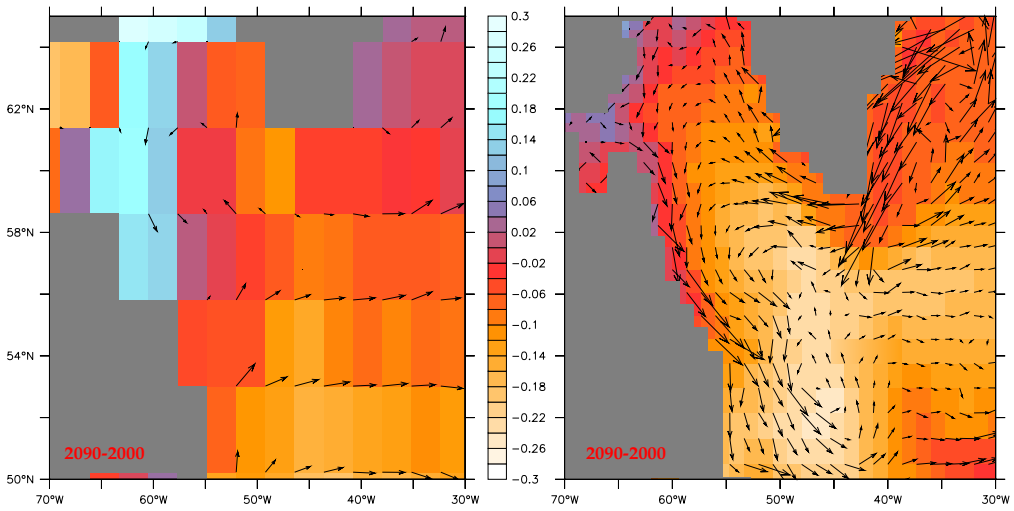

Figure 4.7: *Difference in sea surface density between 2000 and 2100 within the Labrador Sea of MPI (left panel) and CO2 (right panel) in* kg/m^3*. Overlaid are the current velocities between 0-100 m, demonstrating the much higher resolution and consequently more detailed flow field in FLAME4/3.*

Labrador Sea:

A spreading salt anomaly from lower latitudes into the subpolar region reaches the Labrador Sea on its direct path northward and counteracts local decreased surface density fluxes. The result is an only moderate loss of surface density (Figure 4.7, left panel) and hence to an only moderate stabilization of the water column.

In contrast, *CO2* exposes the different response of surface density (Figure 4.5, C) due to a more realistic horizontal circulation at the surface (vectors of figure 4.7, right panel). Apparently, in our model there is no direct connection between the lower latitudes and the Labrador Sea, because any signal spreading from the south follows the subpolar gyre along the North Atlantic Current before entering this area. For that reason, the upper stratification and consecutively the formation of LADW is determined by changes in local fluxes of mainly heat and freshwater. To a certain degree the *preconditioning* mechanism by signals only from the north is an effect as well, although in *FLAME4/3* it seems to be underestimated (see section 2.6.2).

The enhanced surface fluxes together with the warmer and before 2010 slightly fresher East Greenland Current lead to a reduction of surface density (figure 4.5, C) and therefore to a complete shut down of convection within 10 years between 2025 and 2035, when the mixed layer depth allows no more deep water formation (figure 4.9, line). Figure 4.8 shows the evolution of the density structure through the central Labrador Sea at certain time steps of the integration period in March. While during the second half of the 20^{th} century the isopycnal limiting the LADW, after the year 2025 the increasing temperatures lead to stabilization of the water column, so that the renewal is shut off. In the same time the deep basin is filled

with dense NADW coming from the north.
WOOD ET AL. (1999) found in an integration of the *HadCM3* model something interesting in a comparable global warming simulation. When the Labrador convection stops and the overflow density decreases, the circulation around the Labrador Sea also is breaks down. The reason for this response is that the overflow waters become lighter than the interior deep basin, unable to reach this region, so that the cyclonic circulation collapses. However, we cannot find this behaviour in any of the experiments with *MPI* forcing, not even in experiment *NOFRESH*, where the overflows indeed become lighter. Also in the greenhouse gas forcing experiments with *GFDL* fluxes in chapter 5, where in most of the integrations the density of the overflows become lighter, a collapse of the horizontal circulation in the Labrador Sea cannot be found, when the wind-driven gyre is still existant.

The salt anomaly induced in the tropics and subtropics reaches the Labrador Sea not before year 2040 (Figure 4.5, A). At this stage, its impact on the near surface density is consecutively reduced on its way around the subpolar gyre with an excess of surface freshwater fluxes during the whole integration period even in the quasi-equilibrium state.

Furthermore, as a positive feedback mechanism on the shut down of convection, the surface density in the Labrador Sea is further reduced due to the lack of a vertical transport out of this region. The consequence is that the stabilization due to the advective signal is too weak for the stratification to recover and to allow additional deep water formation. Accordingly at the end of the integration period, the surface density is much more reduced in *CO2* than in the *MPI model* (Figure 4.7, right panel). Our uncoupled model allows a deposition of the role of the locally increased freshwater fluxes within the subpolar gyre on the density budget of the Labrador Sea: In *NOFRESH*, all anomalous freshwater fluxes were switched off. Anyhow, the pattern of the formation of LADW is very similar to experiment *CO2* (Figure 4.9, line), where the deep ocean convection breaks down.

This vanishing difference of the mixed layer depth in March between *CO2* and *NOFRESH* (Figure 4.9, dashed) with identical changes in the heat cycle underlines the dominant role of the temperature effect for the surface water's density in the region of the Labrador Sea and consecutively for the formation of LADW.
The stabilizing changes in the freshwater cycle cannot become effective for the Labrador Sea's mixed layer, neither from the surface nor the boundaries. This still holds after 2040, when the strong salt signal has entered the region along the boundary currents (Figure 4.5, A). The reason for this can be studied in comparing *NOFRESHSURF*, in which the anomalous freshwater forcing is in the main reduced to the advective signal coming from the north and in which the mixed layer depth also allows no deep water formation (Figure 4.9, dotted). This weak impact on the deep water formation within the Labrador Sea after year 2040 becomes clear when we look at the role of lateral signals for the deep water formation: After convection has broken down, in our study the system is not able to recover due to an advection of denser water along the boundary currents from the north, if local loss of buoyancy is still reduced.

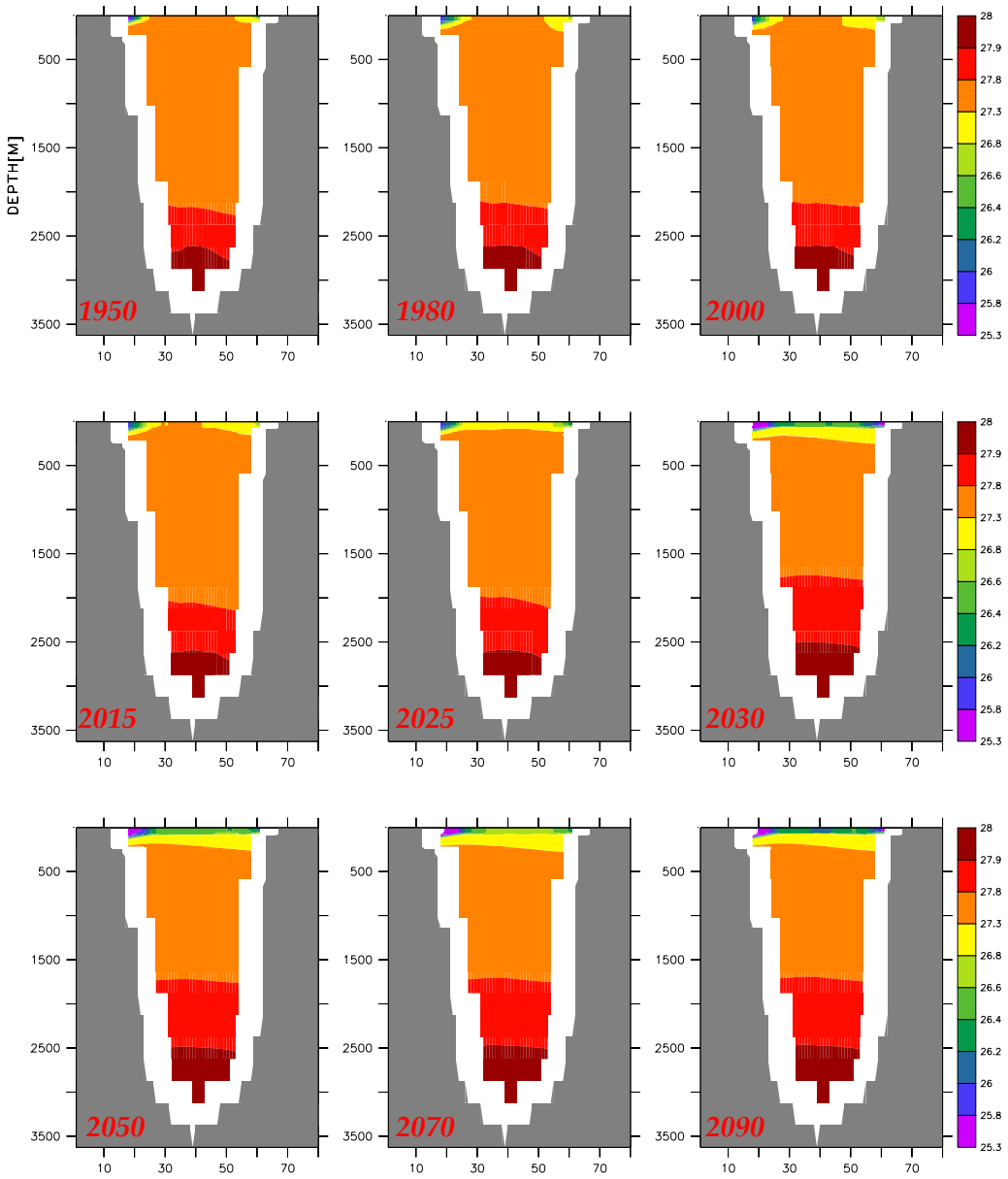

Figure 4.8: σ_Θ *on a section through the central Labrador Sea in March during the integration period. Years are denoted in the figure. During the first half of the* 21^{st} *century, the deep basin is decoupled from surface forcing.*

4.8 Summary of MPI forced experiments

We have investigated the response of different combinations of air-sea fluxes diagnosed from the *MPI* model's greenhouse warming scenario in our regional model of the Atlantic Ocean. The obvious question, whether a more realistic ocean model provides a fundamentally different response of the overturning circulation can be answered with no.

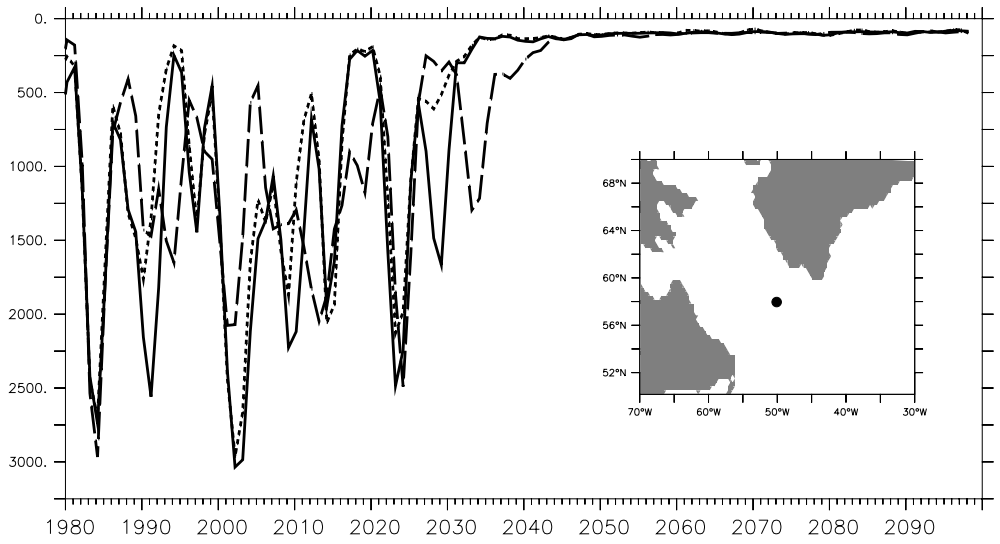

Figure 4.9: *Depth of the mixed layer in the central Labrador Sea at* $58°N$ *and* $50°W$ *of in CO2 (line), in NOFRESH (dashed) and in NOFRESHSURF (dotted) in March (3-year averaged). . The impact of local heat fluxes dominates the response.*

As in the coupled integration of the *MPI* model, the meridional overturning does not weaken significantly. The reason for this behaviour is found to be the enormous gain in ocean salinity during the integration period. In this context several studies with controversial results about the crucial mechanism for the behaviour of the strength of the THC in global warming scenarios have been published. While Mikolajewicz and Voss (2000) reported about the dominating role of changes in the heat cycle, results from Dixon et al. (1999) unmasked the enhanced freshwater forcing to be the crucial reason for the weakening of the overturning. Our ocean's response is somehow in the middle of their positions: Warming of the North Atlantic alone could be strong enough to cause the slowing down of the THC, if the freshwater cycle did not change at all. The impact of locally increased surface freshwater fluxes into higher latitudes solely was found to be relatively unimportant, but the crucial mechanism for the maintenance of the surface density and consecutively the strength of the overturning is the reduced freshwater forcing in *lower* latitudes. Latif's result, that a strong salt anomaly advecting form the tropics is able to stabilize the thermohaline circulation by matching the relatively moderate warming in regions of deep water formation, still holds for our ocean model with a higher resolution and a more realistic representation of the mean state.

Although the THC remains almost constant, the deep water formation within the Labrador Sea completely breaks down after year 2035. The deciding mechanism for this is the locally reduced cooling, leading to an increase of SST as well as a decrease of surface density (Figure 4.5, B and C)

The relative small impact on the meridional overturning cell underlines results form Döscher and Redler (1997), who pointed out, that, if an adequate dense

overflow across the sills can be held up like in *CO2* (Figure 4.5, C) and *NOFRESH-SURF*, variability in the convective regime within the Labrador Sea can not significantly weaken the meridional overturning cell. Focusing on the mechanism for the shutdown in our model, the locally increased heat fluxes into this region during the warming scenario were found to be the crucial factor. Neither local changes in freshwater fluxes nor the inflow of salty water after year 2040 into the region permit a fundamentally differing reaction.

4.9 Discussion and limitation

In our integrations, we unmasked the density of the overflow waters to be the crucial reason for significant changes in the strength of the THC. Consequently the focus has been on a highly realistic representation of the overflow itself, but also on the magnitude of entrainment, after the dense plume crosses the sills. A realistic role of entrainment is very difficult to quantify. HALLBERG (1999) reported of a too low entrainment rate in models with isopycnic vertical coordinates like the *MPI* model, the DYNAMO GROUP (1997) found something similar in z-coordinate models with an isopycnic diffusion operator like *FLAME 4/3*. In both cases, this could put the upper result into perspective: For example, if our model had a too low entrainment rate, the role of the overflows' density flux for the overturning might be overestimated. We focus on the role of entrainment processes in section 5.5.8. There we use different combinations of horizontal diffusion to estimate the role of entrainment. Hence the result is that for the response of the overturning circulation itself, the entrainment rate is relatively unimportant. An experiment with horizontal diffusion and no BBL parameterization is very close to the results provided by the standard *FLAME4/3* configuration.

Normally the role of a lateral salt feedback is to destabilize the overturning system. In this situation the role is vice versa. Due to a suitable *timing* of the signal, the surface waters of the GIN Seas maintain their density and allow further deep water formation. The crucial point in this scenario is indeed the chronological devolution of this scenario. Because there is no direct temporal connection between the strength of the THC and the enhanced evaporation in the tropical Atlantic, the lateral signal has to enter the regions of deep water formation, *before* the winterly convection has broken down. In our study the GIN Seas are a positive example, whereas the response within the Labrador Sea shows the problem: The salt signal follows the East Greenland Current and enters in the region of LADW formation to late for the stabilizing effect to occur.
Similar to the *MPI* experiment, in a global warming integration of the *HadCM3* model, an increase in the surface evaporation rate in lower latitudes was found (THORPE ET AL., 2001). Like in the *OPYC* ocean, the spreading leads to enhanced salinities in regions of deep water formation. Qualitatively this response of the *HadCM3* model is similar though much weaker. Therefore the signal does not balance the local reduction of surface density and the thermohaline index is reduced at about 5 Sv. In their model, the strength of the overturning circulation is closely

connected to the steric height gradient between higher and lower latitudes. By calculating changes in the density contribution they were able to find the impact of certain mechanisms on this response. They reach a new equilibrium of the THC at a 25% weaker level due to a balance of local heating and the lateral salinity effect.
To conclude this chapter, determining the response of the THC in global warming scenarios might not be answered solely by studying the local effects of changes in freshwater and heat fluxes in regions of deep water formation. Another mechanism, namely the lateral transport of signals into these crucial regions must be represented properly, since the convection process itself highly depends on the *preconditioning* within the water column. Together with buoyancy loss at the surface, deep water formation can take place (MARSHALL AND SCHOTT, 1999). In the available study the salt signal is very huge (locally up to 0.8 psu) and relieve an enormous salinity gain in high latitudes (locally up to 0.4 psu). Imagining such large signals from lower latitudes, if they entered the comparatively small regions of deep water formation in the northern North Atlantic, they apparently have an impact on the strength of the thermohaline forcing in the northern North Atlantic.

In this chapter, the main issue was to prove the deviating response of the *ECHAM4/OPYC3* model relative to the majority of global warming simulations. However, huge salinity signals of 0.4 psu in higher latitudes are quite strong. So in the next chapter, we investigate the ocean model's response for a "usual" scenario with a declining overturning index. Beyond examine the general response, we focus on the individual role of different forcing components for the temporal evolution of the overturning function.

Chapter 5

Experiments with GFDL fluxes

5.1 Introduction

In contrast to the experiments performed with diagnosed fluxes from the *ECHAM4/OPYC3* climate model, here we present studies of the response of *FLAME4/3* forced by fluxes from a coupled integration, in which the meridional overturning cell shows a significant weakening during the global warming scenario. In addition to the general response of the ocean model, by integrating several sensitivity studies, we illuminate the specific role of certain components of anthropogenic forcing for the variability and the trend of the overturning circulation. To continue the examination of the ocean components of coupled oceans of different style, as a contrast to the isopycnal vertical coordinate of the ocean in *OPYC3*, here we use diagnosed fluxes from a coupled model with a z-coordinate vertical axis, coming along with a more realistic bottom topography. The fluxes originate from a IS92a-like forcing scenario (namely *gps03*) of the *GFDL R30* coupled ocean-atmosphere-sea-ice model.

5.2 The GFDL R30 climate model

5.2.1 Technical aspects

The coupled model technics and climate variability are capaciously described in Delworth et al. (2002), therefore here we limit to a few catchwords. To give an idea of the greenhouse scenario *gps03* some technical aspects of the coupled integration are presented there.
The ocean component of the coupled model is the *GFDL-MOM 1.1* z-coordinate primitive equations model (Pacanowski et al., 1991). The horizontal resolution is 1.875° longitude by 2.25° latitude with 18 unevenly spaced vertical levels. The vertical thickness of the grid boxes varies between $40m$ at the surface and $677m$ near the bottom. For the parameterization of sub grid processes, methods of Bryan, K. and L. J. Lewis (1979), Redi (1982) and Cox (1987) are used.
The horizontal resolution of the $R30$ atmosphere is approximately 3.75° in longitude by 2.25° in latitude. In the vertical, a sigma coordinate system on 14 unevenly

spaced pressure levels is used. A relative humidity based cloud prediction scheme and a moist convective adjustment (MANABE ET AL., 1965) are used in the atmospheric model. Clouds are predicted whenever the relative humidity exceeds a critical threshold which varies with height (from 100% near the surface to 90% in the upper atmosphere). Where predicted, clouds are assumed to fill the grid box. Precipitation occurs when water vapor supersaturation is simulated, falling as snow when the temperature of the lower atmosphere is below freezing. In this model, a seasonal cycle of insolation is prescribed at the top of the atmosphere, with a solar constant of 1365 W/m^2. The solar constant does not vary during these model integrations. The effects of clouds, water vapor, carbon dioxide and ozone are included in the calculation of solar and terrestrial radiation.
Beside oceanic and atmospheric components, relatively simple formulations of river runoff and land surface are included.

The *GFDL R30* coupled model uses a relatively simple sea ice model that neglects the internal pressure of the sea ice. The sea ice model's lineage can be traced back to the model developed by BRYAN (1969), although modifications have been made over time, several of which are noted in MANABE ET AL. (1990). The horizontal grid spacing of the sea ice model matches that of the underlying ocean model. At each grid point, average sea ice thickness is predicted, but not fractional coverage (i.e., the grid cell is either considered completely ice free or entirely covered by ice of some model-predicted thickness). Thus, the model considers a single ice layer, and leads are not included in the sea ice model.

A well-known problem of coupled climate models is the imbalance between the oceanic and atmospheric component, leading to a climate drift during the integration. In order to reduce the likelihood of such drifts, "flux adjustment" terms are used. These are time-mean fields of restoring and are derived from the last few hundred years of the spinup (MANABE ET AL., 1991).
From a physical point of view, flux adjustments are the attempt to compensate the mismatch between what the ocean receives from the atmosphere and the flux the ocean needs to fit to observations.
The model is run for a number of aspects at the Geophysical Fluid Dynamics Labratory (*GFDL*).

5.2.2 Differences between GFDL and MPI overturning

Since we are not able to investigate a high number of climate models in global warming simulations, we chose the *GFDL* model to prove two fundamentally different types of models. While the *MPI* model has, due to the isopycnal vertical coordinate a somehow idealized topography with e.g. wide passages between Greenland, Iceland and Scotland and consequently unrealistic high transports over the sills, the z-level *GFDL* ocean is quite different. While in the *MPI* model deep water formation mainly takes place within the Nordic Seas, the results concerning the importance of the density signal at the northern boundary of *FLAME4/3* was to some extent expected. In the *GFDL* model, the main region of deep convection is the subpolar gyre, the transport rates over the sills are weaker and more realistic.

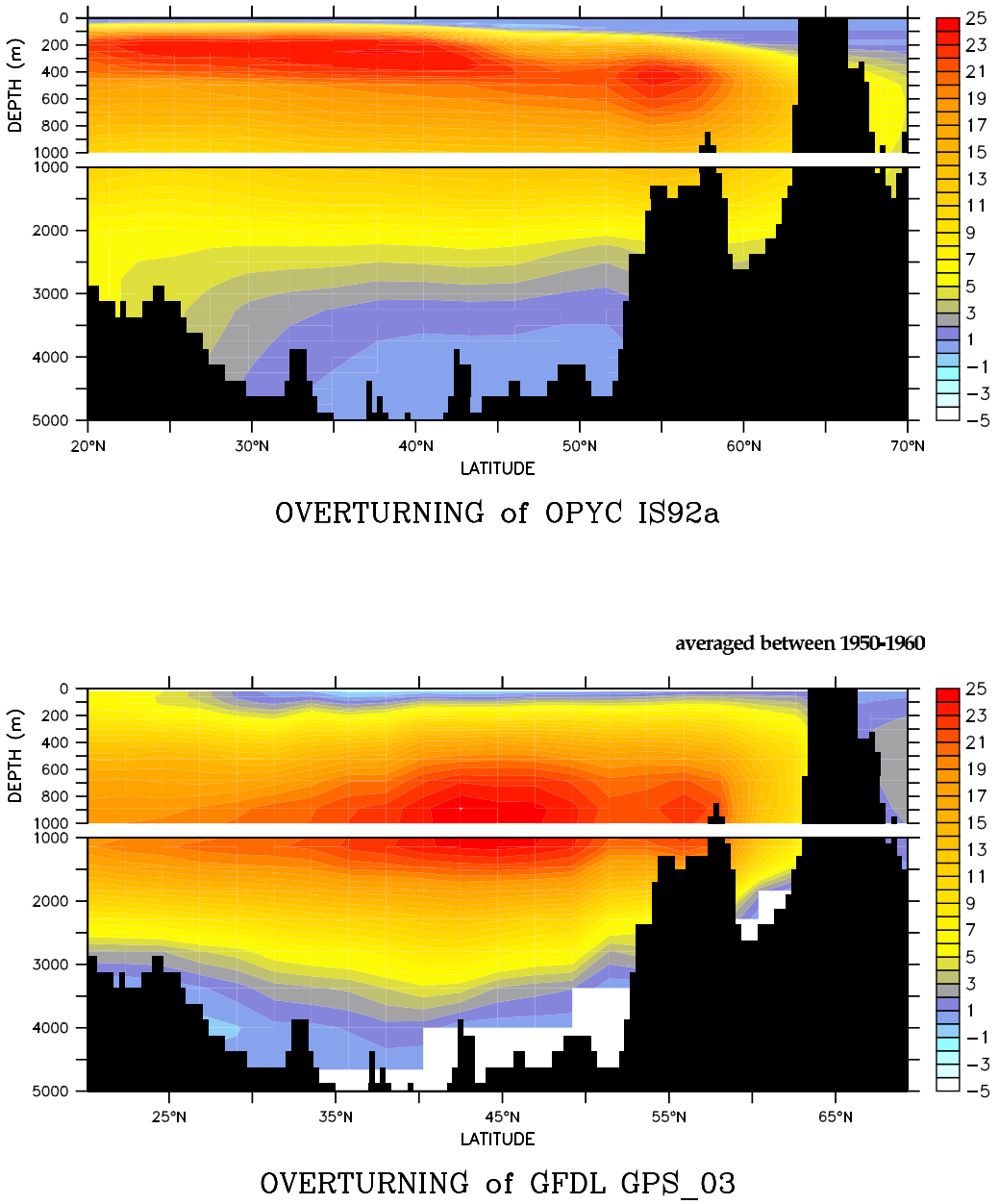

Figure 5.1: *Overturning circulation in ECHAM4/OPYC3 (upper panel) and in GFDL R30 (lower panel), averaged between 1950-1960 (unit is Sv).*

5.2.3 Anthropogenic forcing in *gps03*

As a contrast to the experiments performed with diagnosed fluxes from the *ECHAM4/OPYC3* climate model, here we forced *FLAME4/3* with diagnosed fluxes from the *GFDL R30* coupled model. The applied integration is an experiment called *gps03*, where "gps" stands for **g***reenhouse gases* **p***lus* **s***ulfates*.

Hence, as the name suggests, the direct effect of tropospheric sulfate aerosols was

included in the model as a modification to the surface albedo varying in time and space (HAYWOOD ET AL., 1997).
A suite of *gps* integrations were primarily performed to study the role of initial conditions for the development of the coupled model in global warming scenarios (DIXON AND LANZANTE, 1999). Starting in different years of the spinup, the model was forced with anthropogenic increase of CO_2 and sulfates.
The used fluxes start in year 101 of the undisturbed control integration. Projecting these on the year 1866 with a pre-industrial CO_2 level, the level rises at rates following the IS92a scenario until year 1990 and at a rate of 1% thereafter until 2090.

5.3 Experiments with gps03 output

In this section we shortly describe the different experiments performed with *FLAME4/3* forced by the *GFDL gps03* surface fluxes. Beside the *FULL* integration, in which we implemented the whole set of anomalies to the forcing, we performed a couple of sensitivity studies to illuminate different aspects of the ongoing mechanisms. All experiments are listed in table 5.3. In terms of forcing, *on* denotes that the anomalous anthropogenic forcing is enabled, while *off* denotes that it is disabled (see section 2.3).
The *CTRL* experiment is the one already described in section 2.6 and is used as a reference experiment in chapter 4.

Experiment *FULL*

The experiment *FULL* is integrated with the full set of anomalous anthropogenic forcing in order to study differences of the coupled ocean model and *FLAME4/3*. This is the analog to experiment *CO2* in the suite of experiments with *ECHAM4/OPYC3* fluxes. Additionally it serves as a reference experiment for the sensitivity studies with different combinations of anthropogenic forcing.

Experiments *NONORTH* and *NOSURF*

In experiment *NONORTH*, the northern restoring areas are fixed to the quasi-equilibrium climatology, while the salinity and temperature of the other vertical boundaries (e.g. Mediterranean and southern boundary) are changing as they do in the coupled ocean model.
The surface boundary conditions for heat, freshwater and wind are still anthropogenic. Because of the shape of these terms, for freshwater and wind the forcing is exactly the same as in *FULL*, while the feedback mechanism for the heat flux depends on the ocean's state. Therefore an unrealistic high heating over the northern sponge area takes place (figure 5.20) which can be traced back to the reaction of a nearly unchanged nudged ocean (due to restoring) on an anthropogenic changing atmosphere. Because this region acts as an integral response of the northern ocean, these local high values must be understood as the response of the whole Arctic Ocean in terms of the heat and salt budget.

As a contrast to the former experiment, in experiment *NOSURF* the water mass properties in the northern sponge area are restored to anthropogenic ally changed values. Moreover, for the surface fluxes we kept climatological records.
Again, a constraint must be mentioned concerning these fluxes. While for freshwater and wind stress it is strait forward, the surface heat fluxes are modified in that way, that there is some response of a changed ocean on an unchanged atmosphere. Somehow one can argue that the surface heat fluxes are modified by a natural reaction of the system: Anthropogenic signals from the northern boundary interact with an unchanged atmosphere above leading to changes in the air-sea fluxes.

Experiments *NOBBL* and *EASY*

In contrast to the experiments and to specify some results of the other sensitivity studies, we performed two experiments with *NOSURF* forcing configuration but some modifications to the ocean interior parameterizations. The first one is experiment *NOBBL*, in which the bottom boundary formulation (BBL) (section 2.2.2) is switched of. Since the major role of this parameterization is a more realistic representation of overflows over sills like the Denmark Strait or the Iceland-Scotland-Sill, we chose the experiment *NOSURF* for this parameter study. Because in this experiment the only interannual variability comes from the forcing at the northern boundary, deviations concerning the BBL are expected to be strongest.

To go a little further, we integrated experiment *EASY*, in which not even the BBL but also isopycnal mixing as well as thickness diffusion were switched off. Instead, we used horizontal mixing at $2 \cdot 10^7 cm^2/s$. Additionally, we dredged the Denmark Strait at points between 600 and 1000 m depth to a uniform depth of 1000 m. Again, the model was just integrated with the *NOSURF* forcing configuration in order to feel a maximum impact of the changes at the sill. For both experiments, a new spinup of 50 years was performed, since the climatological state of the overturning function shows a fundamental difference. The overturning cell is much shallower in the experiments without BBL. A lot of different features concerning differences between horizontal and isopycnal mixing in ocean models can be found in literature (e.g. Gough and Lin, 1995; Marsh et al., 1996).
This highly idealized experiment was performed in order to study the role of the overflows for the overturning circulation by switching off all parameterizations, necessary for a relatively realistic representation.

Experiment *NOWIND*

This experiment is identical to *FULL* except that the anthropogenic changes in wind stress forcing are switched off.
Because of the coupled physics of wind and heat forcing, the impact is that the Ekman and Sverdrup part of the anomalous wind stress is disabled, while changes in the heat flux due to e.g. enhanced evaporation are still present in this experiment, because the boundary condition for heat is anthropogenic.
Since the heat fluxes cannot be separated into a wind-caused part and a radiation part offhand, we limit this experiment to the pure Ekman part. One possible way

Name	an.Surface Forcing			an.Vert. BCs		Misc.
	Heat Flux	**Freshw.**	**Wind**	**Temp.**	**Salt**	
CTRL	off	off	off	off	off	
FULL	on	on	on	on	on	rel. *CO2*
NONORTH	on	on	on	off	off	
NOSURF	off	off	off	on	on	
NOBBL	off	off	off	on	on	off BBL
EASY	off	off	off	on	on	*EASY*[1]
NOWIND	on	on	off	on	on	
NOHEAT	off	on	on	off	on	
NOSALT	on	off	on	on	off	rel.*NOFRESH*

Table 5.1: Sensitivity studies performed with *FLAME 4/3* under anthropogenic forcing with *GFDL gps03* fluxes; all experiments are integrated for 140 years between 1950 and 2090.

to handle this problem is to do a regression analysis of wind stress and heat flux in order to extract the wind-caused contribution of the flux. Using this method Eden and Jung (2001) performed some experiments using a regression analysis of the heat flux time series on the North Atlantic Oscillation (NAO) in order to get a long time series of surface forcing depending on the NAO pattern.
This experiment gives indications for a subdivision of the thermohaline and the dynamical part of anthropogenic surface forcing.

Experiments *NOHEAT* and *NOSALT*

Experiment *NOHEAT* and *NOSALT* denote studies with anomalous heat flux respective freshwater forcing switched off. This affects surface forcing as well as sponge forcing at the vertical boundaries. For the former case, the restoring term is limited to changes in salt while temperature forcing is climatological, and for the latter case the situation is vice versa. Again, for the salinity case the surface forcing is straight forward, while *NOHEAT* still can have changes in surface heat fluxes due to the response of a changed ocean state on a fixed climatological atmosphere. Since we use an uncoupled ocean model, we have the ability to distinguish between temperature and freshwater forcing, what cannot be done directly in a coupled mode.
Concerning the northern boundary, a caveat has to be mentioned:
Since in the climate model the water mass properties supplied to the subpolar gyre are a product of formation of deep water masses, the subdivision into temperature

[1] *EASY*: no BBL, horizontal mixing ($2 \cdot 10^7 cm^2/s$), Denmark Strait dredged to 1000 m depth

and salinity forcing at the boundary is somehow idealized. The process of convection depends to some extent on the density of sinking water. Limiting changes in the deep water reservoir to e.g. temperature alone presupposes that the same water is the product of convection. This cannot be assured when the salt signal misses, since the density changes. Nevertheless if one might argue that the whole water column is affected by anthropogenic changes in the restoring area, both regimes, the surface waters as well as the deep water are involved. Therefore even in the region until 70°N the subdivision might be excepted. In section 5.5.2 we argue that the difference between disturbing the surface is quite similar to disturbing the deep reservoir.

5.4 GFDL forcing in *FLAME4/3*

In this section, we show some features of the anomalous anthropogenic forcing felt by *FLAME4/3*. Figure 5.2 shows Hovmoeller diagrams of the surface heat (A) and freshwater flux (B) during the integration period. At the beginning of the experiments, the oceanic heat loss is strongest within the subpolar gyre between 52°N and 57°N and at some latitude along the Gulf Stream between 35°N and 45°N. In higher latitudes, there is net atmospheric heat provided to the Nordic Sea. All these features show a nearly linear evolution during the anthropogenic simulation, leading to a warming of the North Atlantic. South of 30°N, the atmospheric heat fluxes are only slightly modified during the integration and no trend can be diagnosed. The warming is strongest between 60°N and 70°N, a region, in which the deep water formation in this coupled experiment is quite small. In contrast, at the beginning until the year 2000, instead of an increase in surface heat flux (as expected), the subpolar gyre is cooled. The anthropogenic warming starts with the new century. However, in comparison to the heat flux evolution in the *MPI* model, the warming within this region is weaker. Just concentrating on the trend, while the changes felt by the *OPYC* ocean are larger (about $10W/m^2/100y$, figure 4.2), the *GFDL* fluxes change by only $5W/m^2/100y$ between 1950 and 2090.
Looking at changes of the surface freshwater flux, a separation between the subpolar and subtropical region can be made. The freshwater fluxes within the subpolar gyre and in the GIN Seas are increasing, which is quite similar to the evolution of the local fluxes in the *MPI* model. In both integrations the gain is about $20cm/mon/100y$. Relative to the *MPI* model, there are only little higher evaporation rates affecting the subtropical region.

The changes in surface wind stress during the integration period are only marginal, there is no significant trend found in the *gps03* atmospheric winds. This is also quite similar to the *MPI* model. This is in contrast to other simulations with the *GFDL* climate model. E.g. Delworth and Dixon (2000) found an increase of the North Atlantic Oscillation (NAO) in the model.
The evolution of the North Atlantic Oscillation (NAO) index seems to be of great importance for the future of the North Atlantic ocean. Based on 60 years of data from 1935 to 1995, Hurrell (1995) estimated that the NAO accounts for 30% of

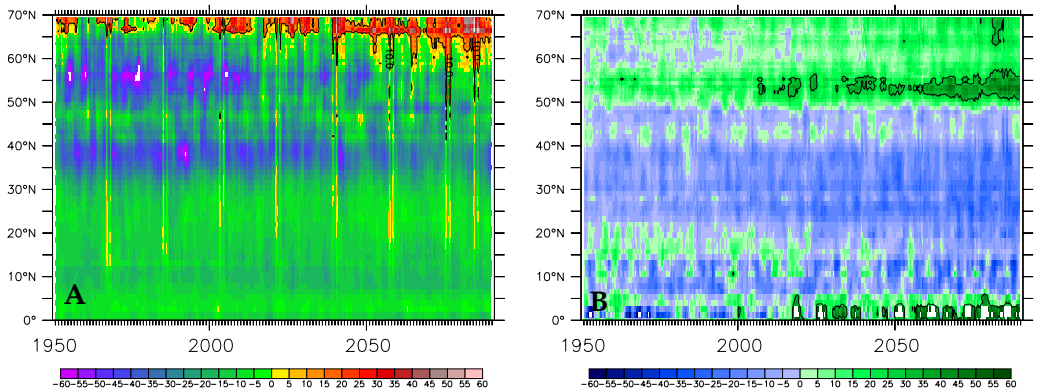

Figure 5.2: *Zonally averaged anomalous heat (A) and freshwater flux (B) in the North Atlantic in FULL; the year 1950 is removed; unit is W/m^2 for (A) and mm/mon for (B).*

the variance in hemispheric winter surface air temperatures north of 20°N. Hence anthropogenic changes in the atmosphere might change the future response of the NAO and hence the effect on the THC. In most coupled models a strong increase of the NAO as observed during the late 20^{th} century cannot be reproduced. During the 21^{st} century, most climate models, when forced in greenhouse gas scenarios, indeed show an increase of the NAO, but the shape of the internal variability as well as the amplitudes differs fundamentally (e.g. Osborn et al., 1999). Perlwitz and Graf (1995) suggest that this deficient simulation of NAO evolution in coupled models could be caused by an insufficient representation of the stratospheric ozone concentration.

Delworth suggested, that, if there is an increase of the NAO in climate models, the associated modified surface forcing could at least for some decades have a stabilizing effect on the thermohaline circulation due to enhanced mixing.

However, both the *MPI* and the *GFDL gps03* global warming scenarios do not show the effect of an increasing NAO realistically (not shown here). The role of changes in the anthropogenic wind stress is explained in section 5.5.7. There the role of wind stress variability mainly affects the interannual overturning variability. For the main trend changes in buoyancy forcing, which could also be related to NAO variability, are the crucial factor.

5.5 The meridional overturning circulation

The response of the overturning function as an indicator for the THC is the central issue of this thesis. Therefore in this chapter we show and discuss its response in the performed sensitivity studies with *GFDL* forcing. By subdividing the different timescales, the role of certain components of anthropogenic forcing are separated.

5.5.1 Changes and variability

First we concentrate on the long-term variability as well as on the trend of the overturning circulation of *FLAME4/3* within the integration period, since one of the frequently asked questions addressed to greenhouse gas forced experiments is the general behaviour of the MOC. Additionally, using results of sensitivity studies, we illuminate the crucial factors for the observed response. Figure 5.3 shows the annual averaged time series of all experiments with *GFDL* forcing. One point concerning the available results of these experiments is the initial response of the model. Since we implemented forcing anomalies not starting at zero, there is indeed an initial response to the singular forcing modification. As a consequence, the annual mean overturning function at the beginning of the experiments does not necessarily start with the quasi-equilibrium state at the end of the spinup.

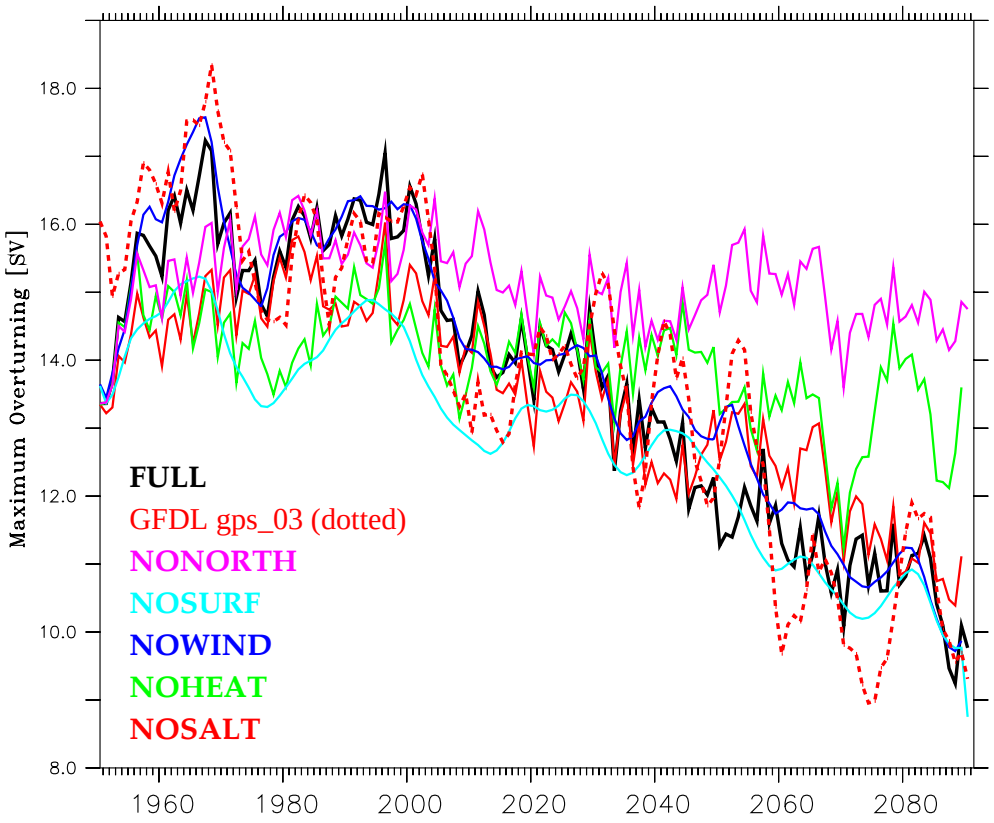

Figure 5.3: *Annual mean maximum meridional overturning function in the North Atlantic in experiments with gps03 forcing as denoted in the figure, the scaled time series of the coupled GFDL experiment is overlaid in the dotted line (unit is Sv).*

As already shown in figure 4.1, the coupled *gps03* experiment shows a significant weakening of the overturning index: between the year 2000 and 2090 the MOC slows down at about 10 Sv, what is a reduction of about 38% from 26 Sv in the middle of the 20^{th} century. In the comparable experiment *FULL* a very similar

result can be found: The maximum strength of the MOC is reduced from 16 Sv at the beginning of the integration period to 10 Sv in year 2090, what is a slowing down of 36% (figure 5.4). So the percentage decrease, what is quite close to the evolution of the heat transport in the case of linearity (section 2.7.2) in the coupled and the uncoupled integration is very similar.

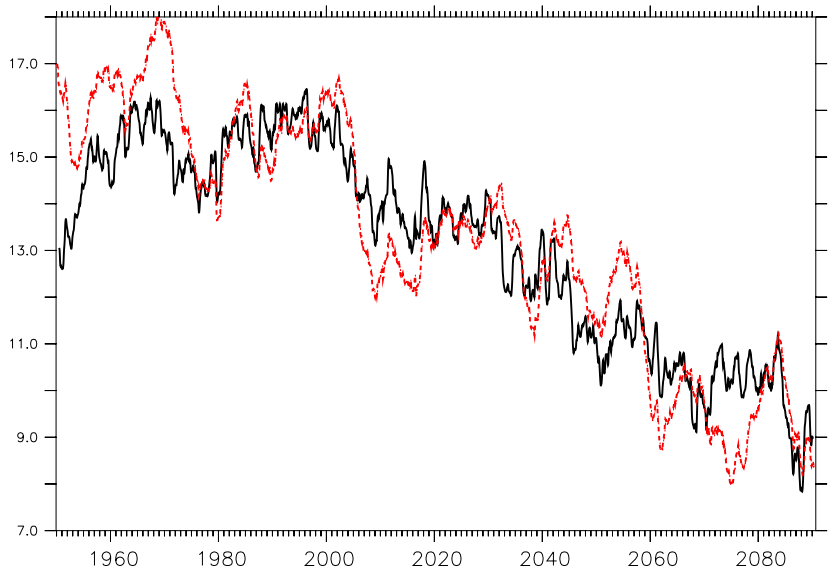

Figure 5.4: *1-year running mean overturning at 40° N and 1000m in experiment FULL (black line) and the coupled GFDL gps03 experiment (scaled, equation 2.13). The comparable surface forcing leads to a similar overturning response.*

But not only the general trend is comparable. The variability on multidecadal timescales is also quite similar. E.g. the two conspicuous maxima of the MOC strength around the years 1970 and 2000 are also evident in both models.
These two periods of high overturning transport can be related to strong atmospheric forcing. In this years, the surface forcing within the subpolar gyre as well as the provided water mass properties are responsible for the behaviour (see section 5.5.2). This response is the consequence of almost all forcing pattern. Only in experiment *NONORTH*, these two maxima cannot be found.
The role of wind stress variability can be seen comparing experiment *NOWIND* and *NOSURF* (figure 5.3, blue and cyan curve) relative to the rest of the experiments. The shape of the index time series is much smoother relative to the others, especially on interannual to decadal timescales. This can be directly attributed to the missing of anthropogenic wind stress forcing, since these two are the only integrations forced with climatological winds. Anyhow, these two experiments differ in the overturning strength due to different surface heat and freshwater fluxes within the subpolar gyre. At the beginning there is an offset of about 1.5 Sv due to surface forcing. Later in the second half of the 21^{st} century, the difference is reduced. This feature can be traced back to the decreasing subpolar surface forcing in experiment *NOWIND* affecting the overturning at that time.

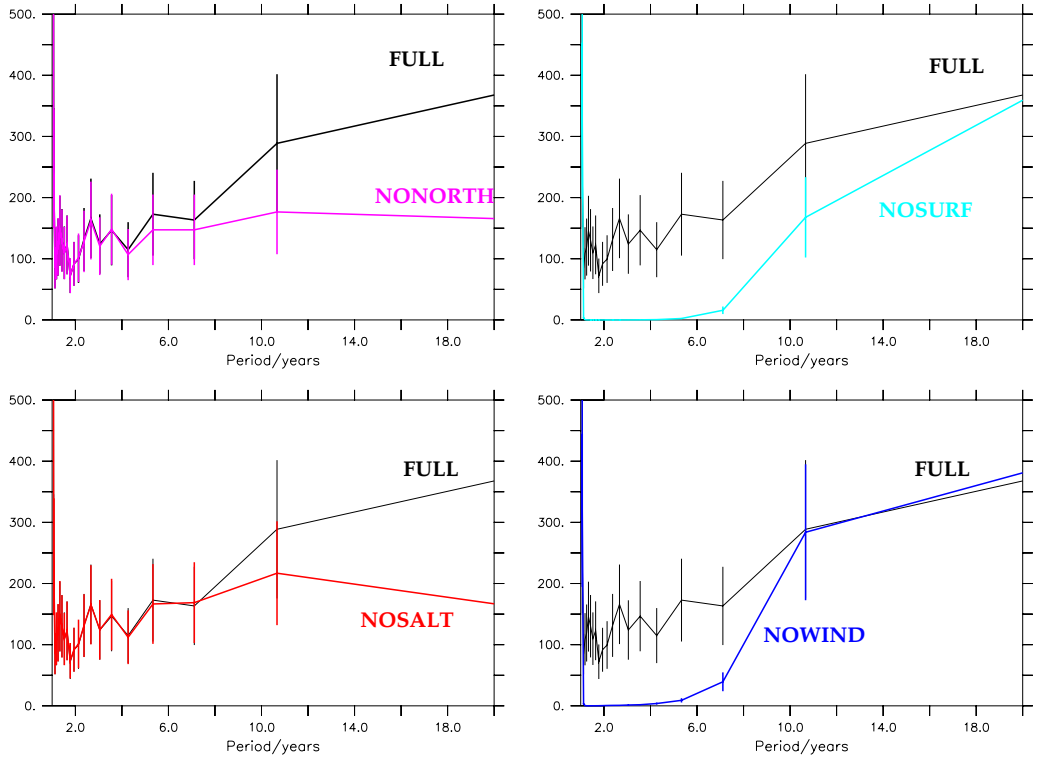

Figure 5.5: *Estimated power spectra of the overturning index of the experiments denoted in the figure. The vertical lines denote standard error estimates.*

The relative influence of the surface heat and freshwater fluxes can be studied by comparing *NOSURF* to *NOHEAT* (green curve). The strength of the overturning index in the second half of the 20^{th} century is very similar in both experiments. The reason is the dominant role of the strong freshwater forcing variability in the Nordic Seas on longer timescales at that time. Since the contribution to the overturning strength in the subpolar gyre is mainly given by changes in the surface heat flux, switching off this part of the forcing has a similar effect as switching of the whole surface forcing, at least on multidecadal timescales.
Anyhow, the impact of freshwater anomalies is more important in the Nordic Seas, as it can be seen by comparing experiment *NOHEAT* in the later part of the 21^{st} century. Here interdecadal variability sets in which is stronger than diagnosed in all the other experiments.

Another approach is to look at the frequency distribution of few of the experiments (figure 5.5). By calculating power spectra of the diagnosed overturning index, the impact of different components of atmospheric forcing becomes visible. Here, three different timescales can be separated: The wind-driven variability on annual scales up to a few years, the subpolar tracer flux variability on decadal timescales and the variability on interdecadal to multidecadal timescales. Very similar on interannual timescales are experiment *NONORTH* and *NOSALT* (upper and lower left panel),

underlining the role of wind stress forcing in the subpolar gyre on these scales. On timescales beyond 10 years, the freshwater variability in the Nordic Seas becomes important. The impact of heat flux forcing is extracted by comparing *NOWIND* to *NOSURF* on interdecadal to multidecadal timescales. On these scale there is much energy in the former experiment relative to the latter.

To summarize the variability on different timescales, the interannual variability of the overturning index is mainly driven by the wind stress anomalies. On timescales of a few years, the wind induced variability is strongest but the heat flux variability comes into play. Decadal variability is determined by surface heat flux anomalies within the subpolar gyre, whereas the long-term behaviour is given by changes in the density field north of Iceland.

5.5.2 The individual role of heat and freshwater fluxes

The role of different parts of surface forcing, namely heat, freshwater and momentum fluxes for the general trend of the overturning circulation is still unclear. Especially in climate models, due to the coupled style, the individual role of these fluxes is difficult to answer. A couple of studies concerning this point show deviating results. While Wiebe and Weaver (1999) found that the atmospheric poleward water transport is chiefly responsible for the weakening of the NADW formation, Rahmstorf and Ganopolski (1999) found heat fluxes to be the dominant factor during the 21^{st} century, while later, changes in the hydrological cycle become important.
To perform studies for a methodical investigation of this question, in coupled models the individual impacts were examined by Mikolajewicz and Voss (2000) and by Dixon and Lanzante (1999).
By performing two baseline integrations under fixed CO_2 respective an prescribed CO_2 increase, the freshwater and momentum fluxes in climate models were diagnosed. Afterwards the models were run with different combinations of air-sea fluxes, using the diagnosed time series of one of the baseline integrations to extract the specific impact of heat, freshwater or momentum. For instance, to estimate the role of freshwater forcing within the global warming scenario, the models were run with a fixed CO_2 concentration but with the diagnosed freshwater fluxes from the anthropogenic experiment. Moreover, for detecting the temperature effect, the models were integrated under increasing CO_2 and freshwater fluxes from the experiment under fixed CO_2. Thus, the different impact of air-sea fluxes for the trend of the MOC in greenhouse gas scenarios could be extracted.
However, the results are very different and allow no clear answer to this point: While Mikolajewicz and Voss (2000) found in *ECHAM4/LSG* that 70% of the weakening of the overturning index could be ascribed to the temperature effect, Dixon et al. (1999) reported that in the *GFDL_R15_b* model the upper procedure adds up to a 65% contribution of freshwater forcing (figure 5.6).
Due to the uncoupled mode of our ocean model, these studies are much easier to perform, in spite of the caveats concerning the northern boundary condition (see section 5.3).

The impact of CO_2 forcing with fixed freshwater fluxes is done in experiment *NOSALT*. Compared to *FULL*, the state in year 2090 reaches at least 65% of the weakening of the overturning cell (figure 5.3, red curve), what is close to the results in ECHAM4/LSG (figure 5.6, a), thin dashed line). Moreover, the structure of the response is quite similar. Both integrations show a quasi linear decrease of the overturning function, starting around the year 2000 without much interdecadal variability.
In contrast are DIXON'S results. With temperature forcing only he found some variability on a timescale of about 30 years (figure 5.6, b), dashed line). The results concerning the impact of freshwater fluxes are correspondingly vice versa. While the experiment with anthropogenic freshwater forcing only (*NOHEAT*) shows much variability on timescales of 20-30 years (figure 5.3, green curve) and only a decrease of 10% during the integration period, the results of the *GFDL_R15_b* model indicate a contribution of about 80% for the freshwater forcing (figure 5.6, dashed curve). Apparently there is much difference in the results concerning the individual impact of surface fluxes.

By investigating the response of different combinations of anthropogenic surface fluxes, an interesting question is the linearity of the experiments. More exact, does an experiment with heat as well as freshwater forcing show a response akin to the sum of the experiments forced by anthropogenic heat respective freshwater fluxes solely?
The left panel of figure 5.7 shows the anomalous overturning function at 40°N in 1000 m depth of *FULL* and a linear superposition of *NOSALT* and *NOHEAT* relative to the first 10 years of integration. Since both sensitivity studies contain anthropogenic wind stress forcing, the impact is somehow taken into account twice,

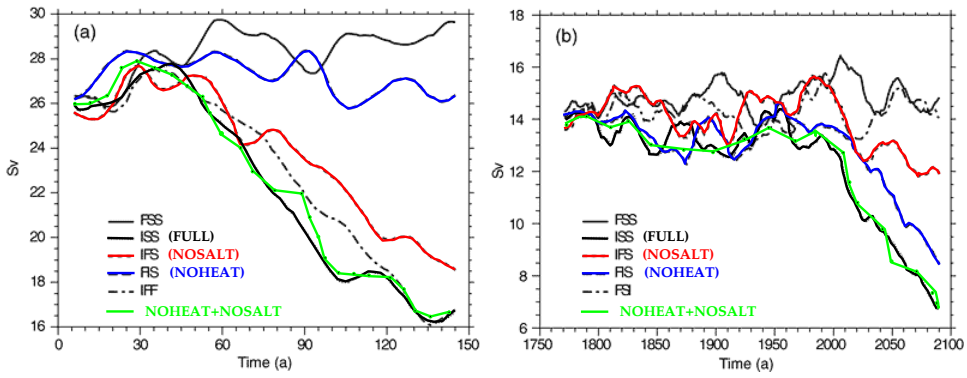

Figure 5.6: *Overturning function at 30°N and 1500 m; sensitivity experiments concerning the impact of different surface fluxes in a) ECHAM4/LSG and b) GFDL_R15_b; the experiments ISF, FIS and IFF correspond to NOSALT , NOHEAT, and NOWIND; source IPCC 2001. Overlaid is the superposed response of experiment NOHEAT and NOSALT, showing a quite linear contribution of the different forcing components.*

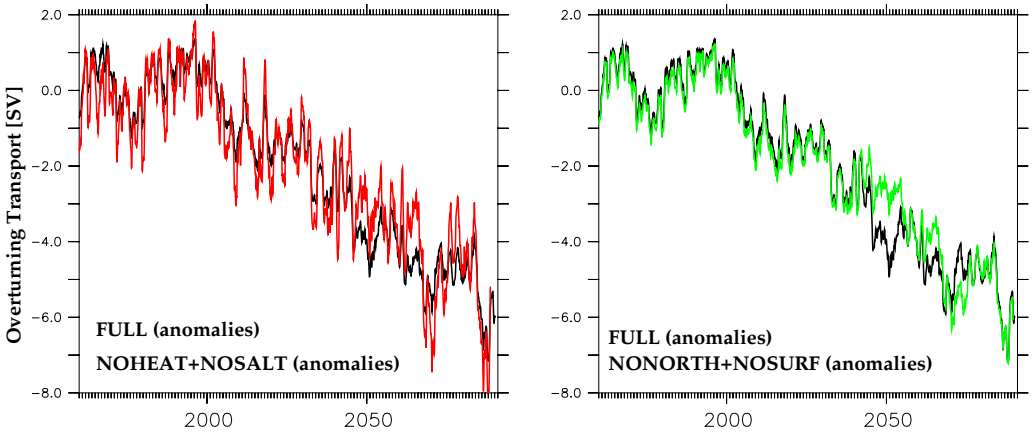

Figure 5.7: *Overturning function anomalies at 40° N in 1000 m depth, experiments denoted in the figure. Superposing experiments with different combinations of forcing show a quite linear response on the individual forcing components.*

what can explain the higher variability on annual timescales of the superposed curve. Nevertheless the impact of heat and freshwater forcing shows a very linear relationship. It is almost perfect until the second half of the 21^{st} century, when the oceanic state is changed so much, that the deep water formation stronger depends on lateral transports relative to the surface fluxes. However, the correlation on annual mean timescales is still quite high ($corr = 0.91$), showing this linear overturning response on heat and freshwater forcing.

Results which *FLAME4/3* find the heat flux to be the crucial factor for changes in deep water formation in the subpolar gyre mainly in the Labrador Sea (Eden and Willebrand, 2001). Following their result, it is not a surprise, that in this region, the response seems to be quite linear. If the heat flux variability accounts for at least 85 % of changes in the deep water formation rate on longer timescales, non-linear effects can be aspected to be small.

The Nordic Seas as the other region of deep water formation, seems to show a similar response as well, which can be denoted to the style of the anthropogenic impact there. Since our model shows no own deep water formation along with an expected non-linear behaviour in that region, the system is somehow simplified. Instead, we prescribe anthropogenic changes in the water mass properties, so that the linear behaviour of *FLAME4/3* is indeed not a surprise (see section 5.5.4 for details).

However, this linear response of heat and freshwater forcing can also be found in both climate model studies (figure 5.6, green curve), a result that underlines the response found in the ocean model.

In a physical sense, this result can be interpreted in the way, that the deep water formation rate into the crucial depth is nearly constant during the whole greenhouse warming scenario, no matter about the properties of the sinking waters. Therefore, anthropogenic changes in salt and temperature in the deep water reser-

voir are to some extent a good approach for changes in the surface fluxes.

Following this idea, we support the argument for the additive response of salt and temperature forcing by tracing the surface variability communicated into the deep basin of the Nordic Seas (figure 5.8). Looking at the anomalous time series of temperature and salinity in this region in different depths, one can trace the sinking waters. These waters reach a depth of at least 600 m, which is approximately the overflow depth. This holds in fact during the whole period of anthropogenic forcing. Here the signals coming from the surface reach the outflow depth even during the whole 21^{st} century. While at the beginning, water of the anomalous temperature and salinity reach a depth of 1500 m, later on the variability signal cannot be found at that depth. However, until the end of the experiment, the signal is transmitted into the outflow depth at about 600 m.
Changes in the deep basin (mainly warmer and fresher) are evolving much slower at that time and can be ascribed to diffusive processes more than to winterly deep convection activities. So, the deep Nordic Seas basin below the sills is somehow decoupled from the surface forcing and hence the overturning variability.
Although the temperature and salinity time series providing the *FLAME4/3* forcing originate from a different scenario and not from the two described above, the sinking reaching at least the depth of the sill can be a reasonable argument for the additive behaviour of the climate model's response of anthropogenic heat and freshwater forcing.
Another interesting feature in figure 5.7 is the behaviour of the climate models at the beginning of the integrations. While forced in a different manner, the curves show the same response in the first couple of years due to the dependency on the initial state. This is also found in recent studies with climate models (LATIF, *pers. com.*) and is the result of internal variability in the coupled system.

The individual role of heat and freshwater flux forcing is still not clear. Since in the subpolar region, heat flux variability dominates the response, in higher latitudes,

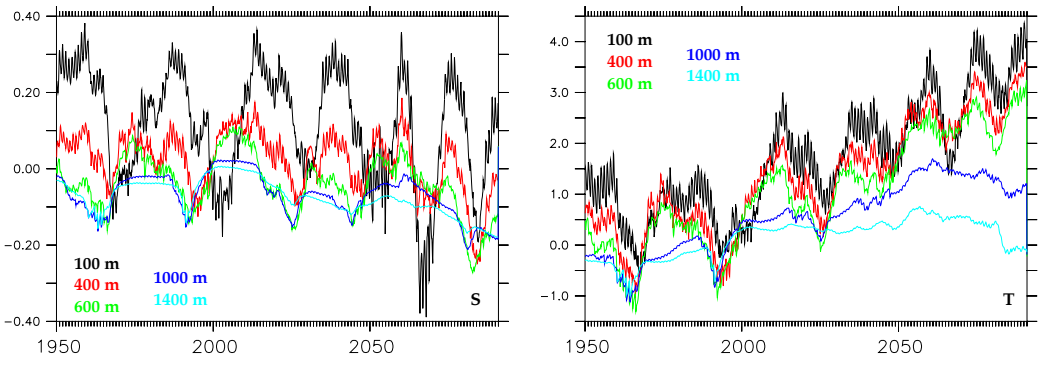

Figure 5.8: *Time series of the salinity (left) and temperature (right) at 70° N and 15° W in the GFDL climate model; the average between 1866-1949 is removed, units are psu and °C.*

both components are important for the variability on longer timescales.

5.5.3 Contribution of different regions

In section 5.5.1 we discussed the response of the overturning function in the experiments in the perspective of different timescales. In former model studies it is shown that even on timescales up to a few hundred years the strength of the MOC in OGCMs strongly depends on the rate of deep water formation in the northern hemisphere of the Atlantic Ocean (e.g. HAY, 1993; LENDERINK AND HAARSMA, 1994). Here we illuminate the impact of anthropogenic forcing in the crucial regions of deep water formation, which are the subpolar gyre and in the Nordic Seas. In this context RAHMSTORF (1999) mentioned some indications, that not only the strength but also the contribution to the DWBC, what is mainly the lower branch of the MOC, might change.

As we can distinguish between different sources of North Atlantic Deep Water (NADW) in *FLAME4/3*, we are able to investigate individual changes to the meridional circulation with their source in the Nordic Sea or in the subpolar gyre. Although our ocean model has no own region of deep water formation north of Iceland (section 2.6), by supplying dense water in that region and hence the overflow waters, we can simulate the impact of changes in convection activity. Nevertheless, being able to control the water mass properties of this region, a caveat is the point that we have to rely on changes in the deep water formation of the coarse climate model's ocean.

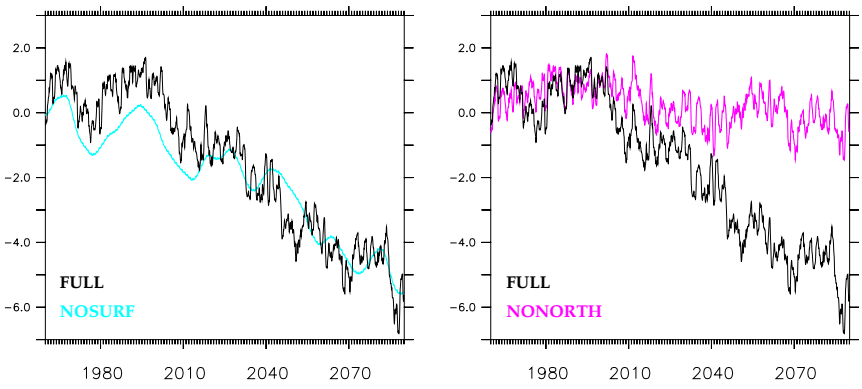

Figure 5.9: *2-year smoothed time series of overturning function at 40°N in 1000 m depth; experiments are denoted in the figure.*

The two experiments we performed with *FLAME4/3* in this context give an indication for the relative role of these two regions. Experiment *NONORTH* contains anthropogenic forcing in the subpolar gyre, more exact at the whole surface of the model, while the water mass properties in the northern sponge are kept climatologically. Since in section 2.6 we showed, that in the quasi-equilibrium state there

is no explicit deep water formation north of Iceland in *FLAME4/3*, this switch assures that only the subpolar convection activity can be affected by anthropogenic fluxes. Vice versa, in experiment *NOSURF* the surface forcing is, except for some heat flux modification, unchanged, while the deep water reservoir of the GIN Seas is changed following the specifications of the climate model. In section 5.5.1 we showed the frequency distribution of the overturning index of these two experiments. The important result was a significant reduction of variability on decadal timescales in *NOSURF*.
Concerning not only this variability but also the trend of the overturning function, we see a remarkable difference in these two experiments: *NOSURF* shows a significant reduction in overturning strength on anthropogenic forcing in the northern boundary; the long-term variability as well as the trend are a good reconstruction of the *FULL* experiment (figure 5.9,left panel). In contrast, in experiment *NONORTH* the trend vanishes (right panel). Instead, anthropogenic changes in the air-sea fluxes within the subpolar gyre become very important on timescales up to a few years. This variability of the surface-forced experiment is very similar to experiment *FULL*, which is forced with the same set of anthropogenic surface forcing in that region.
Again, the question about the linear response of *NONORTH* and *NOSURF* arises. As it can be seen in figure 5.7 (right), superposing the overturning variability of both experiments gives an almost perfect reconstruction for the *FULL* experiment. The results give indications, that there is almost no tele-connection between the subpolar and the Nordic Seas' region in terms of deep water formation in *FLAME4/3*.
Here, a clear distinction between subpolar induced variability and variability in the GIN Seas can be made. This subdivision is already shown in former model studies, although in a different context: Wood et al. (1999) showed results from the *HadCM3* climate model, in which deep water formation takes place either in north and south of Iceland in the climatological state. When in their model the Labrador Sea convection breaks down, the variability on interannual to decadal scales is significantly reduced (their figure 1a). Although the deep water formation in their experiment is shut off only in the Labrador Sea and some deep water formation in the Irminger Sea is still present, this effect can be found in their study.
In contrast to these results, we can put the response found in the *MPI* forced experiments (chapter 4) into perspective. The overturning in the central Labrador Sea broke down due to a reduction in surface heat fluxes. Nevertheless, in that experiment, there was still interannual variability of the surface heat fluxes in the subpolar gyre, leading to some short-term variability in the overturning function in all three experiments (figure 4.6).

Looking at the difference between the two curves in the left panel of 5.9 as a measure for the contribution of the subpolar region to the strength of the overturning circulation, one can see, that the impact is decreasing with integration time. While in the second half of the 20^{th} century the anomalous surface forcing in *FULL* is

responsible for a maximum deviation of 1.5 Sv, in the late 21^{st} century it is much less. Moreover at that time the variability on interannual timescales is reduced.
Merging these results together, the variability on timescales of a couple of years and a maximum amplitude of about 1.5 Sv seems to be steered in the region of the subpolar gyre. In section 5.6 we show the specific response within the Labrador Sea. There, the convection breaks down in the surface forced experiments between year 2015 and 2020. This incident can also be seen in the overturning strength, which is reduced in that period.
At this point, we can resume, that changes in deep water formation north of Iceland seems to be responsible for long-term changes and trends with a much smoother shape. The reason for this long-term variability coming from the north can be ascribed to the reservoir conditions there. While changes in the deep water formation rate e.g. in the Labrador Sea have a quick impact on the overturning strength, in the Nordic Sea, changes in the deep water formation rate is in some way decoupled from the Atlantic basin, leading to a much lower frequency contribution. Experiment *NOSURF* gives an indication, that the gradient of the potential energy provided by the water columns in the north and somewhere in the south is on decadal timescales mainly dominated by changes in the north. *FLAME4/3* does not need an anthropogenic signal somewhere else but in the Nordic Seas to reproduce the overturning weakening of the climate model in the fully forced experiment.

5.5.4 The density structure in the Nordic Seas

By calculating the depth-integrated density anomaly respective the steric height in a lower and a higher latitude, THORPE ET AL. (2001) found a good measure for the overturning in the North Atlantic in the *HadCM3* coupled model. He found the best relation to the MOC index by calculating the steric height gradient between 30°S and 60°N. Concerning the long-term response respective the trend of the overturning strength, results of experiment *NOSURF* provide an indication for the coherency to changes in the water mass properties in the GIN Seas. Implementing only that part of anthropogenic change into *FLAME4/3* gives, aside from some variability on interannual to decadal timescales, a very good reconstruction of the general response of *FULL* (see section 5.5.3). In terms of steric height gradient, this indicates that the southern latitude remains mainly unchanged, while the slope of the gradient is determined by changes in the north. So here we compare changes in the water mass properties in the north and their effect on the overturning function in the different experiments.

If we look at the density structure of the waters, which are communicated into the subpolar gyre, the Denmark Strait Overflow as the densest water mass of the NADW should give a reasonable value for changes in the reservoir in the north. Following this approach, DÖSCHER AND REDLER (1997) found a high correlation between the density of the Denmark Strait Overflow and the overturning strength. Although their model did not include the overflow region, taking the

water mass properties of the DSOW into account, their overturning function was clearly strengthened.

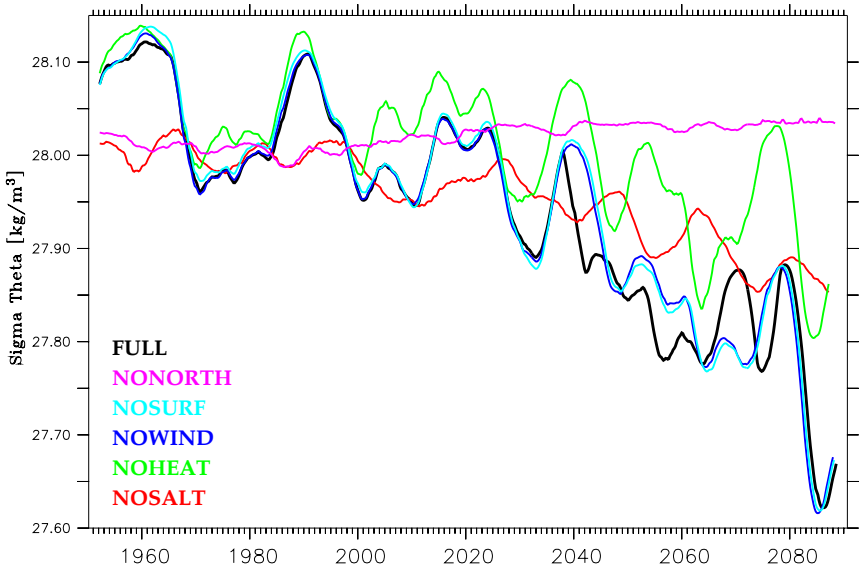

Figure 5.10: *Four years running mean time series of σ_Θ at the core of the Denmark Strait Overflow at 66°N and 28°W in 550 m depth, experiments denoted in the figure.*

In figure 5.10 we show time series of the density at the core of the DSOW of the different scenarios (figure 5.10). Concerning the general response, these curves are quite similar to the structure of the maximum overturning (figure 5.3). Looking at the trend of both the overturning index and the density at that point, figure 5.11 shows a quasi linear relationship at the end of the integration period for all experiments. This holds, even though in none of the available experiments an equilibrium state could be attained.
So, these two figures indicate, that fundamental changes of the overturning function seem to go along with density changes at the sill of the Denmark Strait, what is already mentioned in former studies (e.g. DÖSCHER ET AL., 1994). Whether these changes are the reason for changes in the overturning function or just a response is further illuminated in section 5.5.5. Here we concentrate on the trend and the decadal variability of the density due to forcing differences in the individual experiments.

All experiments except *NONORTH*, which includes climatological deep water properties in the reservoir north of Iceland, show strong variability on decadal to multidecadal timescales in the water mass properties at that point.

The strongest variability is given in *NOHEAT* as the consequence of salinity changes. Due to a strong variability in the freshwater release in the arctic region, this curve shows only little net decrease but jumps up to $0.3 kg/m^3$ in 10 years (figure 5.10, green curve). Relative to experiment *FULL* this gives an indication

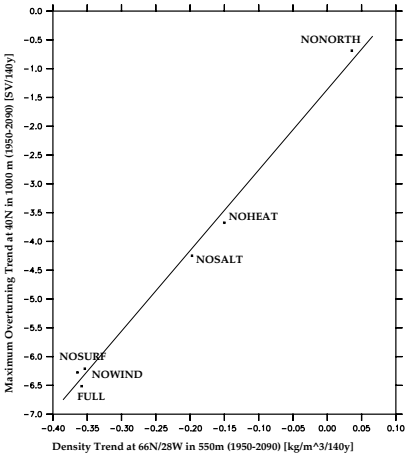

Figure 5.11: *Trends of Denmark Strait Overflow density against overturning strength at 40°N in 1000 m of different experiments with GFDL gps03 forcing.*

for the dominant role of salinity changes (black curve) for the variability on these timescales. So, until the year 2000, both time series show an almost identical response. This can be ascribed to almost constant temperatures of the DSOW until that time. Afterwards, the curves begin to deviate due to slowly raising temperatures.

Therefore the role of temperature changes in the DSOW is somehow different. The amplitude of the temperature induced density variability is less than half as large (experiment *NOSALT*, red curve). Moreover, looking at timescales of a few years in terms of density, the temperature time series is to some extent reciprocal to the salinity variability (figure 5.12, right panel). Positive (negative) temperature anomalies go along with positive (negative) salt anomalies. To some extent both compensate in the density equation. This feature can be ascribed to the precipitation feedback of the coupled climate model: Higher SSTs strengthen the hydrological cycle, leading to an increase of evaporation and consecutively to higher salinities. Therefore in many anthropogenic scenarios, on decadal timescales, changes in SST and surface freshwater flux have an opposite sign (figure 5.12, left panel). However, concerning the long-term variability and the trend, the heating and freshening dominate the density structure in most climate models.
In contrast to the freshwater experiment *NOHEAT*, there is a significant trend in the overturning temperature of about 3 K between year 1950 and 2090 in experiment *NOSALT* due to heat flux changes. The density variability on longer timescales in the deep Denmark Strait is about half as large in this experiment.

To some extent density compensated is experiment *FULL*, (figure 5.10, black curve), at least in the 21^{st} century. Then the variability is much lower than both in the salinity and the temperature experiment. However, the trend is about $0.4 kg/m^3$ in 140 years of integration, which is indeed given by the raising temperatures. Additionally, some kind of linear interaction of temperature and salinity induced

variability with a smaller amplitude as well as the trend can be seen in this experiment.

If we indeed find the density structure of the water column in the north to be the relevant factor for fundamental changes in the overturning circulation in *FLAME4/3*, it becomes clear, why the effect of temperature and salinity shows such a linear response on the overturning function as it is found in section 5.5.2. Without explicit convection in this region (see section 2.6), which could add non-linear dependencies of deep water formation into the system, the water mass properties at the reservoir depth are almost purely given by the sponge term. Nevertheless the impact in the climate model, forced with an individual set of air-sea fluxes as described in section 5.5.2, could provide a different result. Due to the non-linear mechanism of deep water formation a similar behaviour is not necessarily given. Hence instead of a true assertion about the contribution of heat or freshwater forcing to changes in the overturning function, the use of a restoring zone in the north leads to some limitation. Anyhow, in section 5.5.2 we showed that a linear combination of the heat respective freshwater induced variability in figure 5.6 is able to give a good approximation for the combined effect of surface flux forcing even in coupled models without idealized vertical boundaries.

Controlling the reservoir's density by an artificial nudging to prescribed and separated values for salinity and temperature seem to some extent be a good approach for physically realistic forcing of surface heat and freshwater fluxes. In *FLAME4/3* this restoring is an important factor for the relative realistic water mass properties of the DWBC in the subpolar gyre relative to climate models. In chapter 3 we

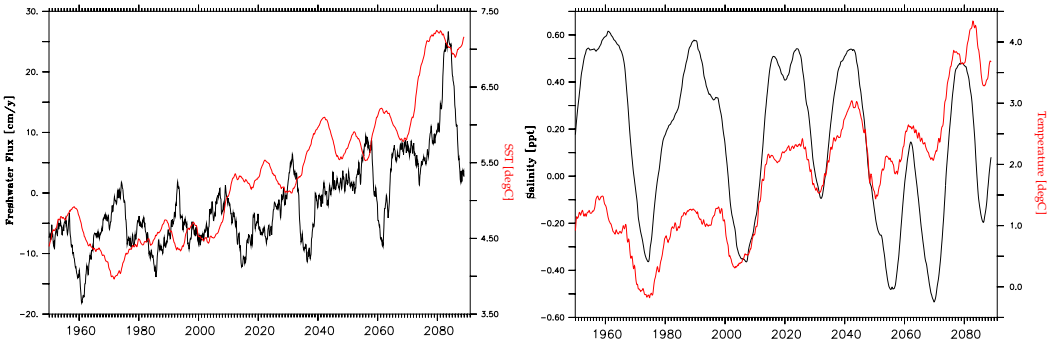

Figure 5.12: *Surface freshwater flux and SST between averaged between 65° N and 75° N and 30° W and 10° E (left) and temperature and salinity of the Denmark Strait Overflow at 66° N and 28° W in 600 m depth (right) of the coupled integration GFDL gps03.*

performed sensitivity studies, which show, how much the oceanic state depends on the water mass properties provided by this area.

Another aspect is the impact of changes in the gyre circulation for the density of the Denmark Strait Overflow. The time series of experiments *NOWIND* and *NOSURF* at that point are very similar during the whole integration period. So, although in the former the anthropogenic surface fluxes are implemented, the devolution of the dense overflow is almost identical to the experiment with no greenhouse gas forcing through the surface. Following these results, the density structure communicated into the subpolar region is indeed mainly determined by anomalous salinity and temperature time series provided in the north. Switching on the wind of the global warming scenario, gives some modification to the density at the sill (*FULL*), especially in the middle of the 21^{st} century. This response is in line with the role of the wind stress in terms of the density transport round Iceland (section 2.7.1). Due to modifications to the wind field, the density transport is modified, leading to changes in the later period of this experiment. Additionally, this role of the wind for the water mass properties at the sill can also be found in the strength of the MOC: The curves of experiment *NOSURF* and *NOWIND* show a very similar shape because of the identical density series between Greenland and Iceland. Some kind of offset on the annual mean can be ascribed to surface tracer forcing within the subpolar gyre. The response of *FULL* includes moreover some variability in the deep water formation rate in the subpolar gyre (see section 5.6).

In contrast to all the other experiments, *NONORTH* has no significant trend in the density of the DSOW (figure 5.10, magenta curve). There is only little increase during the integration period, which can be traced back to an proceeding uncoupling of the dense reservoir from the surface layers (see section 5.7) due to surface warming and freshening. Apparently, there is almost no impact of the (fresher or warmer) anthropogenic signal found in the density of the Denmark Strait Overflow in this experiment. This result underlines the dominant role of the sponge area for the water mass properties in this region and must be attributed to the missing of own deep water formation in *FLAME4/3* north of Iceland. This could alter the water mass properties due to the role of variability in the rate of deep water formation.

However, the implemented changes in the ocean's density profiles cannot be found in observations. DICKSON ET AL. (2002) reported of a "rapid" freshening of the Denmark Strait Overflow between 1965 until 2002 of 0.06 psu. For comparison, the changes prescribed by the *GFDL* model show a strong variability of 0.4 psu during that period with no significant trend. So, finding the density in this region to be the dominating factor is important, but simulating correct density time series at that point seems indispensable for predicting overturning changes.

5.5.5 Timescale of the overturning response

In the idealized sensitivity studies concerning the spreading of density signals from the Denmark Strait sill into the North Atlantic ocean (section 3.3) we found a

timescale of about four years for a density signal from the Denmark Strait to effect the overturning at 40°N.

Investigating the response of the model forced with climate model's fluxes, we would expect something similar for the experiment forced with anthropogenic signals in the sponge area (e.g. experiment *NOSURF*). However, for the experiments forced with time series of combinations of anomalous forcing in the subpolar region as well as in the GIN Seas (experiment *FULL*), the response is expected to be much more difficult to distinguish. Concerning interdecadal timescales, before analyzing the time series we smoothed the data by a 5-years-running mean filter, in oder to concentrate on the long-term variability.

Figure 5.13 A) shows the lag correlation between the maximum overturning function at several latitudes relative to 40°N for experiment *FULL*. As expected, the lag is nearly four years for a signal from 63°N to 40°N. The spreading timescale is about $1\frac{cm}{s}$ and is quite uniformly in the subpolar gyre.
Depending on the combination of forcing, the lag correlation between the density signal at the Denmark Strait and the overturning at 40°N is between two and four years (figure 5.13 B). The experiment with forcing anomalies only in the northern sponge (*NOSURF*) shows the highest correlation, the experiments with mainly strong variability in the GIN Seas water properties show something similar. Since the underlined timescale is give by the salinity signal, *NOHEAT* also has a very high correlation. For the fully forced experiment *FULL*, the correlation is somehow lower. However, this can be traced back to forcing variability within the subpolar

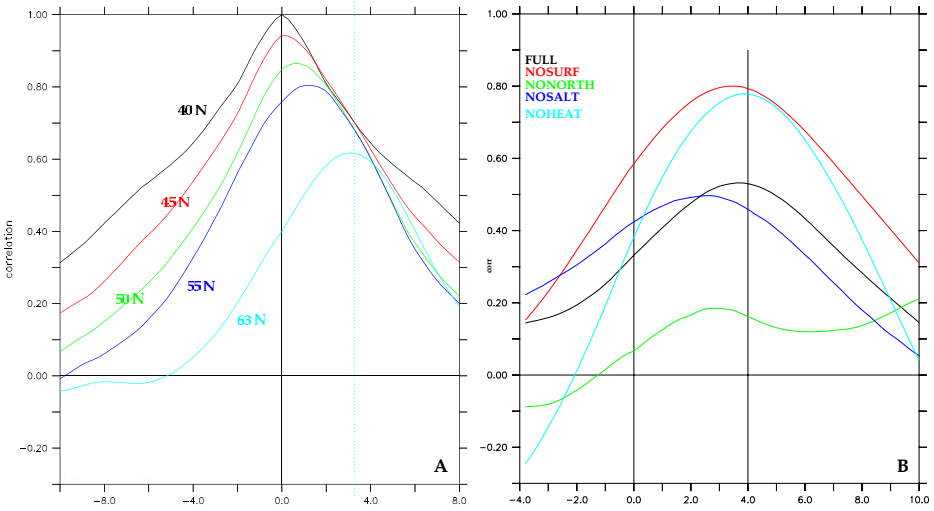

Figure 5.13: *A: Lag correlation of overturning maximum at different latitudes relative to 40° N in experiment FULL; B: Lag Correlation of DSOW density and overturning maximum at 40° N for different experiments; each is smoothed by a 5-year running mean filter.*

gyre.
As expected, the correlation between DSOW density and overturning in *NONORTH* is quite low (figure 5.13,B), green curve). An interesting point is the shorter lag in the experiment *NOSALT* between two and three years, which is almost as large as in experiment *FULL.* (blue curve). In this study the variability of the overturning index on the considered scales is both forced due to heat flux variability in the subpolar gyre and temperature changes in the north. However, the temperature variability in the Nordic Seas is quite low, so that the impact in the subpolar region is seen. This heat flux variability within the subpolar region to some extent seems to accelerate the response of the overturning index on changes in the overflow water mass properties in comparison to experiment *FULL.*

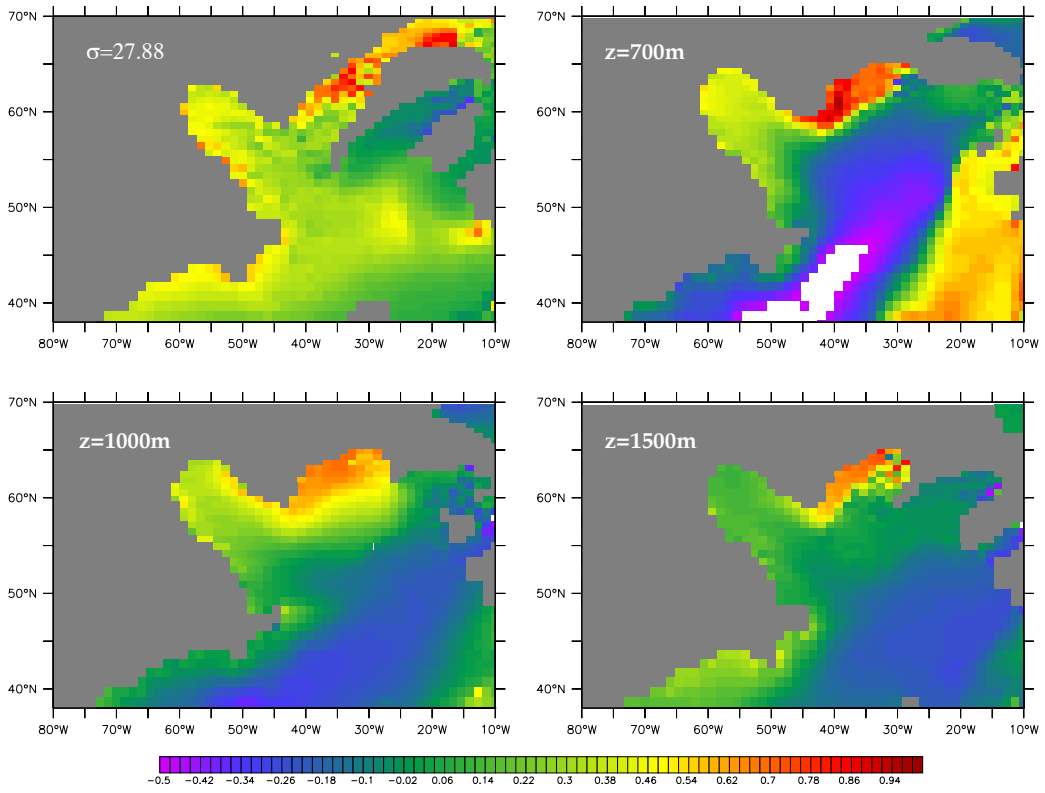

Figure 5.14: *Map of correlation of the overturning function at 40° N in 1000 m and the density in the basin at a lag of 4 years between year 1950 and 2050 in experiment FULL; the vertical position is denoted in the figures, the overturning time series is smoothed with a 10-years boxcar filter in order to effectively eliminate the variability below 10 years.*

Using experiment *FULL*, we are able to calculate a map of this correlation between the overturning at 40°N in 1000 m and the density evolution at all grid points in the North Atlantic for different vertical levels. Since we are interested in variability on at least decadal scales, we smoothed the overturning time series by a 10 years running mean filter, in order to effectively eliminate all higher frequencies. In

figure 5.14, the correlation is shown in four different vertical views. Apparently, the correlation is strongest in the downstream vicinity of the Denmark Strait sill. Following the correlation map on isopycnals ($\sigma_\Theta = 27.88 kg/m^3$ is chosen as a layer covering the whole domain from the sills downstream and being the upper boundary of the Denmark Strait Overflow), nowhere else such a high value can be found. Looking into greater depth, the overflow signal, following the depth contours remains the crucial factor for variability in the overturning function. Remarkable is the decoupling of the deeper GIN Seas. Already at a depth of 700 m, which is only about 50 m deeper than the Denmark Strait sill, the density signal shows no significant coherency to the overturning strength. Below, at a depth of 1000 m respective 1500 m, this still holds. Downstream, in the depth of 700 m, the signal following the East Greenland Current can be found within the Irminger Sea. This feature must be attributed to the variability of the boundary current, which is also affected by anthropogenic changes of the northern sponge area. Indeed this signal spreads faster than the abyssal signal. However, it has less impact on the overturning strength.
The strong minimum in the central North Atlantic is the result of the geostrophic adjustment of the ocean model. When the meridional overturning function strengthens, the core is shifted downward with the consequence that the warmer and lighter branch of the circulation is found in this depth. Therefore the overturning maximum is negative correlated with the density at that depth.
The correlation between the overturning and the density in the vicinity of the sills again underlines and explains the additive behaviour of the individual air-sea-fluxes, we found in section 5.5.2: Since the crucial factor seems to be the density at a relatively shallow depth, in this region convective adjustment is able to mix the surface waters into a depth of about 600 m, no matter how strong the anthropogenic signal is.

These lag correlations give a robust answer to the question, if the Denmark Strait Overflow densities steer the system or if they are a response to changes in the circulation. Since the overturning response follows the density signal with a lag of about four years, it is found to be more the reason for changes in the MOC than a response.

5.5.6 The recoverage of the overturning circulation

Studies about the stability of the thermohaline circulation during global warming experiments often go into the matter, whether the system is in the vicinity of a *point of no return*. In other words, the question arises, if greenhouse warming might cause the overturning to weaken significantly or even collapse without a quick recoverage to today's state on centennial timescales.
Answering this question, in simplified models the possibility for fundamentally different equilibria was examined (e.g. Marotzke and Willebrand, 1990), leading to the result that beyond our present circulation, there are several states possible. The shift from one circulation into another could be caused by relatively small surface forcing perturbations.

Using three-dimensional ocean models with an idealized geometry, the existence of a *deep decoupling oscillator* was found by SARACHIK ET AL. (1996). Accordingly to that theory, forced by a constant atmosphere, the ocean oscillates between two quasi-equilibrium states. The (strong) one is gradually reduced due to increasing freshwater flux into the northern ocean. As a consequence, the overturning circulation declines and falls into the second (weak) state. The recoverage of this weak MOC takes place on diffusive timescales of the order of 1000 years. During that time the uncoupled deep ocean is diffusively filled with warm water, leading to strong hydrostatic instability and subsequently to a *flush* of the order of 100 Sv of overturning. This impact shifts the ocean into the strong MOC situation again. The existence of such an oscillation depends on the rate of freshwater disturbance: For a too strong flux, the meridional circulation is suppressed, for a too weak flux, the strong state reaches a heat flux forced equilibrium.

Due to the anthropogenic forcing time series, we integrated different scenarios for about 150 years only. Therefore, in terms of the MOC recoverage, we can only investigate the oceanic state at the end of the integration period. Looking at figure 5.3, the maximum trend of the overturning index between year 1950 and 2090 is about 6 Sv in 140 years (experiment *FULL*). The strongest oscillations are given in experiment *NOHEAT* with an amplitude of 4 Sv during year 2060 and 2080. This strong variability is traced back to changes in the freshwater budget north of Iceland. This result gives an idea about the system's ability to recover. Following the results concerning the reason for long-term trends (section 5.5.4), the main structure is indeed given by the reservoir density at in the Nordic Sea. Therefore, having the question about the recoverage of a weakened system in mind, for our experiments with a weakening of about 30% it can be answered easily: As long as deep water formation sets in or is strengthened again, the overturning system is able to recover in dependence of the reservoir's density. In today's oceanic state as it is simulated in *FLAME4/3*, a temporal weakening seems to have no long-term impact on the ability of the system to recover. To underline this statement, we integrated *FLAME4/3* in a recovery experiment. Because of the absence of forcing data beyond the 21^{st} century, we performed an experiment, in which we reversed the forcing time series in the the density structure in the Nordic Sea. Starting in year 2090 with the situation of experiment *NONORTH*, we drove the deep water forcing back to the values given in the year 1950. In doing so, in the year 2230 we reach the density values of the starting situation. Looking at the time series of the maximum overturning function, it is no surprise, that it totally recovers (figure 5.15). Again, like the caveats concerning the individual air-sea fluxes (section 5.5.2), this procedure ignores the important question of the ability of the system for deep water formation in the GIN Seas. Instead of being the result of complex air-sea-ice feedbacks, we assumed, that somehow the reservoir of deep water is refilled. This could, for example be the consequence of drastic reduction of anthropogenic forcing.
Although again an argument for the uncoupled ocean, this response is close to results from LATIF (*pers.com.*) in the coupled *MPI* model. They found a relative

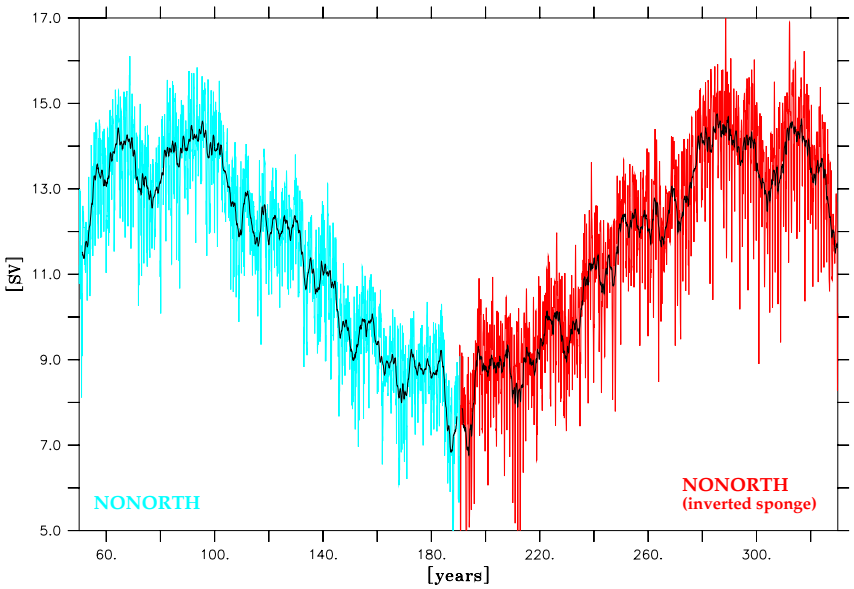

Figure 5.15: *Time series of overturning strength at 40° N in 1000 m depth of experiment NOSURF (year 1950-2090) and of NOSURF with the reversed northern sponge time series (year 2091-2230).*

linear recoverage of the overturning function after CO_2 disturbances are driven back to the present-day's state. Looking at most climate models and their response in greenhouse forcing scenarios, using the overturning index as a measure for the changes (figure 4.1), all models show a more or less linear response to anthropogenic forcing. None of them is close to a bifurcation point, when it is initialized with a present-day's state.

5.5.7 The role of the wind stress

In section 2.7.1 by showing a power spectrum of the overturning index (figure 5.5), the role of the wind stress on the overturning function was investigated. In terms of interannual variability, the wind-driven spinup of the subpolar gyre is the crucial factor of variability. Figure 5.16 shows the differences between the annual mean overturning function of the years 2060 and 2061 of the *NOWIND* and *FULL* experiment. Here, comparing the buoyancy to the wind forcing impact, there is almost no variability ascribed to the former.The wind-induced variability is much stronger. When the zonal wind stress increases (decreases) (related to higher or lower NAO), the southward Ekman transport is strengthened (weakened). This affects the upper branch of the overturning cell, which is reduced (enhanced), as it is found in *FLAME* models by Beismann et al. (2002). This leads to the higher variability found in the right picture. In a study with artifical increased wind stress over the subpolar gyre, Biastoch et al. (2003) showed that the mean strength of the gyre circulation is an important factor for the strength of the overturning function. By attaining a new equilibrium state, they found a quite

barotropic wind-driven response of the circulation around Iceland, which finally affects the overturning function. In section 2.7.1 we showed a similar response in a *FLAME4/3* sensitivity study without any wind stress forcing. However, the implemented wind stress anomalies from the global warming scenarios are not as enduring and have only an impact on shorter scales.

Comparing the differences on longer time scales (2040-2060, lower panel) in the subpolar gyre, the decrease due to buoyancy forcing in experiment *FULL* and *NOWIND* is quite similar. It is mainly given by the surface heat flux trend in the North Atlantic. In lower latitudes, there are some differences due to the variable gyre circulation in experiment *FULL*.

However, we cannot contribute to the point, whether a higher NAO can stabilize the THC, as it is suggested by Delworth and Dixon (2000). Since the implemented anthropogenic surface fluxes are part of changes in the NAO pattern, no separation can be made here. By calculating NAO regression pattern of the surface heat fluxes, Eden and Jung (2001) found, that most of the oceanic variability can indeed be ascribed to NAO forcing. Anyhow, in terms of global warming, the role of the pure wind stress seems to be of minor importance for the trend of the overturning circulation. A limitating point in this context is surely the simulation of deep water formation. The physical processes leading to the renewal of deep water in terms of the gyre circulation, e.g. the *doming* of the water column or the deep convection on relatively small scales (e.g. Marshall and Schott, 1999)

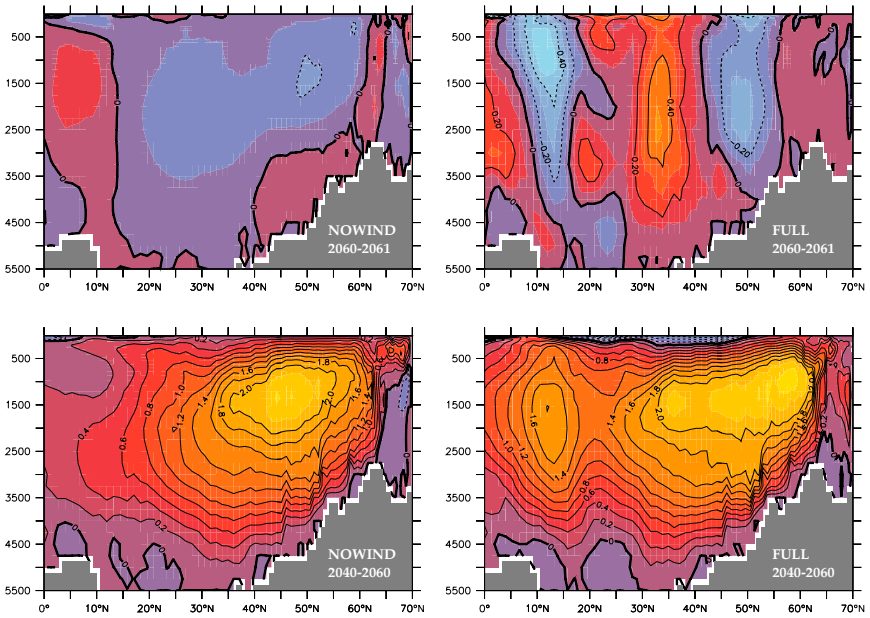

Figure 5.16: *Differences between annual mean overturning cell of the years 2060-2061 (upper panel) and 2040-2060 (lower panel) of experiments NOWIND (left) and FULL (right). The wind stress variability dominates the short-term response, the long-term response is provided by buoyancy forcing.*

cannot be resolved in ocean models properly, so the specific impact of the wind stress might not be realistic.

5.5.8 The overflow representation

In section 5.5.2 and 5.5.3, the sensitivity studies underlined the importance of the water mass properties north of Iceland for the strength of the overturning circulation. These waters are namely the Denmark Strait Overflow Water (DSOW) and the Iceland-Scotland Overflow Water (ISOW). In section 5.5.5 we found a high correlation between the Denmark Strait Overflow and the overturning strength at 40°N. Therefore, here we concentrate on the Denmark Strait Overflow, its representation and its impact on the overturning circulation.

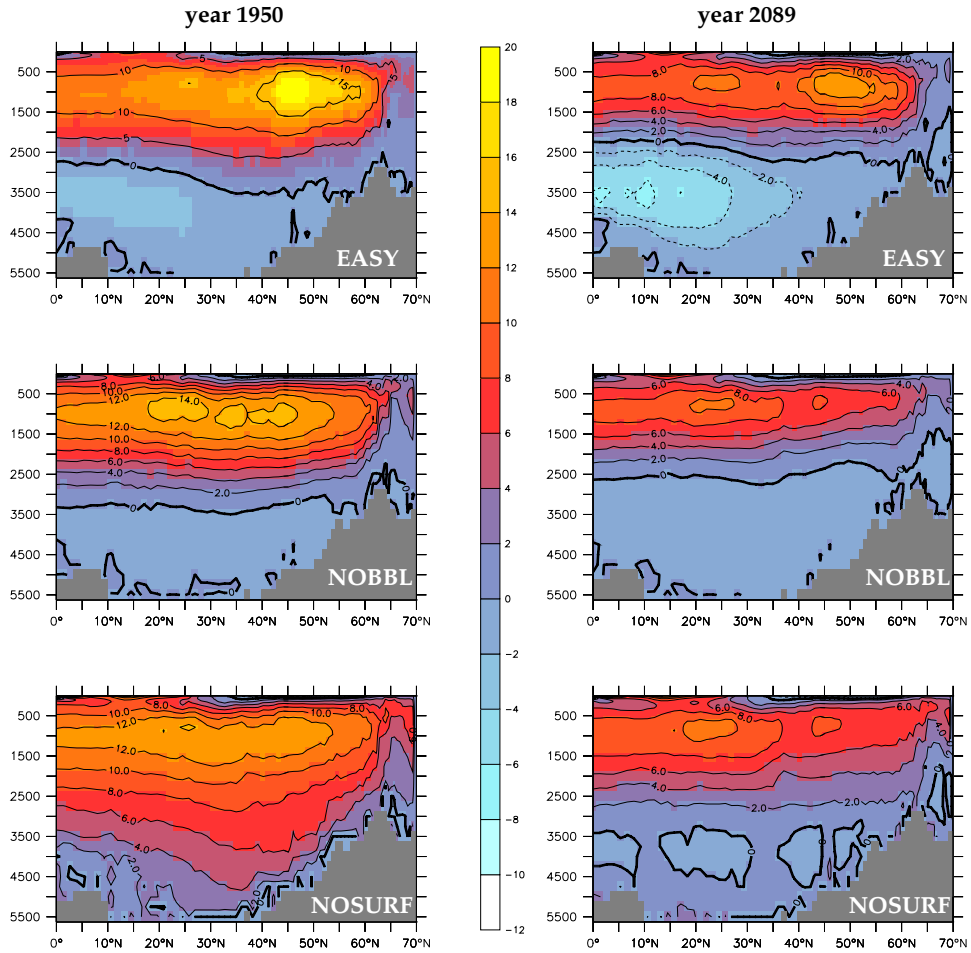

Figure 5.17: *Annual mean overturning function in year 1950 (left) and year 2089 (right) of experiments denoted in the figure, unit is Sv.*

Döscher and Redler (1997) found in MOM-style ocean models that the representation of flows through narrow passages play a substantial role for the THC. Their sensitivity experiments suggest that the presence of a deep and concen-

trated Denmark Strait Overflow makes the overturning circulation less sensitive to changes in the subpolar near-surface buoyancy field. Since most climate models' oceans are clearly unable to represent such narrow passages, they could be too sensitive on long-term variability or even on the impact of global warming. In this study, we already showed that the overturning response of these models does not change fundamentally, even if narrow passages are present like in *FLAME4/3*. In order to prove this result, we performed two more experiments with an even more unrealistic representation of the Denmark Strait Overflow (see section 5.3 for details).

Since the mean state of the meridional circulation is very different in experiments with a different set of parameterizations, we had to perform new spinups for the two sensitivity studies.
In the case without BBL (experiment *NOBBL*), the overturning cell in the North Atlantic is much shallower, the cell of the Antarctic Bottom Water (AABW) reaches from 3000 m depth down to the bottom. In spite of the different shape of the cell, the maximum overturning is very similar to the case, in which the BBL is switched on.

So, although the overflow plume representation is much more realistic at the beginning of *NOSURF*, the strength of the overturning, which is strongly connected to the meridional heat transport, does not significantly depend on this parameterization. As in the BBL case, the overturning weakens with a very similar shape. So, just looking at the MOC as a measure for the oceanic heat transport in the North Atlantic, the ocean model does not depend significantly on a realistic overflow parameterization. This result is already known in former studies with *FLAME* ocean models (Eden, 1999). Although the effect is a much more concentrated plume and reduced entrainment in the subpolar gyre, the maximum overturning strength remains almost unaffected.

Combining *NOBBL* with horizontal diffusion as well as a Denmark Strait of 1000 m depth (experiments *EASY*) leads to an overturning cell which is about 5 Sv stronger but still as shallow as in experiment *NOBBL* (figure 5.17, left upper panel). By dredging the Denmark Strait, the cross section is widened and the street is no more as narrow as before, so that no more realistic overflow is simulated. As a consequence the core of the overturning cell is shifted to the north and is now localized at about 50°N.
While the BBL parameterization already affects the communication of the plume into the subpolar basin, here even the transport of dense water, still supplied from the Nordic Seas, is worse compared to observations (e.g. Girton et al., 2001). With 8 instead of 3 Sv, the transport is more in the vicinity of the isopycnic *OPYC3* model (figure 5.1, upper panel), in which in fact the topography of the passages was as well idealized to receive a reasonable overturning strength. The modifications in experiment *EASY* lead to quasi-equilibrium state with a maximum overturning of 21 Sv in the North Atlantic, which is localized further in the north at about 50°N (figure 5.17). This result shows the limitation of the narrow

streets for the supply of the overturning circulation. An ocean model, forced with identical boundary conditions and also identical rates of deep water formation in the GIN Seas increases its overturning, when the passages are opened in order to get a greater transport.
However, although with a stronger overturning function, this experiment has a quite reasonable meridional heat transport maximum of about 1 PW. So, the *EASY* configuration is somehow tuned in order to permit realistic heat transports although the overturning function is too strong. Jia (2002) compared a number of coupled models and found that the overestimation of the overturning strength in most climate models is compensated by a too warm deep branch of the circulation. She found a mean deviation of North Atlantic Deep Water temperature of about 2.5°C. This leads to a lower slope of the temperature-overturning dependency. Here we have something similar. By enhancing the overturning and the diffusion, both effects are somehow compensated and lead to an oceanic heat transport, which is as high as in the *FLAME4/3* version with isopycnal diffusion and GM90.

In the greenhouse simulation relative to experiment *NOSURF*, experiment *NOBBL* and *EASY* show, concentrating on the maximum strength of the overturning, a nearly identical relative decrease. While the decrease of *NOSURF* from 16.5 Sv to 11.5 Sv is about 30%, in experiment *EASY* the overturning slows down from 21 Sv to 16 Sv, what is a very similar percentage decrease (figure 5.18,A).
Although the surface boundary conditions for heat in both integrations are identical, due to the formulation of the surface heat flux, the heat budget need not necessarily be identical in the North Atlantic of *FLAME4/3*. Since surface heat fluxes respond on changes in the properties of the northward branch, a situation, in which advective changes at the surface lead to changes in the deep water formation rate is possible. However, this effect seems to be small. The heat budget is dominated by the local surface heat fluxes. Nevertheless, the time series of the maximum meridional heat transport is identical in the *NOSURF* and *EASY* simulation. Starting with 1 PW in the 20^{th} century, it is reduced to 0.8 PW in year 2090. Following these results, the shape of the lower branch of the circulation seems

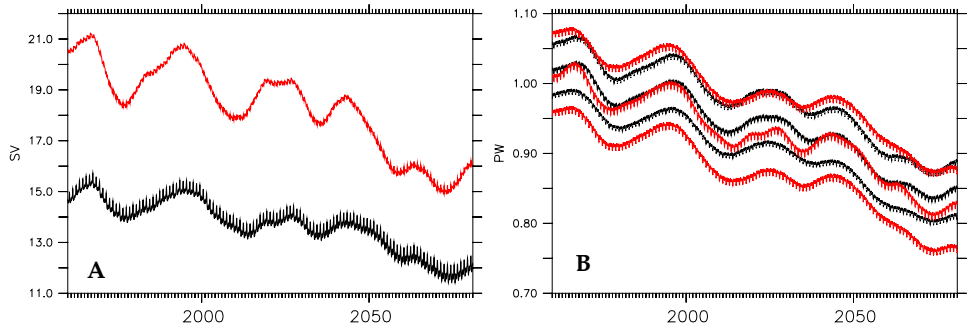

Figure 5.18: *A: Time series of maximum overturning in the North Atlantic; B: time series of maximum heat transport; experiments: NOSURF(black) and EASY(red).*

to be relatively unimportant for the heat transport.
In summary, even in these in a physical sense reduced experiments, the general response of the overturning function and hence the meridional heat transport remains very similar to the behaviour in the greenhouse warming integration of coupled models.
The role of the GM90 parameterization as well as the isopycnal diffusion seems to be quite small in the ocean interior. Results from WIEBE AND WEAVER (1999) and MCDOUGALL ET AL. (1996) indicate that due to the GM90 parameterization the efficiency of oceanic heat uptake during the transient phase of CO_2-increase is reduced. Since in our model the changes in the heat uptake in the crucial region north of Iceland do not primarily depend on the heat uptake but on the restoring towards prescribed values, here no conclusion can be made. Whether this holds for the subpolar gyre is beyond this study. But it seems to be unimportant in *FLAME4/3* in global warming simulations of this style for an integration period of 150 years. Additionally, WIEBE AND WEAVER (1999) found a strong dependency of different subgrid parameterizations in high latitudes, while in an integral sense the ocean has only a weak feedback on global mean surface air temperatures. Again, this statement cannot be proved here, since the impact of deep water formation in the subpolar gyre is relatively unimportant compared to the physical interplay of surface fluxes together with parameterizations in the Nordic Seas.
To get back to the role of the narrow passages, following our results, the crucial point seems not to be the narrow passages, leading to a concentrated signal, but the density signal provided by the northern region. This is forced with the same time series in these experiments, leading to a very similar response.

5.6 The Labrador Sea under GFDL forcing

In comparison to the results with *MPI* forcing within the Labrador Sea in section 4.7, there the response of the *GFDL* forced *FLAME4/3* model in different sensitivity studies in that region is shown.
In the quasi-equilibrium case of *FLAME4/3*, deep water formation within the Labrador Sea takes place every single year. Moreover, there is some deep water formation in the Irminger Sea as well contributing to the overturning strength (see section 2.6 for details).
In former studies, the heat flux variability in ocean models was found to be the crucial factor for changes in the deep water formation rate in this region. Especially the annual cycle of heat fluxes leads to a uniform renewal of Labrador Sea Deep Water (LADW). The decision, whether deep water formation can take place or not is mostly given by the intensity of winterly cooling.

Looking at the differences of the heat flux time series of the the sensitivity experiments (figure 5.19i, upper panel), the dominant role of the local fluxes becomes clear. While in experiment *NOSURF*, although the overturning strength is reduced at about 30%, the surface flux remains almost constant, *NONORTH* and *FULL* show an nearly identical series. Therefore, the impact of changes in lateral

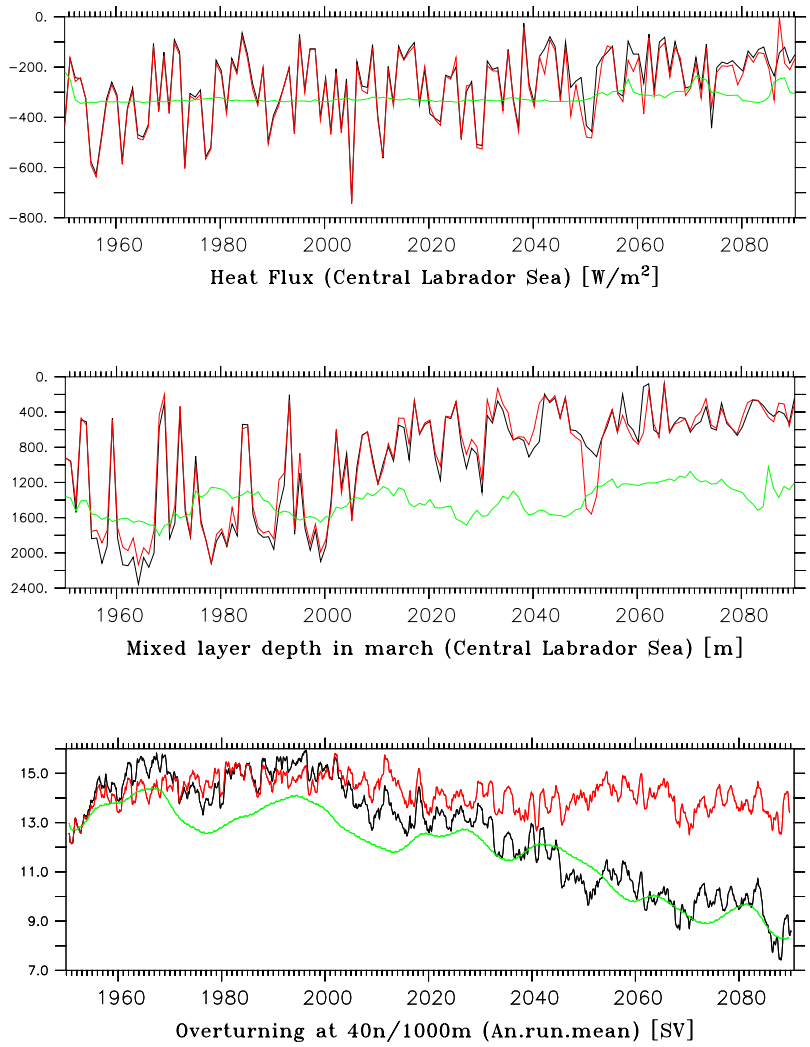

Figure 5.19: *Timeseries of parameters denoted in the figures in the Labrador Sea at 54-58° N and 52-48° W, black: FULL, green: NOSURF, red: NONORTH.*

transports into the crucial region can be neglected in these experiments. Features, where e.g. warmer water is transported into the Labrador Sea by the East and West Greenland Current to be additionally cooled, seem to be relatively unimportant. This was already found in section 5.5.3, where there was almost no interaction found between the two regions of deep water formation.

Nevertheless, this result cannot be found in experiments with higher resolution *FLAME* configurations. The gyre transport of water from the boundary currents was found to be much more important for the properties of the Labrador Sea surface waters. In *FLAME1/3*, errors in the gyre transport into the central Labrador Sea cause the LADW to become too dense in spite of surface restoring to realistic values. Accordingly the convection regime reaches an unrealistic depth. To overcome this problem, some experiments with increased thickness diffusion coef-

ficients have been performed. In these experiments, a strong dependency between the Labrador Sea density and the boundary current properties and transports were found (*Flame Group, pers.com.*).
Looking at the mixed layer depth in the three experiments, a good agreement between *NONORTH* and *FULL* can be seen (figure 5.19, middle panel). As a consequence of local changes in the surface fluxes, their response is almost identical. The reduced cooling during the warming scenario impede the deep water formation after the year 2030. The vertical mixing is reduced to less than 600 m even in wintertime (figure 5.19, center). In contrast to experiments performed with *MPI* fluxes, the deep convection does not stop abruptly, but loses depth between the year 2000 and 2040. This must be attributed to the higher temperatures in the MPI model in that region.
The response in experiment *NOSURF* is quite different. The mixed layer depth remains almost constant, in the second half of the 21^{st} century it is slightly reduced due to lateral transports.

A part of these differences in the Labrador Sea can be found in the variability of the overturning function as well. Looking at timescales up to a few years, the variability is very similar in experiment *FULL* and *NONORTH* (figure 5.19, lower panel). Although the convection in the central Labrador Sea breaks down, the overturning is only slightly reduced in the experiment with unchanged overflow properties. Moreover, although there is still some deep water formation in experiment *NOSURF* in the 21^{st} century, this cannot prevent the trend of the overturning strength.
At the beginning of the global warming experiments, there seems to be much contribution due to variability coming from the subpolar gyre. In the experiments with anthropogenic surface forcing, the overturning strength is at about 1.5 Sv higher than in *NOSURF*. This can directly traced back to high rates of deep water formation between the years 1960 and 2200.

These results underline again results from Döscher and Redler (1997), that, if a sufficiently dense overflow can be maintained, the importance of deep water formation within the Labrador Sea is not so important, if we are just interested in the general behaviour of the overturning function.
To put the results from the integrations of *FLAME4/3* with *MPI* fluxes into perspective, we found a much more abrupt breakdown of the deep water formation in that region. To compare these results, the horizontal circulation of the climate models give a hint about the reason for differences. Since our anthropogenic surface heat flux is a combination of heat flux anomalies and restoring to SSTs (see equation 2.7), both have an impact on the heat flux felt by *FLAME4/3*. Both climate models suffer from a realistic Gulf Stream separation, so the evolution of the Gulf Stream temperatures affect the heat flux over the Labrador Sea in the ocean model. Since in the *MPI* model, the Gulf Stream maintains its strength with increasing temperatures, the anthropogenic heat fluxes are stronger in that model. However, this result is somehow a consequence of the implementation method we used for this study. So the heat fluxes need not necessarily be a result of local

heat flux variability given by the feedback mechanisms within the coupled model. Nevertheless, as in the results found by WOOD ET AL., the Labrador Sea seems to be the region, in which deep water formation is strongly affected by anthropogenic changes in air-sea fluxes.

5.7 The heat budget of the North Atlantic

In the previous sections, we showed that for fundamental changes in the overturning circulation in *FLAME4/3*, the crucial factor is the evolution of the density structure north of Iceland in the Nordic Seas. The caveats concerning the implementation of anthropogenic forcing data and problems about their interpretation are already mentioned in section 2.3. In this context, there are two important points worth to investigate, since they constrain the results of the previous sections in some sense.

The first one is the northern sponge area. In our model, the water mass properties in the vertical restoring zone are given by a combination of lateral signals, restoring salinity and temperature to fixed values as well as surface forcing. Because the restoring becomes stronger, the more the lateral signals diverge from the prescribed water mass properties, the contribution of the different parts cannot be examined this way. However, instead of understanding the sponge region as a modeled part of the ocean, the representation of the Nordic Seas in *FLAME4/3* must be understood as an integral effect of the northern domain. Therefore, all signals from the surface and from the boundary (in fact the restoring terms) must be handled as the response of the polar ocean in order to supply water to the southern basin. Therefore, changes in tracer transports into and out of the restoring area of the uncoupled ocean model should in some way be comparable to the transport changes in the climate model.

The second point is the surface heat flux of the model, which is not totally switched off, when anthropogenic surface forcing is switched off. There remains a residual term, which originates from the change of heat fluxes due to the response of a fixed atmosphere to changes in the oceanic state. So, the experiments still have a degree of freedom concerning the heat flux into the ocean. Therefore the experiment *NOSURF* for example also implies some changes in the surface heat flux due to interactions of a changed ocean to an unchanged atmospheric state. Since in our regional model these two points might have some artificial impact on the overturning circulation response, in this section we calculate SST changes, heat flux changes as well as a total heat budget of subpolar North Atlantic as well as of the area north of 66°N for *FLAME4/3*, when it is forced with *GFDL* fluxes.

Looking at the heat flux during the integration period, the lateral effect on it at the ocean's surface seems to be small. Figure 5.20 shows the differences in surface heat fluxes between the averaged periods of 1950–1960 and 2080–2090. Very similar is the surface heat flux in experiment *FULL* and *NONORTH* (upper left and lower left panel). Both show the strongest heating in the central Labrador Sea. This

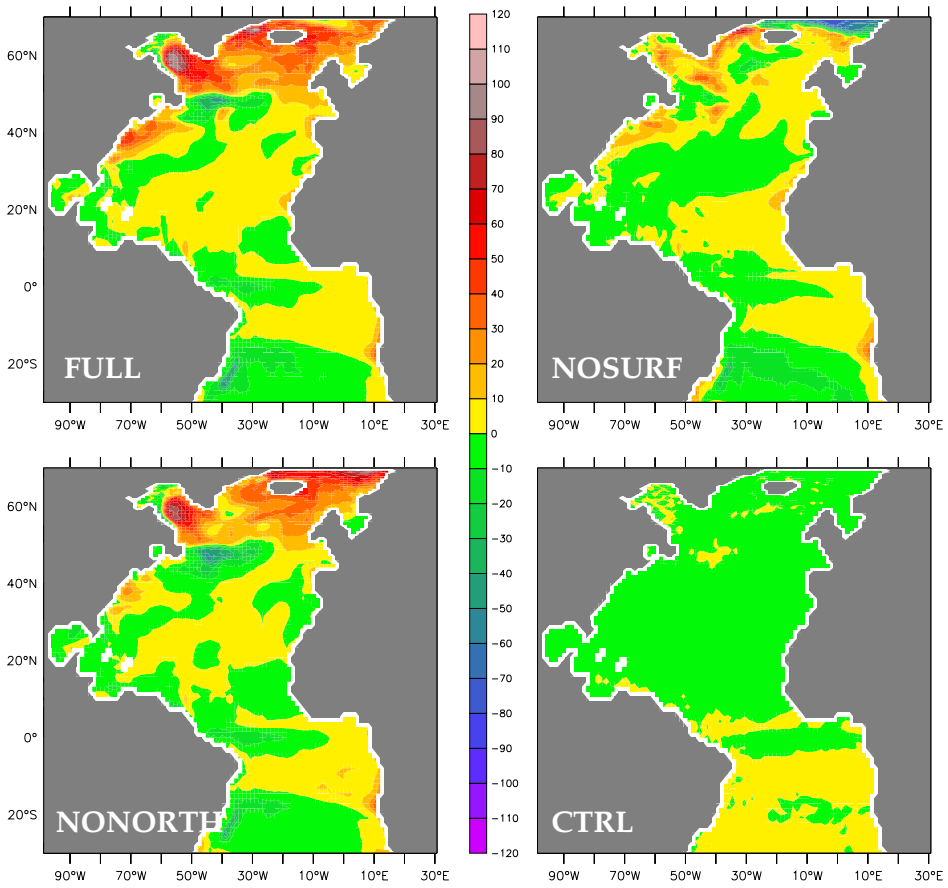

Figure 5.20: *Difference between the heat flux at the beginning of the anthropogenic forced experiments 2080-2090 (averaged) and the end 1950-1960 (averaged) in the experiments denoted in the figure. The local fluxes are mainly determined by local processes.*

confirms results concerning the deep water formation in this area (section 5.6): In *FLAME4/3* it mainly depends on local ocean-atmosphere interactions, so that the lateral impact of water from the Nordic Seas is of minor importance in this case. In the region of the restoring area, the increase in surface heat flux is much higher in the *NONORTH* sensitivity experiment. Here, the ocean temperatures are fixed due to climatological restoring. Therefore, the surface boundary condition works against this constraint with enhanced fluxes. In the Gulf Stream, experiment *FULL* shows an increase in surface heat flux compared to *NONORTH*. The reason is that in the *FULL* experiment, the overturning strength and with it the transport of warm Gulf Stream water is reduced. As a consequence, the strong heat flux into the atmosphere due to evaporation is also reduced, leading to a positive heat flux anomaly into the ocean.

Comparing experiment *NOSURF* the surface cooling is also to some degree reduced due to the remote effect of the implementation of anthropogenic forcing in

the northern boundary condition. However, it is much less than in the experiments with anthropogenic surface forcing (figure 5.20, right upper panel). Only along the East and West Greenland Current changes in the water mass properties lead to some modifications of the heat flux. Here, the cold water from the north becomes warmer due to the anthropogenic signal in the northern sponge. In the climatological integration, surface warming sets in, when the surface waters travel southward. This is now reduced, since the surface waters are already warmer there. Above the northern restoring area, this experiment responds with some increased cooling, since the water is warmed due to the sponge heating. This is in some sense an "uncontrolled" part of the surface heat flux. Although the surface boundary condition is not changing in this case, the flux shows a warming. This is strongest in regions of high velocity in connection with strong temperature gradients such as the East Greenland Current at the southern boundary of the northern sponge zone. In the case of *NOSURF*, the southward transport of cold water is reduced. As a consequence, the upper water masses become colder, leading to a reduced net ocean heat loss within the subpolar gyre. This is a *destabilizing* positive temperature feedback of the ocean model, which is traced back to the surface boundary condition for heat. In a coupled system, this feedback is also possible: A weaker overturning signal leads to a larger meridional temperature contrast and therefore to an increased atmospheric heat transport, leading to less cooling of water in the subpolar gyre (MAROTZKE, 1996). However, this reduced cooling is concentrated in the East and West Greenland Currents, where the strongest cooling within the subpolar gyre in the climatological integration takes place. It has therefore only little effect on the heat budget of the subpolar gyre. The atmosphere is unchanged in an anthropogenic point of view but there are still changes in the surface heat flux due to ocean-atmosphere feedback mechanisms.
The comparison of these three pattern shows the importance of the atmospheric component for the local fluxes. Differences due to lateral transports of water of changed properties are less important.

Comparing the temperature field in 100 m depth for the different experiments with anthropogenic forcing (figure 5.21), the pattern is quite similar to the heat fluxes described above, also underlining the important role of local flux changes relative to lateral transports. As well experiment *FULL* as *NONORTH* show a temperature increase between 1 and 4°C, which is very similar (upper left and lower left panel). Although the overturning circulation is reduced at about 30% in experiment *FULL*, the temperature is relative similar in both experiments at that depth. The strongest increase is given at the subpolar front. This must be attributed to the shift of the subpolar front into the north. Anyhow the heat flux pattern shows no significant increase in that region. Here due to the rearrangement of the horizontal circulation, this temperature increase is given. Comparing the impact of the reduction of the meridional overturning circulation, there are only small differences between these experiments. The heating is a little stronger in the *NONORTH* experiment, since additional to the surface forcing, the oceanic heat transport is mainly unchanged. This difference is strongest in the region, where

the Gulf Stream separates from the coast and transports its properties.

Moreover, in the northern sponge area the situation is of course much more different. Here, experiment *NONORTH* shows no significant changes in temperature, since the water mass properties are fixed. In contrast *FULL* shows a similar response as in the region south of the sills.

Vice versa is the response in experiment *NOSURF*. Although the overturning circulation is reduced at about 30%, the temperatures in 100 m depth are only slightly reduced in some regions of the subpolar gyre (lower left). However, in the northern restoring area, the temperature is increasing due to sponge forcing. Differences to *FULL* due to lateral signals can only be found in the southern end of the restoring zone. Anyhow, at the subpolar front, some additional warming can be found. This can be attributed to the shift of the subpolar gyre in *FULL* and *NOSURF*. Moving northward, the Gulf Stream spreads its water properties further into that region.

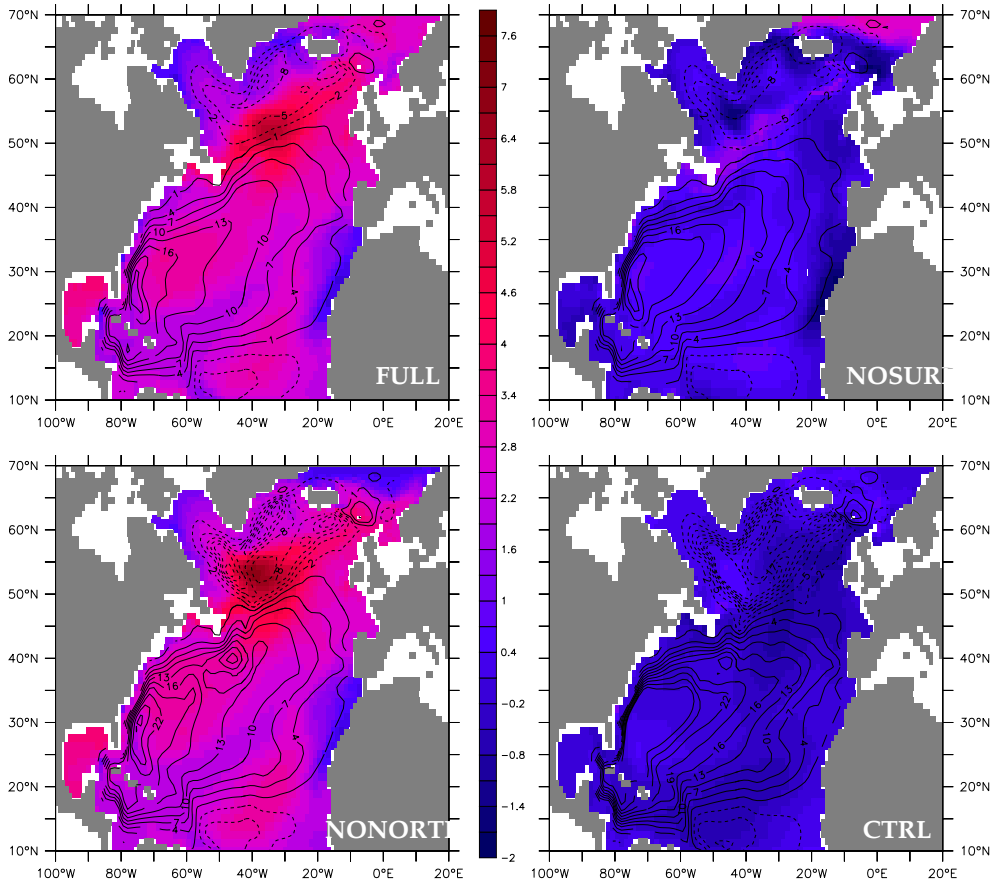

Figure 5.21: *Temperature increase in 100 m depth in year 2089 relative to year 1950; upper left: FULL, upper right: NONORTH, lower left: NOSURF, lower right: CTRL; overlaid is the barotropic stream function at that time. The temperature evolution in the subpolar gyre does hardly depend on lateral signals from the Nordic Seas.*

For comparison, the lower right panel shows the response in the *CTRL* experiment with no significant change in the temperature of 100 m.

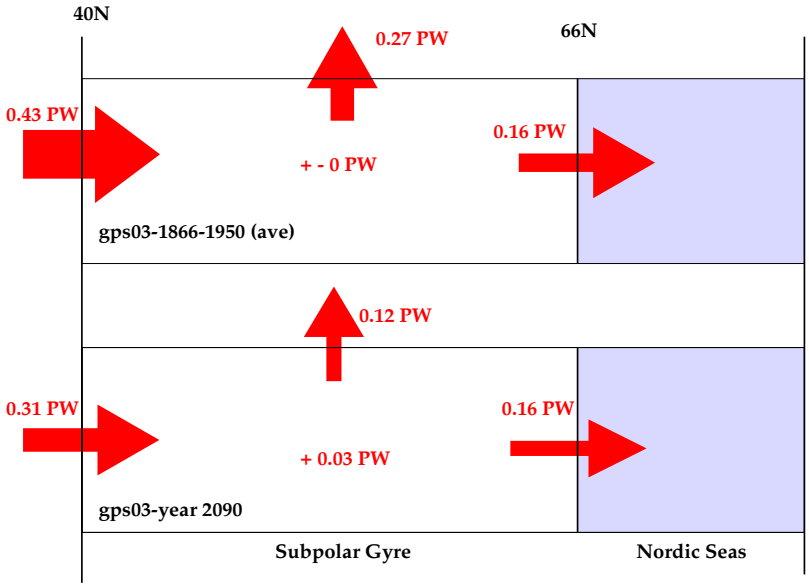

Figure 5.22: *Heat budget of the coupled GFDL model; shown is the average between 1866-1950 (upper panel) and the situation in year 2090 (lower panel); changes in the oceanic heat transport are balanced within the subpolar region.*

To give an overview over the changes of heat budget for some of the experiments with anthropogenic forcing, we calculated the integrated oceanic heat balance for the subpolar gyre. Following e.g. T. DELWORTH ET AL. (1993), the heat budget for a specific volume with closed zonal boundaries in Cartesian coordinates is given by the equation

$$\begin{aligned} \frac{\partial}{\partial t}\int_{x_1}^{x_2}\int_{y_1}^{y_2}\int_{z}^{0} c_p T \rho dx dy dz &= \int_{x_1(y_1)}^{x_2(y_1)}\int_{z}^{0} v c_p T \rho dz dx \\ &- \int_{x_1(y_2)}^{x_2(y_2)}\int_{z}^{0} v c_p T \rho dz dx \\ &+ \int_{y_1}^{y_2}\int_{x_1}^{x_2} Q dx dy. \end{aligned} \tag{5.1}$$

Hereby the change of the heat storage is given by the difference of the transport at the southern and northern boundary of the area as well as by the surface fluxes.

Calculating these terms for some of the performed experiments, we show the results as annual mean values at the end of each integration. Figure 5.23 shows in the upper panel the equilibrium state of *FLAME4/3* with 0.53 PW heat transport across 40°N. Across 66°N, there remains 0.19 PW. Without any significant additional storage in this integration, the residual of 0.34 PW is released to the atmosphere in the subpolar gyre between these two latitudes.

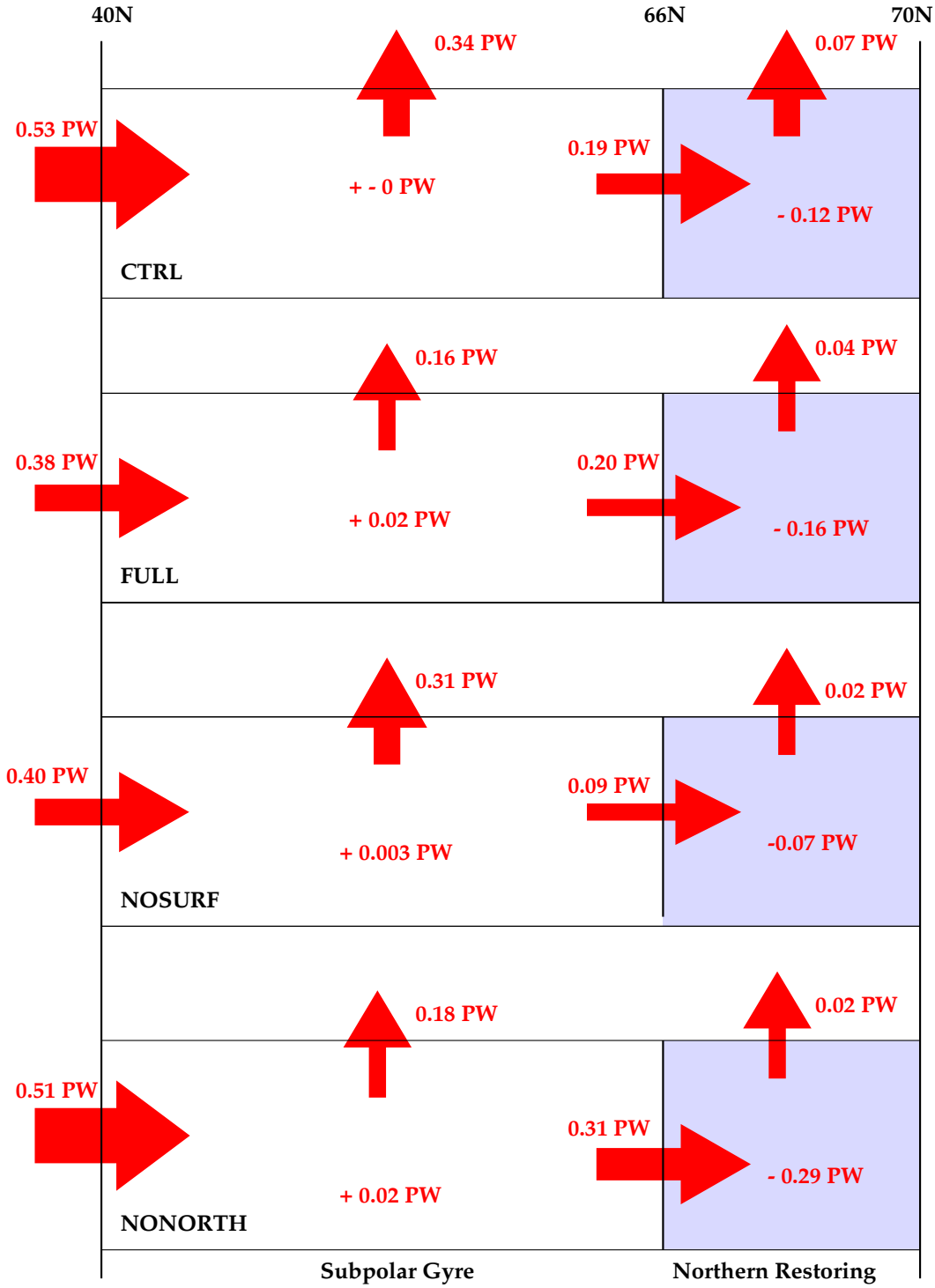

Figure 5.23: *Heat budget at the end of the integration period of GFDL forced experiments within the subpolar gyre. The response is quite similar to the climate model's evolution.*

At the end of experiment *FULL*, the situation is different: By reducing the overturning strength, the northward heat transport declines to 0.38 PW. The budget is balanced by a reduction of surface cooling due to anthropogenic forcing as well as a changed storage within the ocean. Surprisingly, the northward heat transport over 66°N is almost unaffected. Only a slight increase to 0.20 PW is diagnosed. So the heat balance is almost totally closed within the subpolar gyre. This is an important result, since the transport of relatively warm water into the Nordic Seas is of fundamental importance for the ability of the ocean to renew deep water. Comparing the evolution within the climate model, figure 5.22 shows the situation at the beginning and at the end of the coupled greenhouse scenario with the *GFDL* model. Also is that experiment, the transport across 66°N is not reduced while the overturning decreases under global warming conditions, but remains at 0.16 PW. This point is quite encouraging for our method, since the transport across this sill is given by a combination of sponge and surface forcing in the basin. The result, that its evolution is so similar to the coupled integration, justifies the implementation technic. Nevertheless, the communication into the Nordic Seas in this specific climate model is underestimated relative to observations (e.g. TRENBERTH AND CARON, 2001), who found at least 0.2 PW. Therefore possible impacts of lateral transports might also be underestimated.

In terms of transport into the polar region, the two sensitivity experiments *NOSURF* and *NONORTH* show a different result. Due to the characteristics of the northern restoring area the response is to some extent opposed and artificial. In experiment *NOSURF* the overturning circulation is reduced due to changes in the dense water budget in the north. Therefore the northward heat transport, found in the *CTRL* experiment is strongly reduced due to local heating in the north of the basin. At the end of the integration period, there remains 0.09 PW of northward heat transport at 66°N, since the warming sets in from the north. The transport at 40°N is reduced similar to experiment *FULL* and is 0.4 PW at the end of the integration. As we already found in the heat flux pattern over the Atlantic Ocean (figure 5.20) as well as in the temperature distribution (figure 5.21), the *NOSURF* experiment is indeed only slightly disturbed at the surface within the subpolar gyre. The surface heat loss remains 0.31 PW, what is close to the situation in *CTRL*. So, although the atmospheric forcing over the subpolar gyre remains nearly constant, the overturning response can be reduced due to changes the water mass properties in the north. Nevertheless although the heat transport across 66°N is so different at the end of experiment *FULL* and *NOSURF*, the overturning remains so similar. The heat budget of the reciprocal experiment *NONORTH* illuminates the role of the GIN Seas relative to the subpolar gyre from another perspective. The anthropogenic surface warming is quite similar to experiment *FULL*, so that the surface heat loss within the subpolar region is 0.18 PW at the end of the integration. Since we restore to climatological salinities and temperatures at the northern boundary, the additional heat gain of the ocean is transported into the sponge. This leads to an increased heat transport of 0.31 PW at 66°N at the end of experiment *NONORTH*. Furthermore, the transport at 40°N is not affected, although the anthropogenic surface signal affects as well the subtropical and the tropical region.

However, due to the characteristics of the northern boundary condition, the evolution of the heat transport in these two experiments is somehow prescribed. The crucial point concerning experiment *NONORTH* is the fact that, although the averaged temperatures within the subpolar region are rising at 2°C by atmospheric forcing, the overturning, responsible for most of the oceanic heat transport, is only slightly changed.
These two sensitivity studies are indeed idealized, but illuminate the characteristics of different regions for driving the overturning circulation. In some sense the results can be related to Ganopolski and Rahmstorf (2001), who simulated THC variability in the last glacial maximum (LGM) of three different modes of the thermohaline system. Beneath the stable cold climate state during most of the last ice age, there are two different states known. The first one is a warm Dansgaard-Oeschger event (D/O event), in which the Atlantic conveyor belt temporarily advanced into the Nordic Seas and a strong warm anomaly develops over today's subpolar region. During a Heinrich event, the conveyor belt circulation collapsed, a cold anomaly evolved over the midlatitude Atlantic. They assumed that before a Heinrich event took place, a D/O event shifted the crucial region of deep water formation into the Nordic Seas. So, the overturning pulls back into the Nordic Seas before it significantly slows down.
Although somehow in another context, our result, that the northward heat transport over 66°N is not reduced but slightly strengthened, even though the overturning weakens, underlines the dominant role of the Nordic Seas' region for the overturning circulation, even though the subpolar region is already affected by anthropogenic fluxes. Therefore the system is altered due to changes in *local* freshwater and heat fluxes from the atmosphere in the region north of 66°N. Lateral transports are of minor importance for changes in the rate of deep water formation within this region in the northern North Atlantic in the GFDL climate model and also in *FLAME4/3*. This important point confirms the quite linear response of salinity and temperature forcing in section 5.5.2.

In summary, the heat budget of the North Atlantic justifies the studies *FULL*, *NONORTH* and *NOSURF*. The restoring area in the north supplies heat transports very similar to the climate model. Furthermore, the different versions of surface boundary condition for heat supply fluxes into the ocean, as they are expected, so that the results of the former sections are proven.

Chapter 6

Summary and conclusion

6.1 The anthropogenic response

By forcing a non-eddy-resolving model of the Atlantic Ocean with different combinations of diagnosed surface fluxes from greenhouse gas simulations, we investigated the role of a more realistic ocean representation for the overturning and hence the response of the thermohaline circulation. Hereby we implemented air-sea fluxes from two greenhouse scenarios, which differ fundamentally.

6.1.1 Overturning response

In the *MPI* coupled model, the overturning circulation maintains its strength under anthropogenic forcing, while in the *GFDL gps03* integration the overturning is significantly declining. However both coupled models show deficits concerning circulation and water mass properties. Due to the idealized representation of the Denmark Strait and the Iceland-Scotland Overflow in the *MPI* model, the transport from the GIN Seas communicated into the subpolar basin is at 17 Sv. In contrast the better representation of the topography in the *GFDL* model leads to a more realistic but little too weak transport of 4.5 Sv over the sills. In this context, while in the *MPI* model, the deep water formation is principally localized within the Nordic Seas, the *GFDL* model shows deep convection mainly south of Iceland. Other deficits concern the Gulf Stream separation and the simulation of the cyclonic circulation within the Labrador Sea.
However, the impact of these well-known problems in representing the mean state in terms of predicting the THC strength for the 21^{st} century is found to be relatively unimportant. Implementing ocean-atmosphere fluxes from these scenarios in the more realistic ocean model, does not change the individual response significantly: The *MPI*-forced integration leads to an almost complete maintenance of the conveyor circulation as it is suggested by the coupled model. Forced by anthropogenic fluxes, the intensification of the hydrological cycle balances changes in the local heat budget in terms of surface density. In contrast, due to anthropogenic *GFDL* fluxes, an advective spindown of the thermohaline cell in the North Atlantic sets in, which is also quite similar to the result of the climate model in terms of

trend and long-term variability. Following these results, the overturning evolution of the uncoupled model is found to be mainly independent of the deviating representation of the ocean component in the individual scenario. Instead, changes in the atmospheric forcing ultimately determine the ocean model's response.

The Labrador Sea

By integrating sensitivity studies concerning the relative role of different areas of deep water formation, the region of the subpolar gyre was found to contribute to the overturning strength by a maximum of 3 Sv. This value is found in an idealized experiment after 12 years of integration, in which the temperatures were artifically limited from one time step to another. Even though the breakdown of the Labrador Sea convection is responsible for most of this decrease, changes in the surface density within the Irminger Sea also contribute. However, this result seems to be robust even for the higher resolution *FLAME1/3* model. In the anthropogenic forcing scenarios, the maximum impact of the subpolar gyre is smaller, since in these experiments anthropogenic atmospheric fluxes provide modification of convective regions, which are not as area-wide as in the artificial study. In both integrations, the deep water formation in the central Labrador Sea breaks down principally due to local heating within the 21^{st} century with a maximum impact of 1.5 Sv on the overturning circulation. In the experiments forced with *MPI* fluxes, the strong increase of surface temperatures of nearly 3°C in the central Labrador Sea leads to a complete shutdown of the convection. For comparison, in the experiment forced with *GFDL* fluxes the warming is less intense (about 1.7°C). This constrains the deep water formation as well, but due to variability in surface fluxes the mixed layer casually deepens until about 600 m even at the end of the integration period. The reason for this differing response in *FLAME4/3* are stronger local heat fluxes felt by the ocean under *MPI* forcing. However, this surface heat flux variability mainly controls the mixed layer depth and hence the convective events within the Labrador Sea in all anthropogenic experiments. During the integrations with anthropogenic fluxes, lateral transports of water with changed properties remain relatively unimportant.

The Nordic Seas

Concerning the effect of the subpolar gyre, fundamental changes of the overturning circulation, as they are proposed in a number of greenhouse gas simulations, are in *FLAME4/3* generated by changes in the density structure in the Nordic Seas basin. This result remains robust, independent of the main location of deep water formation in the individual coupled scenario. In the experiments with *MPI* fluxes, the density structure of the northern basin is nearly constant. The local warming and freshening in the crucial region is compensated by a strong lateral salt signal with its source in the tropics and subtropics. Switching off this remote effect from lower latitudes leads to a temperature-driven overturning decrease similar to most

climate models. LATIF's argument, that lateral transport of salty water is indeed the crucial factor for the stabilization of the THC, is affirmed by the more realistic ocean model. Moreover, the results demonstrate that for the stabilizing effect to become effective the salt signal indeed has to enter the GIN Seas and subsequently the overflow waters, underlining the importance of the northern basin for the THC. Furthermore by just disturbing the ocean model with the time series of salinity and temperature changes from the *GFDL* climate model in the northern boundary condition, the long-term overturning response of the experiment with all anthropogenic components is almost perfectly reconstructed. This is remarkable, since in contrast to the *MPI* model, in the *GFDL* coupled model the main region of deep water formation is the subpolar gyre and are not the Nordic Seas.
Vice versa, implementing anthropogenic forcing only at the surface of the model, leads to an averaged increase in surface temperature of about 2°C in the whole subpolar gyre. As a consequence, the deep convection in this region ultimately breaks down. Anyway, no trend of the overturning strength can be diagnosed, if the overflows maintain their climatological dense transport.

Linear response

The contribution of different regions for the overturning variability can be carried a little further. Superposing the overturning response of the experiments forced either in the Nordic Seas or at the surface of the model, almost perfectly reconstructs the combined experiment, independent of the timescale we concentrate on. Here we found a nearly linear relationship without substantial interactions between the domains.
By switching off the individual components of anthropogenic fluxes, in the *GFDL*-forced experiments the main trend of the overturning function is induced due to temperature changes. On the other hand strong release of freshwater is responsible for a high thermohaline variability, which however has only little effect on the trend. To some extent, the variability of temperature and salinity on decadal timescales compensate in the density relation due to local feedback processes, leading to less variability in the experiment with the full anthropogenic forcing. Furthermore, superposing the individual effect of heat and freshwater forcing is quite similar to the combined effect on the overturning circulation. Due to the chosen boundary condition and the dominant impact of heat fluxes in the subpolar gyre, this response is not surprising in the ocean models case. However, investigations in coupled models show a similar behaviour. This is indeed surprising, since deep water formation is a non-linear effect, strongly depending on the surface buoyancy forcing. Finding a linear response could therefore ultimately be the consequence of a constant rate of deep water formation into the crucial depth of the Nordic Seas, which is relatively independent of surface density.

Realistic overflows

Since we found that the general trend of the thermohaline circulation is mainly determined by changes in the waters north of Iceland in our configuration of the

ocean model, we investigated the role of a realistic representation of the physical mechanisms like entrainment and diffusivities controlling the communication between the Nordic Seas and the subpolar gyre. In an easy configuration in terms of parameterizations we investigated the anthropogenic response. Choosing horizontal diffusion and no bottom boundary parameterization, high diffusivities lead to a too weak meridional heat transport. To compensate this effect, we idealized the topography in the Denmark Strait, in order to adjust the overturning heat transport. Forced with anthropogenic fluxes from *GFDL*, the relative response of the thermohaline circulation was found to be nearly identical. Following these results, a realistic communication of dense signals through narrow passages is not even necessary for a similar response in the ocean model with greenhouse gas forcing. Primarily the evolution of water mass properties in the northern basin explains differences on greenhouse forcing. If the model's physics are tuned in terms of meridional heat transport, this is found to be the only relevant mechanism for the thermohaline response on global warming in the ocean model at least for the next century.

Timescales

If there is variability in the overflow signals, it takes about 4 years to affect the overturning cell at 40°N and hence the oceanic heat transport. This result is found in idealized experiments with ocean models in both resolution as well as in the global warming scenario with *GFDL* fluxes in *FLAME4/3*.

The individual components of atmospheric forcing can easily be found in the time series of the overturning index. On seasonal to interannual timescales the role of wind stress variability is the crucial factor for the variability of the circulation. However the wind-driven gyre circulation is an essential part of the MOC in the model. Integrating the ocean model in a sensitivity study, in which the wind stress was completely switched off, leads to a reduced overturning function of about 30%. This can be attributed to the role of the gyre circulation around Iceland for the density transport into the subpolar region. However, the wind stress fluctuations in the anthropogenic studies are in the order of the mean but are not as enduring and do not lead to a different shape of the subpolar gyre. Therefore their impact on the long-term variability is small in comparison to the anthropogenic freshwater and heat flux forcing.

On decadal timescales the momentum forcing has indeed almost no effect on the variability and the trend of the THC. Instead surface heat flux forcing in the subpolar gyre becomes important. Multidecadal timescales as well as trends depend on the density signals from the Nordic Seas. As a matter of fact, these anomalies have a much longer timescale, since they are somehow an integral response of the high-frequency surface forcing in the northern ocean.

6.2 Methodical Limitations

The most important defect in our model is the absence of a truly physical representation of processes in the Nordic Seas' basin. As a matter of the vertical boundary condition, the effect of lateral signals for the water mass properties in this region is to some extent determined by the prescribed sponge values. Therefore by integrating greenhouse gas simulations with the regional ocean model, we have to rely on density changes of the climate model's northern North Atlantic being the result of local and lateral impacts there. These are somehow quite unrealistic relative to observations. A number of reasons for this mismatch are apparent: The low horizontal and vertical resolution makes it impossible to resolve the relatively small scales of deep water formation. Parameterizations work to some extent properly, but seem to underestimate lateral effect on the water column. Moreover, calculating realistic buoyancy fluxes at the surface is quite difficult, since interactions between ocean, atmosphere and sea ice include a number of feedback mechanisms on small scales, which are not capaciously understood. A different approach to close boundaries in regional ocean models is the use of open boundaries conditions. However, in these studies, working with an open boundary condition in the north of the model is not expected to modify the results significantly. Since the water mass properties at inflow points are also prescribed in that case, the response would probably be similar.

The second problem is the implementation of air-sea fluxes in the ocean model. Since these are the result of interactions between the atmosphere and an apparently idealized oceanic state, forcing a more realistic ocean model causes problems. E.g. typical air-sea interactions along the Gulf Stream might take place in regions, were no Gulf Stream is found in the ocean model. However, implementing the diagnosed fluxes into the coarse resolution ocean model, this effect is in an integral sense of minor importance for the overturning response. Nevertheless, the Labrador Sea response is to some extent affected by these regime dependent fluxes.

By integrating sensitivity studies with certain components of anthropogenic forcing, local impacts are studied. Here, again due to the implementation of forcing pattern, artifical changes concerning the surface heat flux arise. These are the consequence of interactions between an unchanged atmosphere and lateral transports of SST anomalies. Fortunately, calculating heat budgets, their effect is found to be relatively small.

6.3 Conclusion

The variability of the thermohaline circulation on multidecadal timescales has a number of possible sources, which can be subdivided into three major classes. The first one is one-way forcing from the atmosphere, which can be traced back to stochastic pattern due to short-term weather variability or external forcing e.g. due to the radiation budget in the atmosphere. The second and the third are the

internal variability in the ocean interior respective coupled interactions between atmosphere and ocean (e.g. SARACHIK ET AL., 1996).
In this study, the response of the THC on anthropogenic variability and trends in the atmospheric forcing are examined in a non-eddy-resolving ocean model, neglecting the two latter mechanisms. Since we prescribe the atmospheric pattern independently of the oceanic state, realistic ocean-atmosphere interactions cannot be taken into account. Instead, diagnosed fluxes from the climate models (which could indeed be the consequence of coupled interactions) are forcing the higher resolved ocean model. A subdivision in forcing and interacting parts cannot be made here, even though the atmospheric response to changes within the ocean is still unclear. KUSHNIR AND HELD (1996) found only little impact on SST anomalies in midlatitudes in the atmospheric component of the *GFDL* model. In contrast, TIMMERMANN ET AL. (1998) reported, that in the *MPI* model the THC variability is indeed related to a coupled air-sea mode. By integrating an ocean component in a coupled and an uncoupled version, DELWORTH AND GREATBATCH (2000) diagnosed only little interactions responsible for ocean-atmosphere fluxes. In their model no coupled ocean-atmosphere mode could be extracted. Furthermore, comparing the atmospheric pattern in an uncoupled atmospheric model with the obtained state when it is coupled to a simple mixed-layer ocean, GRIFFIES AND TZIPERMAN (1995) found a very weak oceanic influence on the atmosphere.
However, with an uncoupled ocean model we cannot contribute to this issue. We found a general THC response on one-way atmospheric forcing, which is quite independent of the ocean model's configuration and simulation of the mean state. In the absence of own air-sea interactions, the overturning circulation in the uncoupled ocean with a much more realistic SST pattern behaves similar to the coupled ocean on anthropogenic changes in the atmosphere, what is more in line with arguments for a passive role of the ocean.

The different THC response in climate models

The main scope of this thesis was, to constrain the number of possible reasons for the fundamentally different response of the THC in coupled ocean-atmosphere models, when they are forced by similar greenhouse gas warming scenario fluxes. The available results with the uncoupled ocean model indicate, that a more realistic representation of currents and water mass properties within the tropics, the subtropics and the midlatitudes cannot explain the discrepancies. So, coupling an identical atmosphere to a more realistic ocean component in these latitudes is not expected to converge the predictions of climate models. This holds even for scenarios with a more active role of the ocean. The saline stabilization found by LATIF ET AL. (2000) in the *MPI* model is not a deviating feature of their ocean component. Inducing high salinities in lower latitudes, a more realistic ocean model provides a primarily similar spreading of the signal. A comparable lateral signal from tropical latitudes was diagnosed by THORPE ET AL. (2001) in the *HadCM3* ocean component, which is not able to suppress but to weaken the anthropogenic declining of the THC. In both climate models, due to large scale atmospheric

interactions, the evaporation and hence the salinity in lower latitude rises.
Anyhow, improving circulation, water mass properties and topography is a reasonable approach. A further step must be the integration of global warming scenarios in true eddy-resolving models, in order to manifest the role of geostrophic eddies for the response of the THC. However, parameterizations attending the role of eddies in an integral point of view (e.g. GENT AND MCWILLIAMS, 1990) seem to work properly, if we compare results of different resolution ocean models. It remains questionable and is not yet shown, that fundamental changes in the atmospheric forcing, which we concern in terms of global warming, might indeed lead to a fundamentally different THC response even in models resolving the radius of deformation.
However, diagnosing the response of the THC, it remains an integral parameter of oceanic changes, which is determined by local processes of deep water formation on small spatial scales (e.g. MARSHALL AND SCHOTT, 1999). Improving models in representing the variety of interactions between ocean, atmosphere and sea ice in terms of providing the renewal of deep dense water at least in crucial regions seems to be an ambitious but promising approach.
For the majority of climate models, local air-sea fluxes seem to determine the THC response. An indicator is their quite linear response on different forcing components, which suggests a minor importance of lateral oceanic transports. This e.g. holds for the *GFDL* model, even if the lateral transport into the Nordic Seas is underestimated relative to observations. In the *MPI* model, lateral salinity transport stabilizes the system, but since the response is no direct feedback mechanism of the circulation, the timing of the signal is the crucial factor. A natural negative feedback mechanism within the overturning circulation is the oceanic heat transport, which can also limit the weakening of the THC and whose timing is self-sustaining. Both lateral mechanisms are found by THORPE ET AL. (2001) and explain the only moderate response in the *HadCM3* model.

Individual components of THC forcing

RAHMSTORF (1999) suggests, that not only the strength but also the water mass contribution might alter in global warming simulations, since crucial regions might have different sensitivities concerning changes in anthropogenic forcing. So, in the *FLAME4/3* model, the Labrador Deep Water formation breaks down with an only moderate effect on the overturning circulation. The ocean model's result that fundamental changes of the THC are determined by changes in the density transport from the Nordic Seas is in line with model studies, which indeed can distinguish different regions of deep water formation. WOOD ET AL. (1999) found in the *HadCM3* model a moderate weakening of the circulation, which was traced back to a shutdown of the Labrador Sea convection together with relatively stable response in the north. But also models, which show the main convection events within the subpolar gyre seem to depend on a dense outflow from polar regions to maintain the overturning circulation, as it is demonstrated in our experiments with anthropogenic *GFDL* forcing. In all these experiments, although most of the

heat transport in the ocean is supplied to the atmosphere until 66°N, about 0.2 PW effectively drives the conveyor circulation in the Atlantic Ocean.
Experiments concerning the last glacial maximum by GANOPOLSKI AND RAHMSTORF (2001) act on the assumption, that three different states of the THC were possible. The first one is the stable cold climate state prevailing during most of the ice age with a weak conveyor. This is quite different from today's state, since latitudes north of Iceland are isolated from atmospheric forcing due to an area-wide ice coverage. Below it is the situation during a warm Dansgaard-Oeschger (D/O) event, in which the Atlantic deep water formation temporarily advances into the Nordic Seas. In this situation, a warm anomaly develops in the North Atlantic region. The third climate state is a Heinrich event, with a collapsed THC and therefore a cold anomaly over the mid-latitude Atlantic. Their arguments is, that the necessary condition for a Heinrich event to occur is indeed a D/O event. In other words, for a breakdown of the meridional circulation, the sinking regions advance into higher latitudes, where the further evolution is determined.
However, these climatic states are difficult to compare to today's climate in terms of water mass properties and circulation but also in terms of stability. Anyhow, since we observe deep water formation in the course of global warming scenario integrations mainly in polar regions with moderate temperatures over the North Atlantic, the present climate is in some aspects similar to the D/O situation, in which the strength of the THC is predefined in the Nordic Seas.
So, the relative contribution of the subpolar gyre respective the Labrador Sea to the overturning circulation seems to be more an effect of a warmer world than the cause for a significant weakening of the THC. In this context, observational studies indicate strong deep water formation within the in the early 90s (e.g. LILLY ET AL., 1999; RHEIN ET AL., 2002), while in the years 1998 to 2003 no significant renewal of Labrador Sea Water could be diagnosed (*SFB 460, pers.com.*). In the ocean model, we found a maximum contribution of 3 Sv to the strength of the overturning function with permanent deep water formation in each single year, apparently overestimating the observations.

Another crucial point concerns the effective convection depth. While Labrador Sea Water has to attain a depth of at least 1300 m to contribute to the deep branch of the Deep Western Boundary Current in the ocean model, the necessary convection depth in the GIN Seas is much shallower. Here a depth of 600 m is deep enough to affect the overflow waters and ultimately the overturning circulation. This issue might be important in terms of surface buoyancy loss. Investigating the relative contribution of freshwater and heat flux forcing, climate models indicate different results. While MIKOLAJEWICZ AND VOSS (2000) found a mostly temperature-driven decrease in a global warming scenario which is similar to our results, DIXON ET AL. (1999) ascribed the declining response primarily to freshwater forcing. However, all these simulations show a quite linear response of the thermohaline forcing: The combination of temperature and freshwater induced weakening is a very good reconstruction of the combined effect. Although deep water formation is a non-linear effect, a relatively constant rate of deep water seems to attain

the crucial depth in the Nordic Seas during the anthropogenic forcing scenarios. In these experiments, the basically non-linear effect of lateral transports for the density budget seems to be small. In contrast, THORPE ET AL. (2001) found a more complex picture in a coupled integration with an ocean component with a comparable high resolution similar to *FLAME4/3*. Here, both heat and freshwater flux are important but become responsible for the THC evolution on different timescales. The initial weakening is driven by the temperature effect, on longer timescales, at a lower level a balance between temperature and salinity effects occurs.

In the perspective of the role of different regions of deep water formation, if indeed the impact of changing surface fluxes differs regionally, an integral point of view concerning surface forcing might cause wrong results. PETERSON ET AL. (2002) reported about an increase in river discharge from the largest Eurasian rivers into the Artic Ocean in the 20^{th} century. Anyhow, in an integral point of view, the additional water is picked up by the atmosphere mainly over the Atlantic Ocean, potentially leading to higher salinities there. However, the effect on the thermohaline driven circulation might although not be compensated, since the higher salinities and eventually larger rate of deep water formation in the subpolar gyre might not balance the greater effect in the Nordic Seas. Including all these direct and remote effects, even if the strength of the THC is determined in a relative apparent region, a realistic representation of processes responsible for the density structure there is essential to forecast the THC response.

Necessary model components

Experiments with high resolution ocean models found that if dense signals through narrow passages as they are provided by the Denmark Strait or the Iceland-Scotland Overflow make the Atlantic Ocean less sensitive to surface buoyancy forcing within the subpolar gyre (DÖSCHER AND REDLER, 1997). They deduced, that climate models with wide passages and unrealistic density signals in this case might overestimate the impact of anthropogenic surface fluxes. By integrating an idealized version of the ocean model in terms of subscale parameterizations and topography, we found, that the model is relatively insensitive to entrainment rates, overestimated diffusivities and overflow representation. The general response of the overturning circulation is determined by the northern boundary condition. If the model is adjusted in terms of realistic heat transport, changes in the water mass properties have a comparable effect on the THC. THORPE ET AL. (2001) suggested the meridional gradient in steric height as a good indicator for changes in the overturning circulation. In our case, this deep gradient is basically determined by changes in the north. Beyond shallow warming in lower latitudes, the deep ocean in the tropics and subtropics remains mainly unaffected, although the model is expected to be too diffusive. Therefore, provided by changes at the northern boundary, the THC in these models principally responds as in simple box models.

Detection of climate changes

We might expect the ocean to be less noisy than other parts of the climate system. Therefore changes in surface fluxes, as well dynamic as thermodynamic, to changes in the ocean properties might produce a high signal-to-noise ratio. For that reason, detecting climate changes in the ocean is a useful tool. The detection of anthropogenic climate changes has for long time only been focused on surface temperatures (e.g. Barnett et al., 1999). Following our results, a very reasonable detection parameter could be the density at the sill of the Denmark Strait Overflow or the temporal evolution of profiles within the Nordic Seas. Dickson et al. (2002) reported indeed of a rapid freshening of these waters during the second half of the 20^{th} century. Our results suggest, that for fundamental changes of the MOC and hence the meridional heat transport time series of water mass properties at that outflow point are a good indicator for trends and long-term variability of the thermohaline circulation. Detecting changes in the conveyor circulation in lower latitudes is found to be much more difficult, since shorter-term variability from the subpolar gyre as well as local wind-induced variability interfere the THC signal.

Perspectives

Converging the prognoses of climate models in terms of the THC response is still quite ambiguous. These models must be able to include new scientific conclusion into their representation of the present state. By explicitly modeling processes on smaller spatial and temporal scales, the number of uncertain components in atmosphere, ocean and sea ice must decline in the future. The here presented improvement of the ocean model in terms of the mean circulation, water mass properties, regional distribution of deep water formation and topography is found not to be the crucial step for climate models to converge. Among other present day's simulations this is still a coarse estimation when we keep in mind all the open questions still being unanswered. The next step of improving the ocean's representation is indeed the resolution of the radius of deformation in climate models, in order to include another important physical process explictly. With the higher resolution, the ocean's velocities become less smoothed and more realistic in models, so that the time for interactions between ocean and atmosphere might even change.
Beyond this next step is the simulation of other even smaller processes. At least the approach to simulate surface forced deep water formation properly seems to be essential to get robust predictions of the THC beyond the upper class of models. However including most physical processes like convection, large eddy simulation up to three-dimensional turbulence lies in remote future in the development of climate models (Willebrand and Haidvogel, 2001). Therefore, finding crucial regional processes in today's models could be the starting point for a nesting approach. By at least simulating these regions as realistically as possible, some components of the ocean's role in climate could be revealed.

Bibliography

A.Bacher, J.M.Oberhuber and E.Roecker, 1998: ENSO dynamics and seasonal cycle in the tropical Pacific as simulated by the ECHAM4/OPYC3 coupled general circulation model. *Climate Dynamics*, **14**, pages 431–450.

Baringer, M. O. and J. F. Price, 1997: Mixing and spreading of the Mediterranean Outflow. *J. Phys. Oceanogr.*, **27**, pages 1654–1677.

Barnett, H., K. Hasselmann, M. Chelliah, T. Delworth, G. Hegerl, P. Jones, E. Rasmusson, E. Roeckner, C. Ropelewski and B. Santer, 1999: Detection and attribution of recent climate change: a status report. *Bull.Amer.Meteor.Soc.*, **80**, pages 2631–2659.

Barnier, B., L. Siefriedt and P. Marchesiello, 1995: Thermal forcing for a global ocean circulation model u sing a three-year climatology of ECMWF analysis. *J. Mar. Systems*, **6**, pages 363–380.

Beckmann, A. and R. Döscher, 1997: A method for improved representation of dense water spreading over topography in geopotential–coordinate models. *J. Phys. Oceanogr.*, **27**, pages 581–591.

Beismann, J.-., C. Böning and D. Stammer, 2002: Inter-annual to Decadel Variability of the Meridional Overturning Circulation of the Atlantic: A Comparison of the Response to Atmospheric Fluctuations in three Ocean Models. *CLIVAR Exchanges*, **7**, pages 34–43.

Biastoch, A., R. Käse and D. Stammer, 2003: The Sensitivity of the Greenland-Scotland Ridge Overflow to Forcing Changes. *J. Phys. Oceanogr.*, **in press**.

Böning, C., C. Dieterich, B. Barnier and Y. Jia, 2001: Seasonal cycle of meridional heat transport in the subtropical North Atlantic: Intercomparison of the DYNAMO models and observations near 25 N. *J. Phys. Oceanogr.*, **48** (2-3), pages 231–253.

Böning, C. W., F. Bryan, W. Holland and R. Döscher, 1996: Deep-water formation and meridional overturning in a high-resolution model of the North Atlantic. *J. Phys. Oceanogr.*, **26**, pages 1455–1471.

Böning, C. W., W. R. Holland, F. O. Bryan, G. Danabasoglu and J. C. McWilliams, 1995: An Overlooked Problem in Model Simulations of the Thermohaline Circulation and Heat Transports in the North Atlantic. *J. Climate*, **8** (3), pages 515–523.

Boyer, T. and S. Levitus, 1997: Objective analysis of temperature and salinity for the world ocean on a 1/4° grid. *Technical report, NOAA Atlas NESDIS*, **11**.

Broecker, W., 1987: Unpleasent surprise in the greenhouse? *Climate Dynamics*, **4**, pages 73–79.

Bryan, K., 1969: A Numerical Method for the Study of the Circulation of the World Ocean. *Journal of Computational Physics*, **4**, pages 347–376.

Bryan, K. and L. J. Lewis, 1979: A water mass model of the world ocean. *J. Geophys. Res.*, **84 C**, pages 2503–2517.

Cox, M., 1987: Isopycnal diffusion in a z-coordinate model. *Ocean Modell.*, **74**, pages 1–5.

Cummins, P. F., G. Holloway and A. E. Gargett, 1990: Sensitivity of the GFDL ocean general circulation model to a parameterization of vertical diffusion. *J. Phys. Oceanogr.*, **20**, pages 817–830.

Curry, J. and P. Webster, 1999: *Thermodynamics of Atmospheres and Oceans.* Academic Press.

Curry, R. G., M. S. McCartney and T. M. Joyce, 1998: Oceanic transport of subpolar climate signals to mid-depth subtropical waters. *Nature*, **391**, pages 575–577.

Delworth, T., R. Stouffer, K. Dixon, M. Spelman, T. Knutson, A. Broccoli, P. Kushner and R. Wetherald, 2002: Review of simulations of climate variability and change with the GFDL R30 coupled climate model. *Climate Dynamics*, **19**, pages 555–574.

Delworth, T. L. and K. Dixon, 2000: Implications of Recent Trend in the Arctic/North Altlantic Oscillation for the North Atlantic Thermohaline Circulation. *J. Climate*, **13**, pages 3721–3727.

Delworth, T. L. and R. J. Greatbatch, 2000: Multidecadal thermohaline circulation variability driven by atmospheric surface flux forcing. *J. Climate*, **13**, pages 1481–1494.

Dengg, J., 1993: The problem of Gulf Stream separation: a barotropic approach. *J. Phys. Oceanogr.*, **23**, pages 2182–2200.

Dickson, B., I. Yashayaev, J. Meincke, B. Turrell, S. Dye and J. Holfort, 2002: Rapid freshening of the deep North Atlantic over the past four decades. *Nature*, **416**, pages 832–837.

DICKSON, R. R. and J. BROWN, 1994: The production of North Atlantic Deep Water: Sources, rates and pathways. *J. Geophys. Res.*, **99** (C6), pages 12,319–12,341.

DICKSON, R. R., E. M. GMITROWICZ and A. J. WATSON, 1990: Deep-water renewal in the northern North Atlantic. *Nature*, **344**, pages 848–850.

DIXON, K. W., T. L. DELWORTH, M. J. SPELMAN and R. J. STOUFFER, 1999: The influence of transient surface fluxes on North Atlantic overturning in a coupled GCM climate change experiment. *Geophys. Res. Letters*, **26**, pages 2749–2752.

DIXON, W. and J. LANZANTE, 1999: Global mean surface air temperature and North Atlantic overturning in asuite of coupled GCM climate change experiments. *GRL*, **26**, pages 1885–1888.

DONEY, S. C. and W. J. JENKINS, 1994: Ventilation of the deep western boundary current and abyssal western North Atlantic: estimates from tritium and ^{3}He distributions. *J. Phys. Oceanogr.*, **24**, pages 638–659.

DÖÖS, K. and D. WEBB, 1994: The Deacon Cell and other Meridional Cells of the Southern Ocean. *J. Phys. Oceanogr.*, **24**, pages 429–442.

DOROW, C., 2001: Aufnahme und Ausbreitung von Freon im Labradorseewasser. Diplomarbeit, Christian-Albrechts-Universität zu Kiel.

DÖSCHER, R. and A. BECKMANN, 2000: Effects of abottom boundary layer parameterization in a coarse-resolution model of the North Atlantic ocean. *J.Atmos.Oc.Tech.*, **17**, pages 698–707.

DÖSCHER, R., C. W. BÖNING and P. HERRMANN, 1994: Response of Circulation and Heat Transport in the North Atlantic to Changes in the Thermohaline Forcing in the Northern Latitudes: A Model Study. *J. Phys. Oceanogr.*, **24**, pages 2306–2315.

DÖSCHER, R. and R. REDLER, 1997: The Relative Importance of Northern Overlow and Subpolar Deep Convection for the North Atlantic Thermohaline Circulation. *J. Phys. Oceanogr.*, **27**, pages 1894–1902.

DYNAMO GROUP, 1997: DYNAMO: Dynamics of the North Atlantic models: Simulations and assimilation with high resolution models. Technical report 294, Institut für Meereskunde, Kiel, Germany.

EDEN, C., 1999: Interannual to interdecadal variability in the North Atlantic Ocean. Dissertation, Christian-Albrecht-Universität Kiel.

EDEN, C. and R. GREATBATCH, 2003: A damped decadal oscillation in the North Atlantic climate system. *J. Climate*, **in press**.

EDEN, C. and T. JUNG, 2001: North Atlantic interdecadel variability: Oceanic response to the North Atalntic Oscillation (1865-1997). *J. Climate*, **14**, pages 676–691.

EDEN, C. and J. WILLEBRAND, 2001: Mechanism of interannual to decadel variability of the North Atlantic circulation. *J. Climate*, **14**, pages 2266–2280.

ETOPO5, 1988: Digital relief of the surface of the earth. Worldwide Bathymetry/Topography Data Announcement 88–MGG–02, NOAA, Boulder, CO. Technical report, National Geophysical Data Center.

FISCHER, J. and F. A. SCHOTT, 1997: Seasonal transport variability of the Deep Western Boundary Current in the Atlantic. *J. Geophys. Res.*, **102**, pages 27751–27769.

FLAME GROUP, 1999: FLAME: A Family of Linked Atlantic Model Experiments. Technical report, Alfred-Wegner-Institute, Bremerhaven, Germany.

GANACHAUD, A. and C. WUNSCH, 2000: Improved estimates of global ocean circulation, heat transport and mixing from hydrographic data. *N*, **408**, pages 453–456.

GANOPOLSKI, A. and S. RAHMSTORF, 2001: Simulation of rapid glacial changes in a coupled climate model. *N*, **409**, pages 153–158.

GARGETT, A. E., 1984: Vertical eddy diffusivity in the ocean interior. *J. Mar. Res.*, **42**, pages 359–393.

GENT, P., 2001: Will the North Atlantic Ocean thermohaline circulation weaken during the 21st century? *GRL*, **28**, pages 1023–1026.

GENT, P. and J. MCWILLIAMS, 1990: Isopycnal mixing in ocean circulation models. *J. Phys. Oceanogr.*, **20**, pages 150–155.

GENT, P. and J. MCWILLIAMS, 1995: The wind-driven ocean circulation with an isopycnal-thickness mixing parameterization. *J. Phys. Oceanogr.*, **24**, pages 46–65.

GIBSON, J., P. KALLBERG, S. UPPALLA, A. HERNANDEZ and A. NOMURA, 1997: ECMWF Reanalysis Project. Technical report 1, European Centre for Medium-Range Weather Forecasts.

GIRTON, J. B., T. B. SANFORD and R. H. KÄSE, 2001: Synoptic sections of the Denmark Strait Overflow. *Geophys. Res. Letters*, **28**, pages 1619–1622.

GOUGH, W. A. and C. A. LIN, 1995: Isopycnal mixing and the Veronis effect in an ocean general circulation model. *J. Mar. Res.*, **53**, pages 189–199.

GRIFFIES, S. and E. TZIPERMAN, 1995: Linear Thermohaline oscillator dirven by stochastic atmospheric forcing. *J. Phys. Oceanogr.*, **25**, pages 2440–2453.

HALL, M. and H. BRYDEN, 1982: Direct estimates and mechanisms of ocean heat transport. *DSR*, **29**, pages 339–359.

HALLBERG, R., 1999: Time integration of diapycnal diffusion and Richardson number dependent mixing in isopycnal coordinate ocean models. *MWR*, **128**, pages 1402–1419.

HAN, G. and C. L. TANG, 1999: Velocity and transport of the Labrador Current determined from altimetric, hydrographic, and wind data. *J. Geophys. Res.*, **104**, pages 18047–18057.

HANEY, R., 1971: Surface thermal boundary conditions for ocean circulation models. *J. Phys. Oceanogr.*, **1**, pages 241–248.

HAY, W. W., 1993: The role of polar deep water formation in global climate back. *Ann. Rev. Earth Planet. Sci*, **21**, pages 227–254.

HAYWOOD, J., R. D.L., A. SLIGO, J. EDWARDS and K. SHINE, 1997: General circulation model calculations of direct radiative forcing by anthropogenic sulfate and fossil-fuel soot aerossol. *J. Climate*, **10**, pages 1562–1577.

H.STOMMEL, 1961: Thermohaline convection with two stable regimes of flow. *T*, **13**, pages 224–230.

HUANG, R., 1993: Real Freshwater Flux as a Natural Boundary Condition for the Salinity Balance and Thermohaline Circulation Forced by Evaporation and Precipitation. *J. Phys. Oceanogr.*, **23**, pages 2428–2446.

HUANG, R., M. CANE, N. NAIK and P. GOODMAN, 2000: Global adjustment of the thremocline in response to deepwater formation. *Geophys. Res. Letters*, **27**, pages 74–92.

HURRELL, J. W., 1995: Decadal Trends in the North Atlantic Oscillation: Regional Temperatures and Precipitation. *Science*, **269**, pages 676–679.

IPCC 1992, 1992: *IPCC. Climate Change 1992. The Supplementary Report to the IPCC Scientific Assessment. Contribution of Working Group I to the first Assessment Report of the Intergovernmental Panel on Climate Change.* Cambridge University Press.

IPCC 2001, 2001: *IPCC. Climate Change 2001. The Scientific Basis. Contribution of Working Group I to the Third Assessment Report of the Intergovernmental Panel on Climate Change.* Cambridge University Press.

JAYNE, S. and J. MAROTZKE, 2001: The Dynamics of ocean heat transport variability. *RoG*, **39**, pages 385–412.

JIA, Y., 2000: Formation of an Azores Current due to Mediterranean overflow in a modelling study of the North Atlantic. *J. Phys. Oceanogr.*, **30** (9), pages 2342–2358.

Jia, Y., 2002: Ocean heat trasnport and its relationship to ocean circulation in CMIP coupled models. *Climate Dynamics*, **20**, pages 153–174.

Johnson, H. and D. Marshall, 2002: A Theory for the Surface Atlantic Response to Thermohaline Variability. *J. Phys. Oceanogr.*, **32**, pages 1121–1132.

Kalnay, E., M. Kanamitsu, R. Kistler, W. Collins, D. Dea ven, L. Gandin, M. Iredell, S. Saha, G. White, J. Woollen, Y. Zhu, M. Chelliah, W. Ebiszusaki, W. Higgins, K. Janowiak, J. a nd Mo, C. Ropelewski, J. Wang, A. Leetmaa, R. Reynolds, R. Jenne and D. Joseph, 1996: The NCEP/NCAR 40-Years Renanalysis Project. *Bull. Amer. Meteor. Soc.*, **77**, pages 437–471.

Kawase, M., 1987: Establishment of deep ocean circulation driven by deep–water production. *J. Phys. Oceanogr.*, **17**, pages 2294–2317.

Killworth, P. D., 1996: Time interpolation of forcing fields in ocean models. *J. Phys. Oceanogr.*, **26**, pages 136–143.

Kraus, E. B. and J. S. Turner, 1967: A one–dimensional model of the seasonal thermocline. II. The general theory and its consequences. *Tellus*, **19**, pages 98–106.

Kushnir, Y. and I. Held, 1996: Equilibrium atmospheric response to North Atlantic SST anomalies. *J. Climate*, **9**, pages 1208–1220.

Latif, M., E. Roecker, U. Mikolajewicz and V. Voss, 2000: Tropical Stabilisation of the Thermohaline Circulation in a Greenhouse Warming Simulation. *J. Climate*, **13**, pages 1809–1813.

Lavin, A., H. Bryden and G. Parrilla, 1998: Meridional transport and heat flux variations in the subpolar North Atlantic. *Global Ocean Syst.*, **6**, pages 269–293.

Lazier, J. R. N., 1988: Temperature and salinity changes in the deep Labrador Sea, 1962–1986. *Deep-Sea Res.*, **35** (8), pages 1247–1253.

Lenderink, G. and J. Haarsma, 1994: Variability and Multiple Equilibria of the Thermohaline Circulation Associated with Deep-Water Formation. *J. Phys. Oceanogr.*, **24**, pages 1480–1493.

Levitus, S. and T. Boyer, 1994: World Ocean Atlas 1994,Temperature. *NOAA/NESDIS E/OC21, US Department of Commerce, Washington, DC*, **4**, pages 117pp.

Lilly, J. M., P. B. Rhines, M. Visbeck, R. Davis, J. R. N. Lazier, F. Schott and D. Farmer, 1999: Observing deep convection in the Labrador Sea during winter 1994/95. *J. Phys. Oceanogr.*, **29**, pages 2065–2098.

Macdonald, A. M. and C. Wunsch, 1996: An estimate of global ocean circulation and heat fluxes. *Nature*, **382**, pages 436 – 439.

MANABE, S., K. BRYAN and M. SELMAN, 1990: Transient rsponse of a global ocean-atmosphere model to adoubling of atmospheric carbon dioxide. *J. Phys. Oceanogr.*, **20**, pages 722–749.

MANABE, S., J. SMAGORINSKY and B. K, 1965: Simulated climatology of a general circulation model with a hydrological cycle. *Mon.Wea.Rev.*, **93**, pages 769–798.

MANABE, S. and R. STOUFFER, 1994: Multiple-century response of a coupled ocean-atmosphere model to an increase of the atmospheric carbon dioxide. *J. Climate*, **7**, pages 5–23.

MANABE, S., R. J. STOUFFER, M. J. SPELMAN and K. BRYAN, 1991: Transient responses of a coupled ocean–atmosphere model to gradual changes of atmospheric CO_2. Part I: Annual mean response. *J. Climate*, **4**, pages 785–818.

MAROTZKE, J., 1996: Analysis of Thermohaline Feedbacks. In: *Decadel Climate Variability*, D. L.T.Anderson and J. Willebrand, editors, Springer Verlag Berlin, pages 334–378.

MAROTZKE, J. and J. WILLEBRAND, 1990: Multiple Equilibria of the Global Thermohaline Circulation. *J. Phys. Oceanogr.*, **21**, pages 1372–1385.

MARSH, R., M. J. ROBERTS, R. A. WOOD and A. L. NEW, 1996: An intercomparison of a Bryan–Cox–type ocean model and an isopycnic ocean model. Part II.: The subtropical gyre and meridional heat transport. *J. Phys. Oceanogr.*, **26**, pages 1528–1551.

MARSHALL, J. and F. SCHOTT, 1999: Open-Ocean Convection: Observations, Theory, and Model s. *Reviews of Geophysic*, **37** (1), pages 1–64.

MCDOUGALL, T. J., A. C. HIRST, H. M. ENGLAND and P. C. MCINTOSH, 1996: Implications of a new eddy parameterization for ocean models. *Geophys. Res. Letters*, **23** (16), pages 2085–2088.

MIKOLAJEWICZ, U. and R. VOSS, 2000: The role of the individual air-sea flux components in CO_2-induced changes of the ocean's circulation and climate. *Climate Dynamics*, **16**, pages 627–642.

MITCHELL, J., T. JOHNS, J. GREGORY and S. TETT, 1995: Climate response to increasing levels of greenhouse gases and and sulphate aerosols. *Nature*, pages 501–504.

MONTEREY, G. and S. LEVITUS, 1997: Seasonal Variability of Mixed Layer Depth for the World Ocean. NOAA Atlas NESDIS 14. Technical report, U.S. Gov. Printing Office.

MUNK, W. H. and C. WUNSCH, 1998: Abyssal recipes II: energetics of tidal and wind mixing. *Deep-Sea Res.*, **45**, pages 1977–2010.

Oberhuber, J. M., 1993: The OPYC Ocean General Circulation Model. Technical report 7, Deutsches Klimarechenzentrum.

Osborn, T., K. Briffa, S. Tett and P. Jones, 1999: Evaluation of the North Atlantic Oscillation as simulated by acoupled climate model. *Climate Dynamics*, **15**, pages 685–702.

Pacanowski, P., K. Dixon and A. Rosati, 1991: Ocean Model users guide version 1. Technical report 2, GFDL Ocean Group.

Pacanowski, R., 1995: MOM 2 Documentation, Users's Guide and Reference Manual. Technical report 3, GFDL Ocean Group.

Perlwitz, J. and H. Graf, 1995: The statisticalconnection between tropospheric and stratospheric circulation of the Northern Hemisphere winter. *J. Climate*, **8**, pages 2281–2295.

Peterson, B., R. Holmes, J. McClelland, C. Vörösmarty, R. Lammers, A. Shiklomanav, I. Shiklomanav and S. Rahmstorf, 2002: Increasing River Discharge to the Arctic Ocean. *Science*, **298**.

Philander, S. and A. Fedorov, 2003: Role of tropics in changing the response to Milankovich forcing some three million years ago. *Paleoceanography*, **18** (2).

Rahmstorf, S., 1993: A fast and complete convection scheme for ocean models. *Ocean Modelling*, **101**, pages 9–11.

Rahmstorf, S., 1999: Shifting seas in the greenhouse. *Nature*, **399**, pages 523–524.

Rahmstorf, S., 2003: The current climate. *Nature*, **421**, pages 699.

Rahmstorf, S. and A. Ganopolski, 1999: Long-Term Global Warming Scenarios computed with an efficient Coupled Climate Model. *Climate Change*, **43**, pages 353–367.

Rahmstorf, S. and J. Willebrand, 1995: The Role of Temperature Feedback in Stabilizing the Thermohaline Circulation. *J. Phys. Oceanogr.*, **25**, pages 787–805.

Redi, M. H., 1982: Oceanic isopycnal mixing by coordinate rotation. *J. Phys. Oceanogr.*, **12**, pages 1154–1158.

Reynaud, T., P. LeGrand, H. Mercier and B. Barnier, 1998: A new analysis of hydrographic data in the Atlantic and its application to an inverse modelling study. *International WOCE Newsletter*, **32**, pages 29–31.

Rhein, M., J. Fischer, W. M. Smethie, D. Smythe-Wright, R. F. Weiss, C. Mertens, D. H. Min, U. Fleischmann and A. Putzka, 2002: Labrador Sea Water: pathways, CFC-inventory and formation rates. *J. Phys. Oceanogr.*, **32**, pages 648–665.

ROECKNER, E., K. ARPE, L. BENGTSSON, S. BRINKOP, L. DÜMENTIL and M. ESCH, 1992: MPI Report No.93: Simulation of the present-day climate with the ECHAM4 model: impacts of model physics and resolution. Technical report, Max-Planck-Institut f"ur Meteorologie,Hamburg.

ROECKNER, E., K. ARPE, M. BENGTSSON, M. CHRISTOPH, M. DÜMENTIL, M. ESCH, U. GIORGETTA and U. SCHULZWEIDA, 1996: MPI Report No218: The atmospheric general circulation model ECHAM4: Model description and simulation of present-day climate. Technical report, Max-Planck-Institut f"ur Meteorologie,Hamburg.

ROECKNER, E., L. BENGTSON, J. FEICHTER, H. LELIEVELD and H. RODHE, 1999: Transient climate change simulations with a coupled atmosphere-ocean GCM including the tropospheric sulfur cycle. *JOC*, page 3004 pp.

ROEMMICH, D. and C. WUNSCH, 1985: Two transatlantic sections: meridional circulation and heat flux in the subtropical North Atlantic Ocean. *Deep-Sea Res.*, **32**, pages 619–664.

SANDSTRÖM, J. W., 1908: Dynamische Versuche mit Meerwasser. *Ann. Hydr. Mar. Met.*, page 6.

SARACHIK, E. S., M. WINTON and F. L. YIN, 1996: Mechanisms for Decadal–to–Centennial Climate Variability. In: *Decadal Climate Variability*, D. L. T. Anderson and J. Willebrand, editors, Springer Verlag, Berlin–Heidelberg, pages 157–210.

SCHILLER, A., U. MIKOLAJEWICZ and V. VOSS, 1997: The stability of the North Atlantic thermohaline circulation in acoupled ocean-atmosphere general circulation model. *Climate Dynamics*, **13**, pages 325–347.

SCHMITZ, W. and M. MCCARTNEY, 1993: On the North Atlantic Circulation. *Reviews of Geophysic*, **31**, pages 29–49.

SCHOTT, F., T. N. LEE and R. ZANTOPP, 1988: Variability of structure and transport of the Florida Current in the period range of days to seasonal. *J. Phys. Oceanogr.*, **18**, pages 1209–1230.

SEAGER, R., D. BATTISTI, J. YIN, N. GORDON, N. NAIK, A. CLEMENT and M. CANE, 2002: Is the Gulf Stream responsible for Europe's mild winters. *Q.J.R. Meteorol.Soc*, **128**, pages 1–24.

STEVENS, D., 1990: On open boundary conditions for three dimensional primitiv equation ocean circulation models. *Geophys.Astrophys.Fluid Dyn.*, **51**, pages 103–133.

STRASS, V. H., E. FAHRBACH, U. SCHAUER and L. SELLMANN, 1993: Formation of Denmark Strait Overflow Water by Mixing i n the East Greenland Current. *J. Geophys. Res.*, **98** (C4), pages 6907–6919.

T.Delworth, S.Manabe and R.J.Stouffer, 1993: Interdecadel Variations of the Thermohaline Circulation in a Coupled Ocean-Atmosphere Model. *J. Climate*, **6**, pages 1993–2011.

Thorpe, R., J. Gregory, T. Johns, R. Wood and J. Mitchell, 2001: Mechanisms Determining the Atlantic Thermohaline Circulation Response to Greenhouse Gas Forcing in a Non-Flux-Adjusted Coupled Climate Model. *JOC*, **14**, pages 3102–3116.

Timmermann, A., M. Latif, R. Voss and A. Grötzner, 1998: Northern Hemispheric interdecadal variability: A coupled air-sea mode. *J. Climate*, **11**, pages 1906–1931.

Treguier, A.-M., T. Reynaud, T. Pichevin, B. B. an d J.-M. Molines, A. P. de Miranda, C. Messager, J. O. Beismann, G. Madec, N. Grima, M. Imbard and C. Le Provost, 1999: The CLIPPER Project: high resolution modelling of the Atlantic. *International WOCE Newsletter*, **36**, pages 3–5.

Trenberth, K. and J. Caron, 2001: Estimates of the Meridional Atmosphere and Ocean Heat Transport. *J. Climate*, **14**, pages 3433–3443.

Wiebe, E. and A. Weaver, 1999: On the sensitivity of global warming experiments to the parameterisation of sub-grid scale ocean mixing. *Climate Dynamics*, **15**, pages 875–893.

Willebrand, J., C. Barnier, C. Böning, C. Dietrich, P. Killworth, Y. LeProvost, J.-M. Molines and A. New, 2001: Circulation characteristics in three eddy-permitting models of the North Atlantic. *Progress in Oceanography*, **48**, pages 123–161.

Willebrand, J. and D. Haidvogel, 2001: Numerical Ocean Circulation Modelling: Present Status and Future Directions. In: *Ocean Circulation and Climate*, Academic Press, pages 547–556.

WOCE, 1999: Report of the WOCE/CLIVAR Workshop on Ocean Modeling for Climate Studies. Technical report 165/99, NCAR.

Wood, R., A. Keen, J. Mitchell and J. Gregory, 1999: Changing spacial structure of the thermohaline circulation in response to atmospheric $C0_2$ forcing in a climate model. *Nature*, **399**, pages 572–575.

Wunsch, C., 2000: What is the Thermohaline Circulation? *Science's Compass*, **298**, pages 1179–1181.

Danksagung

Diese Arbeit entstand in der Abteilung *Theorie und Modellierung* des Instituts für Meereskunde an der Universität Kiel.

Mein besonderer Dank gilt meinem Doktorvater, Herrn Prof. Dr. Jürgen Willebrand, der diese Arbeit mit vielen Anregungen und präzisen Fragestellungen gelenkt und begleitet hat.

Vielen Dank an alle aus der Abteilung *Theorie und Modellierung* und hier besonders der *FLAME*-Gruppe, die mit offenen Ohren und Hilfestellungen diese Doktorarbeit erleichtert und mir auf diesem Wege viel beigebracht haben. Dabei möchte ich speziell Joachim Dengg hervorheben, der immer wieder Zeit für mich hatte und mir viele hilfreiche Ratschläge gab. Außerdem sparte er nicht mit kritischen aber besonders auch aufmunternden Bemerkungen.

Herzlichen Dank an meine Familie, die in jeder Hinsicht fast alles unterstützt hat. Zusammen haben wir manch schwierige Situation mit Geduld, Durchhaltekraft und Humor bewältigt und werden das auch in Zukunft versuchen.

Außerdem bedanke ich mich bei allen, die für mich da sind und wissen, dass sie an dieser Stelle gemeint sind.